UiT The Arctic University of Norway

Faculty of Engineering Science and Technology
Department of Computer Science and Computational Engineering

Geometric Modeling- and Sensor Technology Applications for Engineering Problems

Aleksander Pedersen

A dissertation for the degree of Philosophiae Doctor (PhD)

Contents

List of Figures

List of Tables

Preface

The work presented here started as a part of Narvik University College, which now is merged together with UiT The Arctic University of Norway. This thesis has been submitted as part of the requirements for the degree of Philosophiae Doctor (Ph.D.). The research has been conducted throughout the years 2015-2020 under the supervision of Prof. Arne Lakså and co-supervisor Associate Prof. Rune Dalmo.

The thesis is presented as a collection of articles that has been the result of cooperative work with colleagues in the research group. The first chapter consists of an introduction that provides background to this work and connects the included articles. Then follows a section discussing the thesis topics and enumerating the individual contributions. The third section concludes this work, provides some remarks and future research topics. The thesis itself is divided into two separate parts; the first part consists of three articles and a complementary section with application areas on interactive and editable geometry. The second part consists of three articles on sensors and sensor technology.

Abstract

Sensor technology and data collection, processing, interpretation and facilitation of data, analyzing, algorithms, geometric modeling and visualization and related methods are very central fields in engineering applications and for solving specific technical problems. Development in these fields is key to both scientific and industrial development. This thesis tries to combine different aspects of geometric modeling and sensor technology, as well as to facilitate simulation and visualization techniques. It includes;

- Applications and new techniques for geometric modeling, such as design, complex topology, movements and paths, terrain generation and cutting algorithms.

- Sensor technology and a generic information layer as a result of measurements and data analyzing in connection with visualization, modeling, development of hybrid solutions and methods for assessing road conditions.

Linking these two areas forms the motivation behind this work. This study explores many methods for evaluating and analyzing data as well as visualization and data presentation. The aim of the research is to provide a framework where the two seemingly separate areas are connected both as a logical consequence and by seeing common techniques and methods, and that the way we analyze and process information is not limited to one of the areas. Sensor data and measurements can easily be related to geometry in all contexts as a representation technique and vice versa by extracting information from geometry to provide data. The main results that contribute to research fields are: new approaches and representations for complex problems, new and increased knowledge for sensors and measurement techniques, connection of two fields by underlying methods and representations, and new insight into the connection and challenges between the two topics.

Acknowledgements

Numerous people have supported me during my PhD and I would like to give a special thanks to my main supervisor Prof. Arne Lakså for ideas and sharing of knowledge, discussions, support and patience. My co-supervisor, Associate Prof. Rune Dalmo for cooperative work, feedback, discussions and helping me with finishing this thesis. Also, Prof. Børre Bang for invaluable discussions, sharing of ideas and cooperative work. My colleagues, Jostein Bratlie and Tanita Fossli Brustad for common interests, discussions, cooperation and constructive feedback.
I would also like to give gratitude to the U.S.-Norway Fulbright foundation, which provided me with the opportunity to take part in the exchange program and ten unforgettable months in Austin, Texas under the supervision of Prof. Thomas J.R. Hughes.
Moreover, I am grateful to the Faculty of Engineering Science and Technology, UiT The Arctic University of Norway, and the department of Computer Science and Computational Engineering for giving me the possibility to work on and finalize this thesis. I would also like to give my gratitude to Stipendiatprogrammet Nordland Fylke for financing a major part of this project.
Also, a part of this thesis has been conducted as a work package for the Interreg-Nord project "WiRMa" (project ID 20201092).
Last but not least, my friends and family, especially my mom and grandparents, who have always believed in me and given support during my entire studying career.

Part I

Introduction

1

Background

Through years of research, numerical simulations have become a key technology in both scientific and industrial applications, as well as product development. Simulations of real-life large scale problems where models become increasingly complex, is still challenging, despite the growing capabilities of modern computers. Finite Element Methods (FEM) are among the most used and well known methods for solving partial differential equations (PDEs). FEM is used to find a numerical solution for PDEs and can be applied to a wide variety of problems. There have been, and still are, research topics on both local refinement and adaptive finite elements. There are however, some bottlenecks which account for a lot of the computational cost, for example in mesh generation. Constructing meshes of good quality in the sense of geometry for complex constructions, both for computations as well as visualization, can be a difficult and expensive task. Isogeometric analysis(IGA) was introduced by Hughes et.al in [13], which tries to bridge the gap between Computer Aided Design (CAD) and Finite Element Analysis (FEA). In general, this integration means using the same functions for constructing the geometry as for performing analysis and there is no need for any mesh generation. Typically, in CAD systems the geometry representation is trimmed using intersection curves, which make the boundary for the faces and will therefore lead to basis functions that are not restricted to the face accordingly. B-Splines/NURBS is the de facto industry standard construction used for this purpose. NURBS (Non Uniform Rational B-Spline) is incorporated into almost all commercial software and industry standards used in CAD. NURBS is actually a B-Spline in the projective space and, when mapped to the Euclidean space, it becomes a rational function increasing the

degree of freedom for B-Splines. Some variants of B-Spline/NURBS which try to reduce the amount of data are: T-Splines [76], PHT-Splines [20, 21], Locally refined B-Splines (LR B-Splines) [22, 37] and Hierarchical B-Splines [87, 27]. Most of the different research environments which conduct research either using or developing spline constructions, often require specific properties and thus new spline constructions are developed from scratch or extended from existing constructions.

The work carried out during this project has been twofold, therefore this thesis is divided into sections based on the two different areas. The background information will also mainly focus on the two separate parts, one consisting of geometry and the other one on sensor technology.

This chapter connects some of the basics within splines, geometry, data analysis, sensors and technology. The goal is to give the reader a better basis for following the theory introduced later in the articles and summaries.

In Section 1.1 of the first part on geometry, to include a broader audience I will give the reader a brief historical perspective of previous work. The main matter from the field of geometry in this thesis is best described by interactive geometric modeling, surface construction, irregular geometry and analysis.

Sections 1.2 and 1.3 of the second part on sensors and sensor technology, consist of testing, developing and analyzing sensor data. The data used and gathered here is from a very broad selection of technologies, such as smart-phones, stand alone sensors i.e. accelerometer, gyroscope, mobile road sensors, measuring equipment i.e Dynafor LLX2digital load indicator and radar.

The last part about scientific research and innovation, Section 1.4, describes how this thesis can be connected to innovation within both geometry and sensors.

1.1 Blending splines

This section gives an explanation of suitable geometry for IGA purposes with a blending type spline construction. To show how the blending splines might arise as one of the alternatives for suitable geometric representation in several aspects, such as IGA and interactive and editable geometry, a brief review will follow of the history of blending splines and their development over time.

Historically, blending of curves and surfaces is not a new technique, however

this thesis includes a new blending construction. Before entering the history of blending splines we show how it started and what kind of development lead to this specific research. B-splines/Bézier are blending of points and, if we also consider blending with vectors we can include Hermite interpolation. We can also relate to earlier constructions such as Coons Patch [12] and Circle Splines [90], which are similar to the blending type spline construction used in the first part of this thesis. For further notice we look at blending in a more general perspective and only consider the blending function (B-function). A B-function is a permutation function, mapping $[0, 1] \rightarrow [0, 1]$, where the first derivative is monotonically increasing, and symmetric around a center point $[0.5, 0.5]$.

There is a long list of examples of how blending has been used and developed over time. We find that the development of surface construction with arbitrary smoothness [92], Modeling surfaces from planar irregular meshes [54] and Modeling surfaces from meshes of arbitrary topology [53], are a selection of such development and groundwork for some of the research in this thesis, specifically for blending and surface construction.

In (1.3) we can see one of the first definitions of Expo-Rational B-Splines and there have been several simplifications which will be explained below. One of many advantages of using this blending construction compared to ordinary polynomial B-Splines, is not only the possibility to have a position connected to the control points, but also orientation and scaling. The result of this is a base for an easy interactive modeling tool with very accurate design possibilities, with local support equivalent to a first degree polynomial B-Spline. Imagine creating a model based on scanned data that can be divided into smaller local surface, and can be used in blending to create a flexible, accurate and easy to use tool to do local deformations. Such deformation can come from contracting a muscle to create a bump, for example a biceps contracting. Blending splines is a spline construction where local geometry is blended together to create global geometry. It was first introduced through the Expo-Rational B-Splines (ERBS) [17, 42] and the Generalized Expo-Rational B-Splines (GERBS) [15] constructions. The research was first communicated at the international conference "Mathematical Methods for Curves and Surfaces" in Tromsø, Norway in 2004, and there still is an ongoing research effort at UiT The Arctic University of Norway. With the generalization, non expo-rational basis functions were introduced, such as the Euler Beta Function B-Spline (BFBS) basis. BFBS are polynomial splines and, as such, can be represented as linear combinations of polynomial B-Splines. Other examples of generalized basis functions used with blending splines are Logistic ERBS (LERBS) and the original scalable subset. The different constructions vary in the way they are constructed; some require heavy integration and are more complex in implementation, others consist of explicit and exact computable functions.

This can make the different constructions suitable for different aspects and applications of interactive geometric modeling and IGA.

The examples and evolution of blending splines are shown below, starting with how an ERBS function $f(t)$ can look like.

$$f(t) = \sum_{k=1}^{n} l_k(t) B_k(t) \tag{1.1}$$

where l_k are local functions blended together by a blending function B_k.

$$B_k(t) = \begin{cases} \dfrac{\int_{t_{k-1}}^{t} \psi_{k-1}(s)ds}{\int_{t_{k-1}}^{t_{k+1}} \psi_{k-1}(s)ds}, & if \quad t_{k-1} < t \leq t_k \\ \dfrac{\int_{t}^{t_{k+1}} \psi_{k-1}(s)ds}{\int_{t}^{t_{k+1}} \psi_{k-1}(s)ds}, & if \quad t_k < t \leq t_{k+1} \\ 0, & \text{otherwise} \end{cases} \tag{1.2}$$

where

$$\Psi_k(t) = e^{-\beta_k \frac{|t-((1-\lambda_k)t_k+\lambda_k t_{k+1})|^{2\sigma_k}}{((t-t_k)(t_{k+1}-t)^{\gamma_k})^{\alpha_k}}}. \tag{1.3}$$

The integral in the denominator for $B_k(t)$ is denoted as the constant scaling factor. $B_k(t)$ is defined on R and its support is $[t_{k-1}, t_{k+1}]$, which is the minimal possible support for continuous B-Splines to satisfy the partition of unity. In [41], Laksaa has provided a thorough analysis of the properties of ERBS, furthermore the five basic properties are discussed below.

Property 1

Every basis $B_k(t)$ is positive on the interval $t_{k-1} < t < t_{k+1}$ and 0 otherwise.

Property 2

The set of basis functions $B_k(t)$ for $k = 1, 2, \ldots, n$ form a partition of unity on $(t_1, t_n]$. It follows that if $t_k < t \leq t_{k+1}$ then $B_k(t) + B_{k+1}(t) = 1$

Property 3

A Lagrange form of polynomials holds for $k = 1, 2 \ldots n$ and the basis $B_k(t_k) = 1$

Property 4

Every basis function $B_k(t)$ is C^∞-smooth on R

Property 5

All derivatives of all basis functions are zero at their knot t_k. In fact they are zero at every knot

Properties 1, 2 and 3 are basic properties for both ERBS and linear B-Splines. **Properties 4 & 5** are unique amongst the spline basis functions, and are influencing the way we can use ERBS. In order for the two unique properties to be true, there are some restrictions regarding the intrinsic parameters $\alpha, \beta, \gamma, \sigma, \lambda$ used in (1.3). The default values are $\alpha = \beta = \gamma = \sigma = 1$ and $\lambda = \frac{1}{2}$. Adjusting these parameters yields different shapes of the ERBS basis function. Regarding **Properties 4 & 5** they are restricted by the intrinsic parameters by:

- $\sigma \in 0 \cup N$, for **Property 4** at both intervals $k-1$ and k
- Either $\lambda > 0$, or $\lambda = 0$ and $2\sigma < \alpha$, for **Property 4** at interval k and **Property 5** at interval $k-1$
- Either $\lambda < 1$, or $\lambda = 1$ and $2\sigma < \gamma\alpha$, for **Property 4** at interval $k-1$ and **Property 5** at interval k for exterior knots and $k-1$ for interior knots.

The reason for mentioning **Properties 4 & 5** in a more detailed version here is the interest they raise regarding the analysis of blending splines. Points on the geometry where the function derivatives are zero handles singularities when performing analysis and calculations. Where the derivatives are zero at the knots, the derivatives can be set explicitly.

Another important property connected to (1.3) appeared after adding even more restrictions to the intrinsic parameters; $2\sigma_k = (1+\gamma_k)\alpha_k$. The result of this was a sub-set of the ERBS called the Scalable Subset and Ψ is reduced to

$$\Psi = e^{-\beta \frac{|t-\alpha|^{(1+\gamma)\alpha}}{(t(1-t)^{\gamma})^{\alpha}}},$$

and with the same default intrinsic parameters ($\alpha = \beta = \gamma = 1$ and $\lambda = \frac{1}{2}$) it gives

$$\Psi(t) = e^{-\frac{\left(t-\frac{1}{2}\right)^2}{t(1-t)}},$$

and since this restriction reduces ERBS to a sub-set where the integrals are independent of the knot-vector itself and depend only on the parameters in the knot interval, the scaling will be a constant and using the default set of intrinsic parameters gives

$$\left[\int_0^1 \Psi(t)\right]^{-1} \approx 1.6571376797382103.$$

Another sub-set of ERBS is the logistic ERBS (LERBS) [19] which was also the

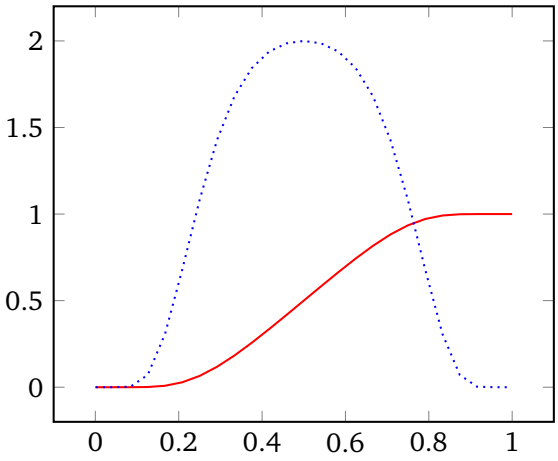

Figure 1.1: Logistic version of the blending function (solid) and its first derivative (dotted)

result of a change in variables. The original LERBS blending function is

$$B(t) = \frac{1}{1 + e^{\left(\frac{1}{t-1} + \frac{1}{t}\right)}}, \tag{1.4}$$

where the domain is $[0, 1]$. For analysis purposes a change in domain from $[0, 1] \longrightarrow [-1, 1]$ is beneficial and (1.4) changes to

$$B(t) = \frac{1}{1 + e^{\left(\frac{2}{(1+t)^a} - \frac{2}{(1-t)^b}\right)}},$$

where $a = b = 1$ is the default values. Another related logistic function is

$$B(t) = \frac{1}{1 + e^{\left(-2\frac{t}{\sqrt{1-t^2}}\right)}}.$$

Blending splines summary

The reason for reducing the original (1.2) is to decrease computational cost. Computing the integral of Ψ is expensive and by introducing the scalable subset we get an easily computable infinitely differentiable (1.3). If we recall the formula for a second degree B-Spline curve

$$c(t) = \begin{pmatrix} 1 - w_{1,i}(t) & w_{1,i}(t) \end{pmatrix} \begin{pmatrix} 1 - w_{2,i-1}(t) & w_{2,i-1}(t) & 0 \\ 0 & 1 - w_{2,i}(t) & w_{2,i}(t) \end{pmatrix} \begin{pmatrix} c_{i-2} \\ c_{i-1} \\ c_i \end{pmatrix},$$

where

$$w_{d,i}(t) = \frac{t - t_i}{t_{i+d} - t_i},$$

Regularized Beta Function	Euler and Legendre	
Trigonometric function	Szilvsi-Nagy and Vendel [82]	2000
Rational function	E. Hartmann [35]	2001
Fabius function Approximation	Olofson [55]	2019
Expo-Rational functions		
- Non-symmetric type	Navau and Garcia [54]	2000
- Symmetric Integral type	Dechevsky, Lakså and Bang [43]	2004
- Rational based symmetry	Ying and Zorin [92]	2004
- Symmetric logistic type	Zanaty and Dechevsky [19]	2013

Table 1.1: Introduction of several B-functions

and the index i is determined by $t_i \leq t < t_{i+1}$. If we now use a B-function to make a permutation of the $w(t)$, we get the following expression

$$c(t) = \begin{pmatrix} 1 - B(w(t)) & B(w(t)) \end{pmatrix} \begin{pmatrix} 1 - B(w(t)) & B(w(t)) & 0 \\ 0 & 1 - B(w(t)) & B(w(t)) \end{pmatrix} \begin{pmatrix} c_{i-2} \\ c_{i-1} \\ c_i \end{pmatrix}. \tag{1.5}$$

Here the $B(w(t))$ (another notation is $B \circ w(t)$), will still maintain all the properties of a regular B-Spline. We get a B-Spline with continuity properties that is increased by the order of the B-function used. In the case of ERBS, we know that the B-function has an order of infinity, so the curve in (1.5) will be C^∞-smooth. In the blending spline type construction we choose to use a second order B-Spline that imposes the least possible support, we keep hermite interpolation properties, but still maintain a higher order continuity depending on what B-function we use. In (1.6) we have replaced the control points with local functions.

$$c(t) = \begin{pmatrix} 1 - B \circ w_{1,i}(t) & B \circ w_{1,i}(t) \end{pmatrix} \begin{pmatrix} c_{i-1}(t) \\ c_i(t) \end{pmatrix}. \tag{1.6}$$

A selection of B-functions is shown in Table 1.1. As we see, there are several variants of the original B-function and from the latest contribution in [55] a new blending function based on trigonometric and polynomial approximations of the Fabius function arose.

1.1.1 Local geometry - functions, curves and surfaces

A blending spline (1.1) is blending together different geometries, local geometry, using a blending function. The only requirements for the local geometry is that it has a parametric domain. In general there are no restrictions regarding the type we are blending and blending two different geometries can be done. Representations such as scalars, vectors, polynomials, trigonometric functions are included.

1.1.2 Applications

Blending splines has also created a platform for further **R** & **D**, with several fields of interest in both research projects and teaching. Blending splines has been used for different types of modeling, including interpolation, approximation and compression, local refinement, deformation of objects, simulations and also including wavelets [5, 94, 32, 6, 70, 89, 52, 16]. Furthermore, even though blending splines and example areas have been investigated, there is still a wide field of unexplored territory including the emerging new field of interest, namely IGA. One of the possible advantages of blending splines in the context of IGA [18, 39] is to utilize the basis for both geometry and analysis, which could make a big difference for hardware, time consumption and enable the development of an integrated system for modeling and simulations. A short survey is given below of projects previously conducted at Narvik University College(NUC) and still being explored at UiT within the field of blending splines.

Application of GERBS in Computer Aided Design and Analysis (CADA) [94]: Presented a hierarchy of smooth and piecewise continuous constructions founded on the family of GERBS, and studies the resulting representation in the framework of geometric modeling and finite element analysis(FEA). Constructions proposed in [94] provide new and alternative tools for use in both geometric modeling and FEA, where the domains presented consist of flexible and minimally supported smooth basis functions on tensor products meshes and polygonal domains. Current methods applied in IGA are mostly based on Non-Uniform Rational B-Splines(NURBS) with specific rules relating to the dependence of basis functions, the ability to represent watertight surfaces and smoothness conditions.

Interactive modeling[5]: Presented tools for interactive modeling, using local refinement by knot insertion, splitting or blending. The geometry can be both modified and well suited for different geometrical objects. Figure 1.2 is illustrating a refined tensor product surface, where local surface patches are blended together.

Surface deformation over flexible joints[32]: Presented a surface deformation using blending splines and applying an affine transform on the elements of a skeleton framework consisting of connected bones together with Hermite type of local geometric surfaces, the surface can be deformed to "fit" the bones and their movement. The current implementation does not take into account any type of volume conservation or self intersection, but as Figure 1.3 shows, the results can be promising and using blending splines seems to be a good fit for this type of deformation.

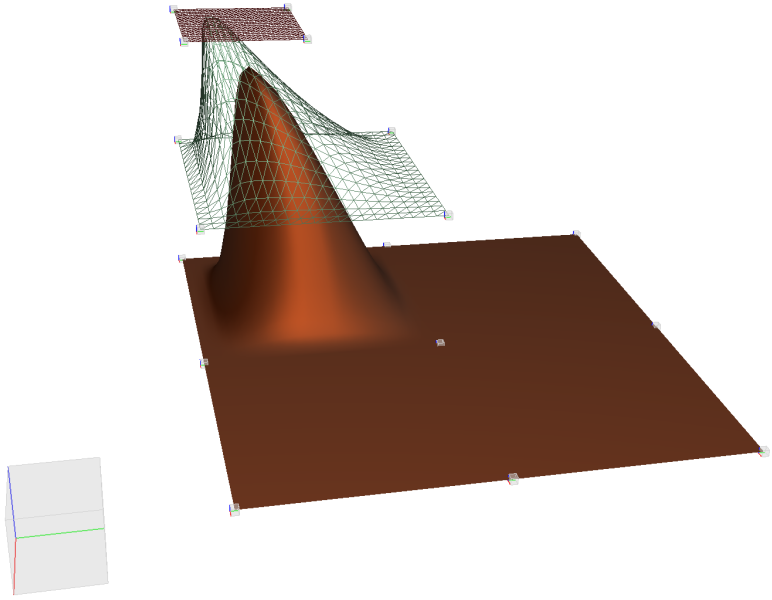

Figure 1.2: Locally refined GERBS surface using blending splines, figure from Bratlie [5]

Smooth rendering[6]: Presented smooth rendering using the graphics processing unit(GPU) based on the tessellation shader architecture with render block types. Results show promising visualizations for use in computer games or computer generated images. Figure 1.4 shows a "Tower" surface created using blending splines and the smooth rendering with four render blocks.

Surface deformation and simulation[66]: Presented ideas for an environment with object-object or fluid-structure interaction (FSI) together with the blending splines resulting in interactive simulators. This is also one of the

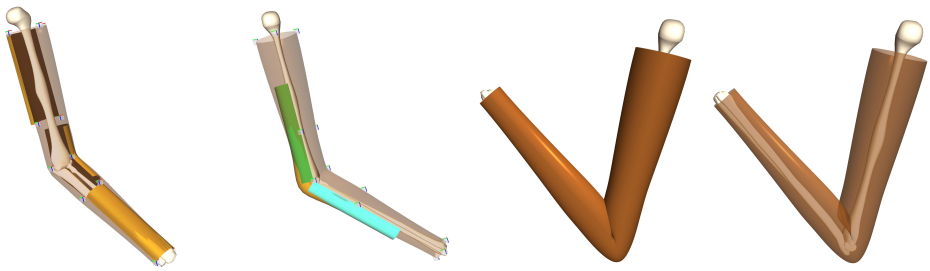

Figure 1.3: Skinning done with GERBS, figures from Haavardsholm [32]

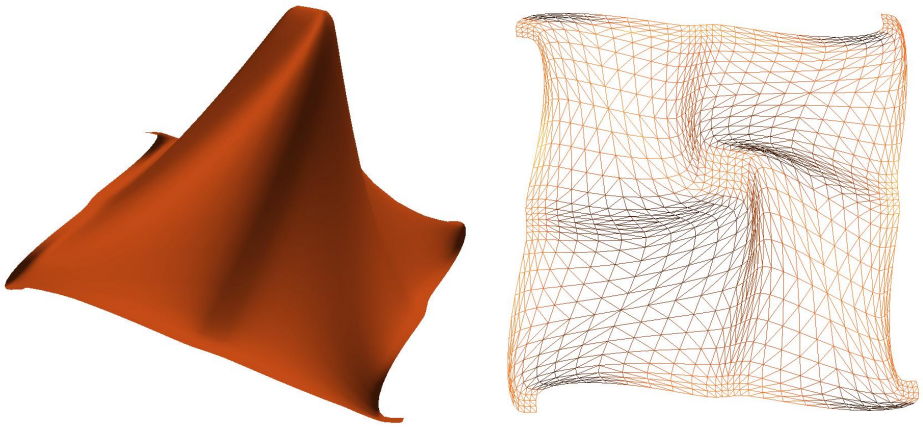

Figure 1.4: Solid and wireframe shading of a "Tower", figures from Bratlie [6]

properties discussed in phase field modeling, which is included in a later section. Based on local refinement, the geometry can be deformed by applying localized stresses/forces. For graphical purposes, different visualizations can be applied, for example curvature(Gaussian and mean), as in Figure 1.5. In the OpenGL Shading Language(GLSL) we can utilize the geometry shader to perform calculations directly on the GPU. The geometry shader requires information regarding the geometry, such as derivatives and curvature. From the surface on the right hand side in Figure 1.5 we can see some geometric discontinuities. One of the reasons for using the blending spline construction and what we call knot multiplicity is exactly to create geometry with such discontinuities. These holes and the surface itself are still mathematically C^n-smooth while being geometrically G^0-smooth. Even with such irregularities, the surface and definition still covers the entire domain and can be evaluated at any point. What is also interesting here is to see how local the construction is, and it is not difficult to create small dents that do not influence the entire surface, but only a very small part.

Spring and wave simulation[89]: Presented surface deformation by employing differential equations(functions on the local surfaces), here in the form of spring and wave equation. This is of course not restricted to local surfaces, but rather the control points or grid. Applying calculations directly on the local geometry, which is then blending together by blending splines to form the global geometry, which is then updated whilst calculations are being performed. This creates a degree of freedom and the user can interact with the object(this case surface), even when the calculations are running. This type of simulation and connection to the basis functions was one of the next steps towards IGA without using a combination and extraction operator. The local geometry here is also surfaces of a lower degree, and from the Figure 1.6 on the right hand side we

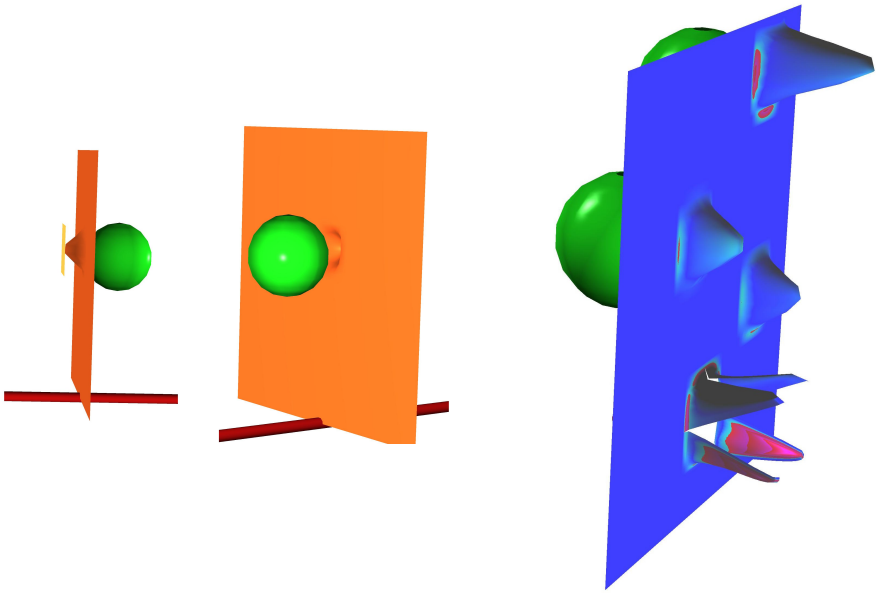

Figure 1.5: Indentation and splitting scenario in Shooting simulator, figures from Pedersen [66]

can see these surfaces. The control points of the local surface(blue) have had positions and derivatives changed in relation to the partial differential equation employed here. This is done in real time in a simulation environment. Here the wave equation is performed directly on the local geometry, creating the wave motion on the global geometry by blending.

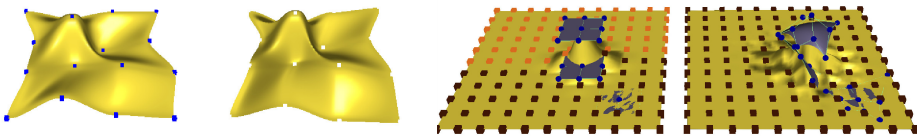

Figure 1.6: Spring and wave equation using blending splines, figures from Wang [89]

Flame behavior visualization[72]: Presented a three-tensor ERBS volume to visualize the behavior of flames. The local volumes used here are Bézier volumes and Figure 1.7 visualize a slicing plane through the volume for three different time steps. The volume can also be used to simulate the behavior

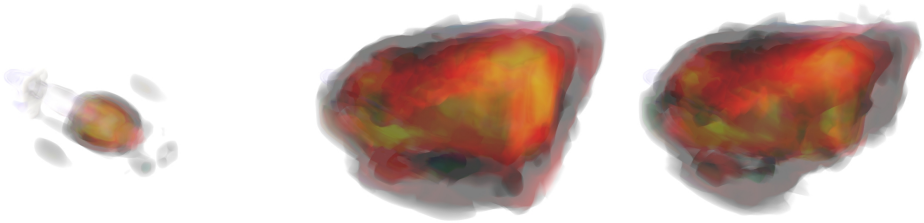

Figure 1.7: Flame behavior using ERBS volume with Bézier volumes as local volumes, figures from Rasmussen [72]

of the flame, but this would require some analysis that was not part of this specific project, but could be a future task. One aspect that was investigated here was the effect of rotating the local volumes creating wavelike motions in the global volume, which is possible based on the way blending splines work, Section 1.1. In this case, the volume was combined with existing data to visualize and simulate the behavior of flames. Just like in the previous sections, Section 1.1.2, we perform deformation on the local geometry and, by blending this together, we get a complete domain. One of the main reasons for this work and the utilization of ERBS volumes was to create a very simplified, but yet realistic model based on scaling and rotation of the local volumes. Comparing the simplified model to the data obtained was the next step in the process.

1.1.3 Mechanics and perforation

The first part of this thesis was focusing on IGA and analyses on surfaces with discontinuities, that is, creating suitable geometry with holes that forms a basis for analyzing perforation and penetration problems on a thin plate. Such analysis problems can be, but are not limited to, effects of tension and loads during and after penetration and/or perforation, crack propagation, phase field modeling and fracturing mechanics. To connect structural and material properties with geometry in basic and advanced mechanics, we apply spline theory and blending techniques.

All solid mechanics problems have some fundamental components:

- Relationships between stress and applied forces and how the stress can vary within a body, also known as mechanical equilibrium.
- Strain relative to displacements is known as the geometric compatibility.
- Closing the loop for solvable system of equations, is the material consti-

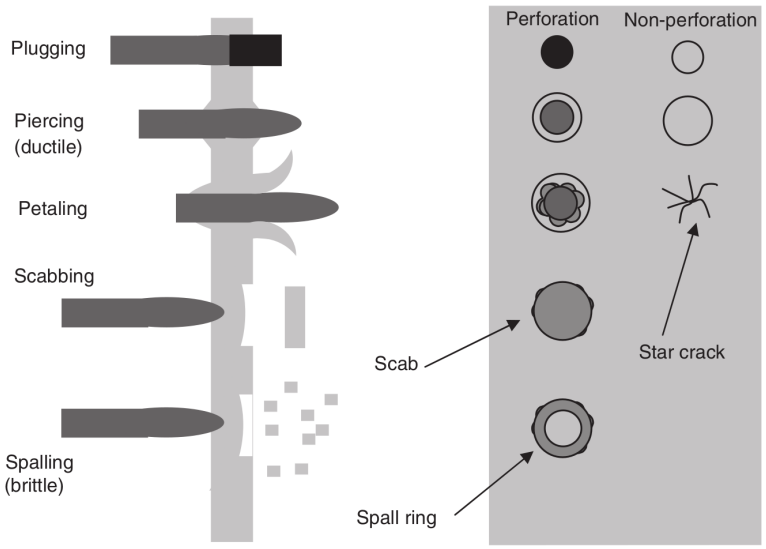

Figure 1.8: Target failure modes from [9]

tutive law that governs how stresses are related to strains in a body.

Generally the two first statements lead to partial differential equations (PDE's), whereas the last statement yields algebraic equations for elastic materials, including ODE's for more complex materials. Deflection profiles, bending of beams, moment distribution, stress analysis, principal stress, shear yield strength, stress distribution are some components of the solid mechanics.

1.1.4 Basics of ballistics

Terminal ballistics is the regime a projectile enters at the end of its flight, where it collides with a target. The terminal effects of the projectile depend on both the design and mission of the bullet as well as the material properties of both projectile and target. Penetration, perforation and indentation are three of the terminal effects that can occur.

Penetration refers to the impact case in which the projectile enters the target, whereas perforation is the case in which the projectile passes completely through the target. Indentation is a deformation of the target, where the target remains intact without any failure.

Considering a metal target, penetration and perforation failure modes consist, according to [9], of plugging, piercing, petaling, scabbing and spalling, see Figure 1.8. The theory of penetration and perforation are very different

depending on the target- and projectile material. Furthermore, not only the material properties make a difference, the velocity of a projectile can also differ from way below 200 m/s to above 1000 m/s. Such varying conditions lead to different problems, thus, each spectrum of velocity benefits from different techniques. The higher the speed is, the more energy the projectile will have when it hits the target, and impacts with speeds greater than 12.000 m/s will create such a high rate of energy exchange that some of the colliding materials will vaporize.

There are in general three different scenarios of deformation: either the object is not deformed because the external forces are too low compared to the resistance of the object's material, the object is deformed permanently, but not damaged in any way, or the object can be damaged by cracks, penetrations and perforations. When talking about a damaged object, this is often the case for the area that is affected by the external force, and when dealing with projectiles, this area can be relatively small compared to the size of the object. Since developing a simulator that takes care of all of the above mentioned scenarios is a complex task, it is desirable to study each case individually.

If the external force applied to the surface at a section is less than the force needed for deformation, the surface will appear unaffected by the projectile. On the other hand, when the applied stress exceeds the elastic limit, the deformation of an object will become permanent, and we would see an indentation in the material. We note that how this indentation is calculated and visualized depends on the method of choice.

Furthermore, when a metal is exposed to a force, such as a bullet, the metal will start to vibrate. The vibrations of the metal can not be observed directly due to their small amplitude as a consequence of the speed of sound in a metal being much higher than in air, or any other liquid, and the deformation due to the vibrations are very small. The speed of sound in a metal will vary depending on the structure and composition of the metal. This property may even vary internally in one single object. Therefore, it can be very difficult to calculate the exact speed in a metal, even when the composition is known. In a volume medium the wave speed takes the general form

$$v = \sqrt{\frac{elastic\ property}{inertial\ property}} = \sqrt{\frac{B}{\rho}},$$

where B is the bulk modulus and ρ is the density.

With solids, the wave speeds are different in all directions, in different geometries and there is a difference between transverse and longitudinal waves. The idea of a wave traveling through the metal when it is exposed by a force from

the bullet inspired us to try the wave equation system with the help of the discretization method.

If we look at the properties during a perforation/penetration of a thin plate, we can use phase field modeling, for problems with interfaces, and also prediction of crack propagation [4, 30, 84].

1.2 Application

A sensor is usually referred to as a device which detects change in quantity, such as light, heat, motion, gasses and pressure. Today, we know that sensors are incorporated into almost everything and the technology itself is still in development. For instance, a smart-phone has several sensors, such as accelerometer, gyroscope, magnetometer, microphone, touch screen, GPS, pedometer and barometer.

There is still a debate about who started the development of the first sensor technology, but this is mostly a question regarding the type of sensor. For instance, Wilhelm von Siemens and Warren S. Johnson both invented temperature sensors. Warren invented the electric thermostat, while Wilhelm was said to use the temperature sensitivity of electrical resistance in different materials [14].

Collecting and processing data is a necessary aspect of our technologically advanced society, which can be related to many fields, such as monitoring different events, controlling environments, or for decision making purposes to mention a few examples. An illustration of the connection between fields is shown in Figure 1.9.

During this technological development we are experiencing, where we now have smarter cities, cars and to some extent self driving vehicles, the need for assessing road conditions increases. One of the more difficult seasons is, of course, winter time, specifically in northern regions where the weather can be rough. There are already cameras, equipment and other measuring techniques out there. Safety and consistency in moving vehicles is important, and this is only achieved when the road network is maintained to a certain standard. By utilizing users' mobile phones, [34], proposes a road condition monitoring framework to detect anomalies on the road surface by analyzing the accelerometer and gyroscope data recorded using smart-phones. In [57, 56], an image recognition system for road surface condition classification was proposed using low cost cameras mounted on regular vehicles.

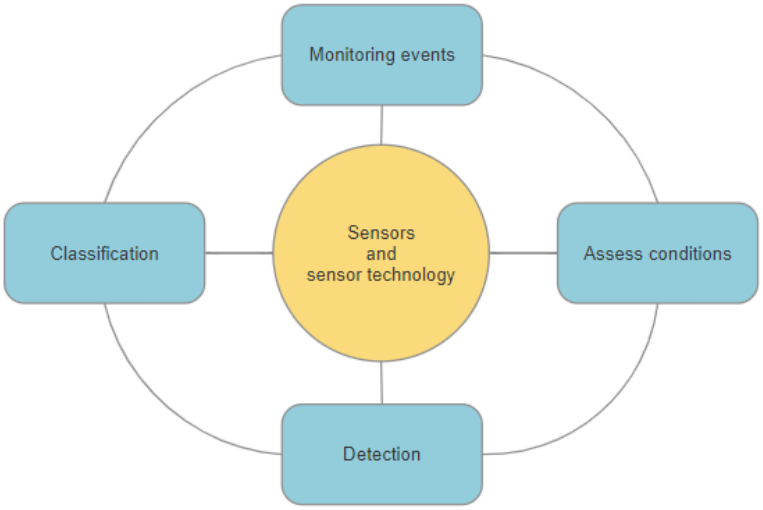

Figure 1.9: It is very difficult to summarize sensor technology into one specific theory, since every branch has its own characteristics. The sensor technology used in this thesis can be divided into four different categories; Monitoring, assessing conditions, detection and classification. This is just a simple and very broad list of the sections in which most of the technology can be found, for example, optical sensors for assessing road conditions or measuring temperature and humidity.

Using sensors and developing applications using a smart-phone have been thoroughly tested in applications where, for example, position and orientation estimation using inertial sensors have been used [38]. Other uses for smartphones include indoor positioning [78], signal processing algorithms for position measurements with mems based accelerometer[23], [65]. In [59] the author studied simple methods for evaluating the trajectory of a 3D pendulum, and literature show usages when combining algorithms with phone sensors for physics and mechanics problem purposes.

1.2.1 Technology descriptions

This section describes the technology used for project work and research papers. Two optical sensors, the Road Conditioner Monitor 411 (RCM411) and Mobile Advanced Road Weather Information Sensor (MARWIS), and the On-Board Diagnostics II (OBD-II) link reading car information combined with experimental devices such as a radar (Walabot) constitutes the sensors used in this thesis for winter road assessment. For the digital twin setup and prototype development, the DEUS XP Metal Detector was utilized and mounted using a special Celestron smart phone adapter. The technical descriptions are a limited overview gathered from [7].

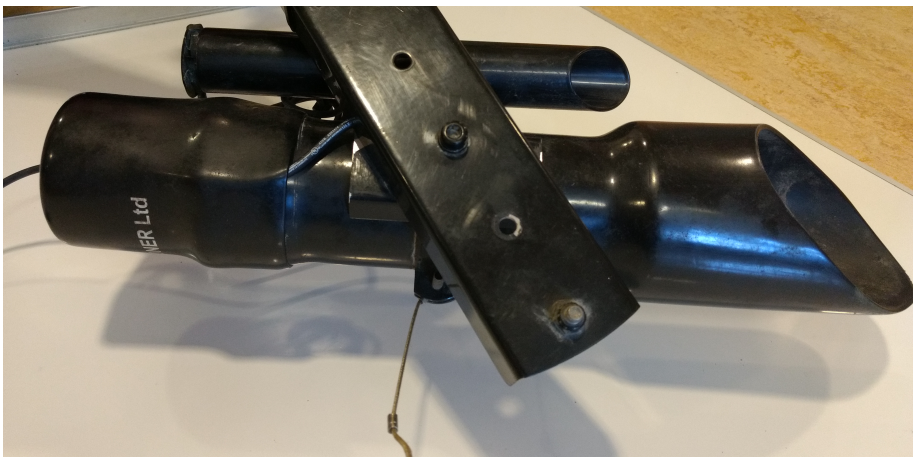

(a) RCM411.

(b) MARWIS.

(c) OBD-II.

(d) Walabot.

(e) DEUS XP Metal Detector with Celestron smart phone adapter

Figure 1.10: Selected technology used in this thesis

Teconer - RCM411

Road Condition Monitor RCM411 (Figure 1.10a) [33, 1, 83] is an optical sensor based on spectral analysis that evaluates the surface condition by measuring the optical reflection signal on the road surface. Information on surface conditions, friction, and water layer thickness are some of the variables the sensor outputs. In addition RCM411 uses an IR-thermometer (RTS411), supplied by Teconer, installed to the RCM411-frame. This thermometer gives feedback on air temperature and surface temperature. RCM411 is designed to be mounted on the rear of a vehicle on a 50 mm tow ball, with the sensor pointing down towards the wheel track. Data from the sensor is transferred to a mobile phone using Bluetooth, then communicated to selected servers. This provides the opportunity to see real-time updates on surface conditions on a mobile phone app or online at `https://roadweather.online`.

MARWIS

Mobile Advanced Road Weather Information Sensor (MARWIS) (Figure 1.10b) [48, 49] is an optical sensor that captures the reflecting behavior of the road surface at varying wavelengths to give feedback regarding the road conditions. In addition MARWIS has three other integrated sensors for measuring temperature and humidity. The data received from the sensor includes surface conditions, friction, water layer thickness, ice percentage, temperature (surface, ambient, and dew point), and humidity (relative and relative at ground temperature). MARWIS can be mounted on a truck or a car using a custom rack attached with magnets, and there are three ground-to-sensor distance options depending on the MARWIS model: 0.5 m, 1 m, or 2 m. Data from the sensor is transferred to a mobile phone using Bluetooth and can be viewed in real-time using the MARWIS app [73]. The app has automatic upload of received data to a server (the ViewMondo-Server), which gives the opportunity of downloading, visualizing, and analyzing the measurements on the ViewMondo software platform [50].

OBD-II

On-Board Diagnostics, Second Generation (OBD-II) (Figure 1.10c) [79, 80] is a computer-based system monitoring the performance of engine components. The system was originally designed to reduce emissions from vehicles and became a requirement in the US in 1996 on all newer vehicles. Later on other countries adopted similar laws, including Canada, parts of the European Union, Japan, Australia, and Brazil. The OBD-II system in a vehicle can be accessed via a Diagnostic Link Connector using a device called a scan tool or OBD-II

adapter. Various information can be obtained from the diagnostics, e.g. status of the "Check Engine" light, diagnostic trouble codes, and hundreds of real-time parameters (i.e. speed, RPM, coolant temperature, etc.). Most scan tools are compatible with third-party OBD software and mobile apps (e.g. via Bluetooth) that displays and saves information, and allows interaction with the OBD-II in the vehicle.

Walabot

Walabot [88, 81] (Figure 1.10d) is a pocket-sized 3D imaging sensor that uses radio frequency technology to illuminate the area in front of it and sense the returning signals. The sensor supports short range scanning and distance scanning, with the possibility to extract 3D image data, 2D image slices, raw signals, and the sum of raw signals in an image. Data collected from the sensor is processed and sent through a USB cable to a host device (e.g. a Raspberry Pi). Depending on the model, the Walabot can be used in areas such as in-room imaging, in-wall imaging, object detection, motion sensing, and sensing of dielectric properties of materials. In addition many competitions have been held that focus on finding new use cases for the Walabot, some examples can be found at [93].

DEUS XP Metal Detector

DEUS XP Metal Detector is a regular metal detector which consists of two coils, a search coil and a detector coil as well as a set of control logic. The search coil generates an electromagnetic field, and the detector receives the replicated field generated by the metallic objects, Eddy currents [8]. The output from the metal detector is then transferred to the control logics which emits an audio signal indicating the type of material. The audio signal can then be recorded and used for analysis purposes.

Smartphone

The smartphone is used as a processing and data collection device, utilizing the built-in sensors and hardware. Examples of such sensors:

1. Accelerometer
2. Gyroscope
3. Rotation vector (attitude composite sensor)

4. Microphone

For the simplest motion-based representation, the accelerometer is used to detect movement changes in the x, y, and z-axis. The gyroscope is used for orientation by measuring the rate of rotation for the three-coordinate axis. The rotation vector is an attitude composite sensor reporting the orientation relative to an East-North-Up coordinate frame by integrating the underlying accelerometer, magnetometer and gyroscope readings. The microphone has its own reporting mechanism which can be invoked using the android library.

1.3 WiRMa project

A section of this thesis is due to the work done in the WiRMa project (Winter Road Management (project ID 20201092)). We were included in the work for one of the work packages for this project. In short, this package consisted of assessing hybrid measurement techniques and what kind of sensor technology could be useful for winter road surface condition classification.

This project aims to achieve an efficient level of readiness for very changeable and rough weather conditions in the arctic traffic and road patterns. Through the WiRMa project, partners from Norway, Sweden and Finland will do research on and demonstrate a profitable, industrial and network based system for decision support for winter road maintenance. This will be achieved by exploiting smart equipment, sensor technology, real time analysis and using predictions and simulations.

The research group from UiT was responsible for work package number 4 - Winter road condition information. Described by:

- Functional condition indicator and serviceability of winter roads
- Vibration measurements and indirect methods for winter road condition monitoring
- Optical measurements methods of winter roads
- Optical reflectance based sensor technology for road surface measurement
- Optical ellipsiometric based sensor technology for road surface measurement

- Hybrid measurement method techniques for winter roads

During the startup we carried out a comprehensive initial study [69], where we wanted to explore the use of commercial and experimental technology for surface measurements. This includes a list of commercial sensors such as RCM411 and MARWIS, whereas on the experimental front we tried to employ a radar kit, Walabot, and also see if it is possible to combine other already existing technology in a car. Every car has on-board diagnostics (OBD) interface, where one can use a special gadget to read the data parameters straight from the car. The data parameters available can vary from car to car. Since we in most cases already utilize a smartphone while driving, it can be used for gathering data as well, such as video, sound and other sensor information. There was also a more comprehensive paper [7], which has a more in-depth analysis of the data and sensors used in the WiRMa project, and a study [63] on the pull force for heavy haulers when sanding the road surface to increase friction.

1.4 Scientific research and innovation

In [24], Fagerberg, Mowery and Nelson state that innovations are as old as mankind, and we, as people are always looking for ways to improve. If we define innovation in a more modern term, we see innovation as a new idea and a creative process. Innovation as such exists in all fields, ranging from behavioral science, geography, artificial intelligence (AI), as well as geometry and technology. If we look at innovation at a basic level and focus on geometry and sensor technology, there are several key aspects of innovation worth taking a look at. In this section I discuss some key developments for geometry and sensor technology. As people are naturally curious, we get new and exciting products, methods, ideas and creative thinking, and we always try to find solutions to problems.

Geometry

Starting with innovation in geometry we first need to differentiate between geometry and geometric modeling. Geometry is a branch of mathematics concerning shapes, sizes, positions and space properties, whilst geometric modeling studies methods and algorithms for a mathematical description of such shapes. Geometric modeling is central in Computer Aided Design and Manufacturing (CAD/CAM) and illustrating computer aided geometric design by means of interesting applications. We find several signs of innovation in geometry [28]; if we look at the late 1700 and early 1800, Gaspard Monge introduced and gave lectures on descriptive geometry [2], which increased the knowledge about

design processes and led to an enormous increase in design possibilities for architecture and industrial design [46]. Examples of such processes are origami, folding studies and curved surfaces.

The use of geometry is not limited to a particular field such as design and industrial purposes, we find geometry is one of the important factors in the development and behavior of robotics [45] and scientific visualization.

It is not just in architecture and design where geometry is important. Even in an artistic setting such as music [77] we find connections to geometry. The innovative process here is the way we use geometry and symmetry to explain "Why is music good, or what makes people like certain types of music?".

We can look at a more intuitive application of geometry, such as in simulators, and connect this field to innovation. Simulators themselves do not undergo a specific innovative process, but rather the type of simulators and realism they bring to the user. Of course there are some specific things that a user would notice immediately, such as the look and feel of a simulator. This process is the result of innovation, whether it is technological processing power(computers) or within the field of geometry, analyzing and representing reality. There are hundreds and thousands of different simulators available to those who want to try out and practice different fields, for example, fishing, farming, flying, sailing, diving, shooting, etc.

Interactive and editable geometry has been the center of attention for several years now, and several existing tools for analysis still use geometry in the form of meshes and mesh generation. This subject has been thoroughly researched and is still an ongoing field, whereas new techniques such as interactive geometry and spline techniques are emerging. These methods also constitutes the base for further research into IGA and other tools for analysis and editable interactive geometry. If we use ERBS (1.1) as an example, this has previously been discussed to be one very useful spline technique which increases the design capabilities of such tools. Another advantage of such improvements and development of different techniques is the implementation on a computer. With this development we can emphasize other, more important purposes and instead utilize the processing power of modern computers for computations such as in simulations and complex algorithms.

If we take a closer look at the development of car design and design processes, we see a large leap in design methods and manufacturing. This is both due to innovation and the way we look at design, as well as in geometry, where we are going from a manual process in the late 1950's to analog computers. The early computer numerical control machines (CNC machines) could employ the use of lines, circles, parabolas and other geometrical functions, but there was still no

signs of freeform curves, much less surfaces. What we then see in 1959, when Citroën hired Paul de Faget de Casteljau, is the introduction of De Casteljau's algorithm [25], which recursively evaluates an existing mathematical expression, the Bernstein polynomials [47].

Sensor and sensor technology

If we look at the development of sensors and sensor technology, we need to start at the beginning, with the concept of connected devices. This concept dates back to 1832 when the electromagnetic telegraph was initially discussed [71], which communicated with each other through the transfer of electrical signals. The era of sensors did not start until around 1860 and there is still a debate about who started the development of the first sensor technology, but this is mostly a question regarding the type of sensor. For instance, Wilhelm von Siemens and Warren S. Johnson both invented temperature sensors. Warren invented the electric thermostat, while Wilhelm was said to use the temperature sensitivity of electrical resistance in different materials [14]. The definition of a sensor is a device or measuring unit that can respond to different physical phenomena such as temperature, moisture or pressure to name a few of the vast amount.

The best way to differentiate the technological growth and advancement from innovation in the field of sensors, is to look at some separate usage areas instead of sensors in general. The technological development is of course one of the major reasons for sensor usage, but usually this development is based on what kind of sensors we need and their purpose. An example of such development is the advancement for structural health monitoring [29].

There are so many fields and applications for sensors, even today we still see a vast amount of new sensors and areas being developed and researched. One of the really interesting aspects is the use of wearable sensors for market learning and networking, where we can shape the opportunities out there through innovation CITE. This is not only with regards to market purposes, but also for tracking and monitoring as a result of preemptive behavior in health and/or other perspectives [31].

As we described in a previous section about CAD/CAM, there is also research focused on Computer Aided Design Software Innovation that uses Virtual Reality(VR) and VR technology [26]. This is researched based on the VR technology's sensory expression system and virtual control system to create a realistic feeling with increased man-machine interactive feedback, which ultimately tries to improve the user's immersive experience and artistic freedom.

The last thing worth mentioning here is the emerging term, Smart City, a global innovation hub for sensor technology. This "hub" has grasped the entire field of sensor technology and surveillance equipment and taken it to another level. If we only look at a little section of this broad field, we can see that many of the areas described above are a part of this. A little peek into the world of smart cities show us, for example, that there is a huge amount of wasted energy in buildings and working environments, which with the help of sensors and technology, could be significantly decreased and help the efficiency, distribution and cost [44].

2

Motivation

Serious gaming and virtual reality is one of the fastest growing industries in the world, and by utilizing the expertise at NUC, we have the potential to be at the leading edge of this field. The PhD project is defined as research within interactive virtual modeling and editing capabilities, and can be connected through applications such as product development, virtual design, games, learning systems, simulators, development of virtual worlds, and more.

In late 2015 I applied for a U.S-Norway Fulbright grant, which I was lucky enough to receive, and in July 2016 I started a ten month exchange program in Austin, Texas. I was under the supervision of Prof. Thomas J.R. Hughes and the research group led by him. The research group was focused towards advanced mechanics, which was very educational, and during this period I was able to attend several courses on both basic and advanced mechanics at master and doctorate level. During my stay the research group organized and arranged several workshops and presenters from different universities came to lecture. I made several connections for future work and cooperation between our common research groups as well as significantly improved knowledge in mechanics and analysis.

Based on the introduction I would like to follow up on my reasons to divide the thesis into two parts, as well as the reason for both topics. We know from experience and years of research that numerical simulations and technology have become key aspects in both science and industry. During my work with geometry and sensors, both subjects have driven me to investigate areas where

we have trouble finding solutions to key problems, such as irregular geometry in the setting of applied, interactive and simulation purposes. As for the second part, in early 2018, we were asked to be a part of a project called WiRMa (Winter Road Management), more specifically, one of the work packages which aimed to estimate/focus on road conditions using sensor technology.

Next I wanted to take a closer look at some other areas which use sensor technology. If we then take a look at sensors in general, we can see that many areas in science use sensor technology, and if we look at just a simple problem, such as positioning indoors without using signals and Global Positioning System (GPS), there is almost no solution, or at least the error of the solution is increasing so fast it does not apply to long periods of time.

What connects both fields are the fundamental building blocks for each of the two seemingly separate areas, namely data, analysis and mathematical methods. That is, why and how they are utilized to evaluate and present data. Methods such as interpolation, expansion series, least squares methods, regression and standard deviation are the foundation which is employed before the data is suitable for evaluation and visualization. The main contribution is methods and constructions which employ techniques on data for visualization and analysis purposes where partial information is not adequate.

2.1 Research questions

The main goal of this thesis has been to explore techniques and methods for data collection, processing and analysis and visualization. Sensors are and will be even more important for obtaining data, interpretation and processing are basically closely linked to the sensors and as such are a study in seeing the possibilities and limitations. When proceeding in processing, analysis and use, numerical calculations, geometry and algorithms for building curves / surfaces / volume are important. Non-regular geometry will be especially important.

However, the topic is so large that the thesis bears some resemblance to "random samples" in the subject. This has led to a division of the theme, ie i) sensors and basic interpretation and ii) geometry and processing.

At the same time, the underlying methods and data that form the foundation of the two parts are very similar.

The four specific objectives that are explored in the interactive and editable geometry section are a special construction for irregular geometry on analysis

suitable geometry, representation and analysis of geometry for a practical setting on railway tracks, a geometrical approach to the simple pendulum motion in 3D and applications where data is analyzed and visualized using blending splines.

The three specific objectives for sensors and sensor technology are a study on how the friction increases during targeted sanding and its impact on heavy hauler pull force, a visualization of sub-ground metal objects and also a preliminary study on winter road assessment with a possible hybrid setup consisting of several sensor technologies.

Despite having two separate parts, there are common research questions:

Overarching questions

1. Can we use geometrical approaches for visualizing data and facilitate different application areas, such as sensor technology?

2. Are there similar methods for both areas, geometry and sensor technology?

Based on the two quite different topics, it has been natural to divide the research questions further into two parts.

Interactive and editable geometry

1. Does blending splines constitute a basis for analysis suitable geometry?

2. Is it feasible to include both analysis suitable and interactive geometry in the same applications?

3. Can alternative representations provide new insight into common complex problems?

Sensors and sensor technology

1. How can we visualize sensor data in such a way that the message is clear, concise and informative for an end user?

2. Do solutions based on sensor technology offer enough or is it advantageous to employ a hybrid setup when analyzing certain conditions?

3. Can we utilize sensor data for different scenarios using similar visualization techniques?

Part II

Thesis overview and methodology

The author of this thesis has decided to divide the completed work into two separate research areas. The first part is general mathematical/geometric modeling and analysis of differential geometry, where experimental programming and implementation of algorithms are used to test both constructions and analysis. The second part is in general more practical, using sensors and sensor technology, and how we can use these sensors to create better tools for understanding certain conditions and give a more user friendly interface. Many of these sensors are able to output a lot of data, and they can be used for analysis purposes and in many cases, used for prediction, recognition, classification, detection and much more. The thesis is divided into four parts. Part I is an introduction to the history of blending and blending techniques, sensor technology and development and project work during this work. It also includes the motivation behind the present work and the main research questions. Part II includes details of the main focus areas and also an overview of the thesis with specific contributions, both individual and cooperative work. Part III concludes the dissertation and has notes for future work. Chapters 1-6 constitute Part I, II and III. Part IV is an Appendix, presenting the research papers covering interactive and editable geometry, and sensors and sensor technology. Each of the individual papers are included as separate appendices. Appendices A, B, C, E, F and G are paper reprints of either published or sent for review research articles. Appendix D is unpublished relevant research which contributes toward the main goals of this thesis and consists of conference presentations and proceedings.

Method and approach

Since the thesis consists of two seemingly separate areas, the methods and approaches vary depending on the scenario and particular case we have explored. Each of the research papers included in this thesis has a problem formulation, an introduction which is trying to connect the research with similar research fields, a method step imposing a solution for the problem, results showing how the solution worked and concluding remarks describing the outcome of the study. The overall approach for interactive and editable geometry has been to explore methods and different representations using data sets, whether they are gathered from sensors or purely synthetic data. The sensors and sensor technology is approached a little differently, where the data gathered is analyzed with respect to quality and used further for visualization purposes. Both fields are connected through data and analysis, but represented differently. Even though the methods and approaches are quite different for the two areas, the foundation is data collection and analysis, which is seen in the research presented in this thesis.

3

Research objectives

The purpose of this work has been to explore the usage of blending splines in an applied setting in interactive geometry with a main focus towards surfaces with discontinuities, i.e. holes. However, with the inclusion of project work, the author has been delving into the world of things, with sensors and sensor technology in terms of arctic conditions. The main goal of the first part has been to employ methods for geometry suitable for editing and interactive modeling. Secondly, the goal for sensor technology has been to explore possible new techniques for measurements and analyzing, as well as new technologies. This include a combination of technologies to create hybrid measurement tools and customization of different devices.

In the two following sections for interactive and editable geometry and sensors and sensor technology we will give a brief overview of the various overarching research objectives connected to their respective fields.

Interactive and editable geometry

1. **Geometric modeling** has been a rapidly developing collection of mathematical methods for describing the shape of an object in computer graphics [11] and computer aided design and manufacturing. Computer Aided Geometric Design [3] applies mathematics, supported by interpolation and approximation theory to design geometric models for object shapes. Representing geometry

with discontinuities, such as holes, and still maintaining a complete domain is explored using Coons patches and Boolean Sum surfaces in Appendix A and D.

2. **Interactive geometry** is to create and utilize the underlying constructions in geometric modeling to create editable and interactive models when working in CAD environments. One such environment is Rhinoceros 3D [74]. CAD and CAGD tools rely on several operations to create splines suitable for modeling. These tools are, but not limited to, evaluation, refinement and knot insertion. Appendix A presents a construction for modeling arbitrary holes using double knots creating G^0 surfaces. A study on railway track geometry with respect to curvature, modeling and analysis is presented in Appendix B. In Appendix D we present a collection of application areas such as modeling, analysis and terrain approximation using a blending type spline construction.

3. **Isogeometric analysis** is trying to bridge the gap between CAD/CAGD and Finite Element Analysis(FEA) [13] to create geometry suitable for analysis with respect to, among others, computational time and post processing. The main idea with IGA is to use spline spaces introduced for the geometric representations, instead of the regular FEM function spaces. IGA was introduced as a new method for analyzing problems governed by partial differential equations, such as solids and fluids [36]. Constructions in Appendices A, B and D are among an interactive geometry modeling and parametric design platform which can be suitable for IGA. One of the key features of using IGA is refinement of the basis without changing the geometry or the parameterization for analysis purposes without communication between the model and CAD description.

4. **Simulation environments** represent a key role in analysis and modeling. Problems vary from mechanics [75] and elasticity to networks and multi-agent simulation environments [51]. Mathematical modeling, mechanics, elasticity and simulations are common for Appendices A-D. Each of the contributions in Appendices A-D are either solved or implemented using in-house software and simulation tools.

5. **Mechanics and ballistics** are a very central when discussing limitations and properties of structures. A specific field dedicated to surfaces undergoing stress opens up a collection of different problems. Being able to model surfaces and volumes are key for composite structures where strength and structural analysis is required. Such constructions are explored in Appendices A and D.

Sensors and sensor technology

6. **Prototype development** is often used to create incomplete or partial applications when testing new methods and is not limited to phone applications, but for simulation software as well. Appendices A-G are examples where prototype development has been used to create applications for different purposes, i.e. geometric modeling, constructions and smart phone applications.

7. **Phone sensors** are a great source for data and are often required when investigating problems. Understanding and working with sensors has been key throughout the second part of this thesis and in Appendices E-G such data sources have been used extensively with respect to analysis and assessment purposes. Both Appendices C and F have results which identify the reverse engineering methods using phone sensors with specific physics problems. Among other things, free fall, pendulums and a selection of motion equations are evaluated using smartphone sensors such as acceleration and gyroscope [85, 86, 40, 10].

8. **Hybrid measurement technologies** with recent advances, such as usage of sensor nodes, both static and mobile, and performance measurements on such node networks are becoming attractive, where trade-offs between cost, energy consumption and performance are evaluated [91]. In Appendix G we have conducted a study on hybrid sensor technology for winter road assessment. In combination with **Phone sensors** and **Prototype development**, a hybrid system with a mobile phone and a metal detector was created and an analysis is given in Appendix F.

9. **Road conditions** play a crucial role in dealing with risk assessment and safety precautions. In Part IV we performed an initial assessment of potential friction force increase using a special sanding instrument attached to heavy haulers. Dealing with slippery surface conditions, heavy haulers are struggling to create enough friction and the specialized equipment releases sand/gravel from a dispenser in front of the wheel. There are many potential methods to evaluate road conditions using both mobile and stationary equipment. To increase road safety, especially where conditions can lead to difficult or impossible situations, we rely on solutions based on simpler and cheaper technology. In Part IV we present a study on hybrid sensor technology for winter road assessment using both commercial and experimental technologies.

4

List of Papers

This section is providing the paper titles and references to their respective publisher. The thesis consists of six papers and one section for conference proceedings/presentations. The papers included in this thesis as appendices are reprints of the original published articles in order to ensure a uniform format. The reprints are identical to the original articles, nothing is added, subtracted or changed.

Appendix A. *A. Pedersen, J. Bratlie, R. Dalmo. Spline representation of connected surfaces with custom-shaped holes. In Large Scale Scientific Computing, Springer International Publishing 2015. Pages 394-400 [68]*

Appendix B. *A. Pedersen, T.F. Brustad, B. Bang, R. Dalmo. Alternative representation of railway track geometry. In proceedings. International Heav Haul Association 2019. [64]*

Appendix C. *A. Pedersen. Geometrical approach to a simple pendulum motion in 3D for large initial angles. For review in The Physics Teacher Journal. 2020 [59]*

Appendix D. *A. Pedersen. Application areas and conference contributions. (Multiphysics - Sofia, Bulgaria 2014), (Mathematical Methods for Curves and Surfaces (MMCS) - Tønsberg, Norway 2016) and (Curves and Surfaces (C&S) Archachon, France 2018). Multiphysics [62]*, MMCS [58], CS [61]

Appendix E. *A. Pedersen, T.F. Brustad, B. Bang. Targeted sanding and its impact on heavy hauler pull force and surface friction. For review in Journal of Cold Region Engineering. [63]*

Appendix F. *A. Pedersen. Altering perceptions, visualizing sub-ground metal objects. Published in Emerging Science Journal 2020. Pages 205-213. Volume 4. [65]*

Appendix G. *A. Pedersen, T.F. Brustad. A Study on Hybrid Sensor Technology in Winter Road Assessment. In Safety Journal 2020. Volume 6 Nr 1. Article Nr 17. [69]*

Papers describing the research project and a brief history of blending splines are incorporated into the introduction of this thesis and omitted from the contribution list, but can be found in:

1. *A. Pedersen. Interactive modelling and simulation using blending techniques. Published in Norsk Informatikk Konferanse - Open Journal Systems 2015. [60]*

2. *A. Pedersen, B. Bang. Blending type spline constructions: A brief overview. In AIP Conference Proceedings 2015. Volume 1690. [67]*

Paper the author has co-authored or given as a talk at a conference, and is also omitted from the contribution list:

1. *T.F. Brustad, A. Pedersen, B. Bang. A field study of sensors for winter road assessment. Published in Transportation Research Interdisciplinary Perspectives 2020. Volume 7. [7]*

4.1 Paper contributions

Below is a short summary of contributions for the individual works. The individual research papers are included as reprints in Part IV, Appendix. The summaries are connected to the research questions for each individual contribution, which are discussed further in the conclusion part of this thesis.

4.1.1 Interactive and editable geometry

Appendix A: Spline representation of connected surfaces with custom-shaped holes

This paper explores a blending type spline construction where the geometry has discontinuities, but still analysis suitable with the requirement that the surface can be evaluated at every point. The two main findings are:

1. A new construction creating geometry with holes using local refinement tensor product surfaces. The geometry is discontinuous, i.e. G^0, while being mathematically smooth i.e. C^k and covering the complete parametric domain.

2. A concrete example is presented: a surface with a hole in the center is constructed using compact C^k-smooth tensor product surfaces with a Boolean Sum surface technique i.e. Coons Patches. The construction is based on inner and outer boundary curves.

Appendix B: Alternative representation of railway track geometry
In this paper we explored a different representation of railway track geometry where a B-spline curve is compared to a segmented railway curve consisting of straight, clothoid and circular segments. In this study we used a part of the Ofotbanen railway and compared the B-spline curve with the segment curve with respect to curvature.

3. The B-spline construction using both uniform and non-uniform parametric domain matches the curvature of the segment curve completely for the clothoid and closely to the line and arc.

4. By employing a B-Spline representation of degree 3 (an energy minimizing spline) the curvature for the entire railway track is consistent with the segmented curve.

5. The curvature of the segmented curve was discontinuous in the joints, where the B-Spline curve had a continuity of a higher degree. This, in theory, should give a better transition, even though there were some oscillations on the curvature plots.

6. Increasing the degree of the B-Spline is minimizing the oscillations of the curvature and also increasing the smoothness of the curve.

Appendix C: Exploring simple methods for the nonlinear 3D pendulum
In this paper we wanted to explore other methods for representing the pendulum motion in 3D. The approach is based on geometrical considerations which simplify calculations and reduce a complex problem into a simpler and easier to solve problem using geometry. There is however a need for correction steps since the solution is an approximation using linear time steps.

7. The motion for a simple pendulum with large initial amplitudes was evaluated using Taylor expansion of two well known equations of motion leading to a geometric predictor corrector method.

8. The proposed geometrical approach matches the solution from a classical numerical method solving the equation of motion in its nonlinear form.

9. The period comparison of the solution using large initial angles of 90° and 135° is exactly matching the solution using Runge Kutta 4.

Appendix D: Blending spline applications and contributions
These contributions are either extended further work based on previous papers or applications where modeling of geometry using sensor data was explored. The application areas were separated into three sections: Surface construction with arbitrary inner and outer boundaries, a heat diffusion problem and terrain and level curves.

10. The construction presented in Appendix A is extended with both inner and outer boundaries with respect to modeling geometrical discontinuities such as holes from penetration and perforation. The extended construction is preventing the zero derivatives were the previous solution had vanishing points in the joints between the inner and outer boundaries.

11. A preliminary analysis of a heat diffusion problem with respect to the constructions from Appendix A and the extended version in Appendix D.1. An concrete example is provided showing that the construction is valid for the heat diffusion problem and the surface can be evaluated at every point.

12. Construction of terrain geometry with respect to modeling using terrain information such as level curves:

    (a) Two concrete examples are provided showing the blending of geometry using two approaches.

    (b) Specific intersection algorithms were developed to create intersection curves between a plane and the blending type spline construction. Concrete examples are provided showing the exact intersection curve for the intersection algorithms.

4.1.2 Sensors and sensor technology

Appendix E: Targeted sanding and its impact on heavy hauler pull force and surface friction
In this paper we performed a case study on heavy haulers pull force and how the friction is affected before and after using targeted sanding. The field experiment was performed on a closed track, and using a special weight attached to the truck and trailer to measure the pull force exceeded by the truck before and after sanding. The friction was measured using a RCM411 sensor before and after sanding.

13. A study of the effects of sanding on a low friction surface with sensor measurements have been provided and shows an increase in pull force.

14. Custom measuring equipment to estimate the increase in pull force before and after sanding was employed between the truck and trailer resulting in five measurements.

15. The average value of surface friction was measured to 0.24 using a (Road Condition Monitor 411) RCM411 sensor with several runs to insure a more reliable result and base for further analysis.

16. Based on the proposed model an increase in friction was estimated (from 0.24 to 0.48 before and after sanding), and hence, the pull force after sanding increased.

Appendix F: Altering perceptions, visualizing sub-ground metal objects
In this paper we explored the possibility of enhancing the visualization of a metal detector using a smart phone mounted to the metal detector frame using a custom Celestron Smartphone Adapter. The goal was to achieve a better visualization where partial information is not adequate. By processing the data recorded, and employing evaluation and visualization techniques, a prototype application was developed to present the solution.

17. A custom mount attaching the smart phone to the metal detector was used to combine the two systems providing better analysis tools.

18. A prototype application with initial analysis and user interface for assessing the sound from the metal detector and movement pattern was developed successfully during the experiments and testing.

19. A specific algorithm was created to convert the preliminary sound signal to a frequency domain representation.

20. A specific algorithm was created for coloring the movement pattern from the motion recorded on the smart phone using the data from the Fourier analysis.

21. A calibration step and error analysis are conducted using standard deviation and a moving average of the motion trajectory.

22. The concrete examples are smaller field tests performed to illustrate the algorithms and visualization technique.

Appendix G: A Study on Hybrid Sensor Technology for Winter Road Assessment
This paper is a preliminary study on various sensors with a special interest towards creating possible hybrid sensor technology in winter road assessment. The selection of different sensors that we tested was 2 commercial sensors; Road Condition Monitor (RCM411) and Mobile Advanced Road Weather Information Sensor (MARWIS) and 5 experimental technologies or techniques; Walabot, Video, Sound, OBD-II and Smartphone. The data was collected by performing three test routes where we analyzed different properties on each run.

23. An evaluation criteria table to establish common grounds between the different technologies is created to find connections between technologies which could lead to potentially decreased risk and, hence, increase safety for all road users.

24. Preliminary experiments with respect to possible road surface characterization are presented in a hybrid technology setting and the sensor variables: friction, surface temperature, and road state is consistent when driving the same test route twice.

25. A data collection method is established and visual analysis of preliminary data is presented showing promising results towards hybrid technology that can complement each other in a beneficial way.

26. Lower cost alternatives such as OBD-II, video, sound and smart-phone data can provide a new dimension to winter road assessment.

Part III

Conclusions and future work

5

Concluding remarks

In this thesis, two main themes have been explored: Interactive editable geometry, and sensor technology as well as the use of sensors. The two seemingly separate topics may seem somewhat incoherent, but based on the common research questions and the underlying methods for each of them, there are both similarities and they are interrelated. The most important findings show that both fields use data and evaluation methods that are the same, and both topics can be easily related to geometry in all contexts. The way we analyze and process information is not limited to any of the topics, and data can be represented using geometry such as curves, surfaces, volume and objects with even more parameters. Data can also be retrieved from geometry by evaluation/calculations, which the sensors actually perform. The main work has then been to process the information and present the data in different ways depending on use and relevant areas.

Based on the research questions for interactive and editable geometry, the results show that: Blending splines constitute a new spline technique with very interesting properties for analysis suitable geometry; the applications and studies provided show that there are advantages and disadvantages where interactive simulations and analysis is not suitable nor sensible; alternative representations definitely provide new insight into problems which are too complex and perhaps not solvable by ordinary methods.

Based on the research questions for sensors and sensor technology the results show that: Depending on the scenario, different visualization techniques are

necessary to insure informative and concise presentations; exploration of hybrid setups show several advantages depending on which conditions and the type of assessment that is to be made, especially with respect to areas where there is a lot of information and uncertainties; the studies provided in this thesis include similar visualization techniques using a rich set of data.

With that said, the main result from the two parts conducted during the period of the research project can be summarized as follows:

1. New constructions of editable and interactive geometry with respect to modeling tools and simulation frameworks is presented. In Appendices A and D we presented a method for constructing irregular geometry by knot multiplicity and interactive editing of local geometry. This construction is able to model exact inner and outer boundaries by Hermite interpolation of the boundary curves. In Appendix B we conducted analysis of the segment curves constituting a railway track, and the possibility to estimate sections which were prone to wear. The analysis was performed using a third degree B-Spline as a basis for minimizing energy. A least squares method was used to create the control points for the B-Spline construction and a mean squared error MSE estimate between the original segment curve and the energy minimizing spline was presented. In Appendix C we presented an approach to the simple pendulum in 3D for large initial angles using a geometrical approach where the pendulum trajectory is approximated using a Taylor expansion series combined with an error correction step. The method proposed is a form of predictor corrector in the sense that we where calculating the next step using information from the previous steps and then employ a correction step.

2. A set of engineering application areas such as railways, modeling physical problems and terrain generation have been investigated. In Appendix B a framework for analyzing curvature and error estimates was proposed and applied to an existing railway track, Ofotbanen. In Appendix D, Section 2, a preliminary analysis using the construction from Appendix A was conducted using a heat diffusion problem. The proposed method presented initial results visualizing the heat diffusion using two different parameterizations on the geometry. In Appendix D, Section 3 we presented terrain generation methods and an intersection algorithm. The two proposed constructions both utilized a blending type spline construction, but differed in the approach of creating local geometry, where Bezier and horizontal planes where utilized. The blending construction provides a new array of properties which are suitable when editing the terrain as well as creating interactive modeling tools. A preliminary error estimate was conducted using a difference plot between the new constructions and the triangulated surface. Intersection curves were constructed using

an algorithm which calculates the intersection between a slicing-plane and the surfaces from the blending constructions.

3. Sensor technology provides in many cases a new layer of information for further analysis. They are often cheap, small devices with a single purpose of recording information about the environment surrounding the device. In Appendices E-G we provide results using a vast range of different sensor technologies, such as sensors for temperature, humidity, ice and water thickness. Combining such information with proprietary devices provides the ability to alter perceptions and create a new layer to existing solutions. Appendices E and G both present analysis of existing technologies with possible new solutions. In Appendix F a visualization of sub-ground metal objects using smart phone sensors and a custom mount to a metal detector is presented.

4. Winter road assessment and estimating road conditions are necessary tools for road maintenance and increasing safety in regions with critical conditions. In Appendix E we presented preliminary results of targeted sanding and its impact on heavy hauler pull force and surface friction. The initial results show an increase in pull force up to 50%, which estimated provides a significant increase in surface friction. In Appendix G we presented initial results on hybrid sensor technology where both commercial and experimental technologies where tested. A summary of the initial results where presented in a table to be used for future comparison of new technologies.

6

Future work and comments

The two main topics have explored various applications and techniques for both analysis and visualization, but there are still areas which need a more thorough study. The main focus for future work is related to answering the uncertainties with respect to the research questions and objectives such as:

1. An interesting topic that requires further investigation is the use of blending splines where the local geometry can inherit certain properties, i.e. material and geometrical properties such as stiffness, hardness, conductivity, etc. We can then use this geometry with properties and apply constraints, such as a Partial Differential Equation (PDE) on each separate local geometry (curve, surface,. . .). When utilizing the interpolation properties of the blending spline, we can model boundary conditions as well as more complex geometries, while still being able to generate a solution and refinement for the PDE. Using the blending spline basis as the basis function for a PDE (the same function space) the representation of both the PDE solver and geometry is exact.

2. Interaction between the PDE solution and geometry can be handled separately, with typical modeling problems such as Fluid-Structure-Interaction (FSI). Other cases are expected to belong to multiphysics. As mentioned in Section 1.1, **Properties 4 & 5**, we were describing the possibility of having irregular geometry and the connection to multiphysics could include discontinuities such as intersection between objects(typically two different phases, fluids and solids).

3. The construction presented in Appendices A and D should be investigated further with respect to modeling arbitrary holes in application areas such as, but not limited to, fracturing and basic ballistic failure modes (plugging, piercing and petaling). The current results show promising modeling properties which can be utilized in the context of ballistic failure modes and a preliminary visual similarities between plugging was presented.

4. The analysis and method proposed in Appendix B should include a study on targeted curvature with a possible change of transition curves. By utilizing a different transition curve, many areas which are prone to wear could be eliminated.

5. Regarding Appendices E, F and G, the sensor technology used and information recorded could be visualized in different settings such as Virtual- and Augmented- Reality solutions. The information could be interpreted differently depending on the presentation platform, hence, all future solutions should investigate new visualization techniques and technologies.

6. Appendices E and G provide results on hybrid solutions and several of these fields should be investigated further with a special focus on simpler and cheaper solutions such as smart-phones, OBD-II and camera technology. The combination of such cheap solutions with artificial intelligence (AI) could promote new and enhanced solutions.

7. An extension to the simple pendulum solution proposed in Appendix C could include following a parametric curve embedded in any surface or volume and not restricted to a sphere surface. By utilizing the proposed method, a solution could include rolling spheres on a terrain surface.

8. The methods and constructions proposed in Appendices A and D provide easier structure and constructions with respect to analysis and intersections, and a thorough analysis should be performed. The initial results form a basis for further research which should be conducted in future works.

Bibliography

[1] J. Autioniemi et al. *Intelligent Road*. Tech. rep. Lapland university of Applied Sciences, Luleå University of Technology, Finnish Meteorological institute, 2015 (cit. on p. 26).

[2] Walter William Rouse Ball. "A Short Account of the History of Mathematics." In: 4th ed. DOVER PUBLICATIONS, INC. NEW YORK, 1960, p. 466 (cit. on p. 29).

[3] Wolfgang Boehm, Gerald Farin, and Jürgen Kahmann. "A survey of curve and surface methods in CAGD." In: *Computer Aided Geometric Design* 1.1 (1984), pp. 1–60 (cit. on p. 41).

[4] M. Borden, T. Hughes, and C. Landis. "Isogeometric Phase-field Modeling of Brittle and Ductile Fracture." In: *COMPLAS 2015* (2015). Videos of Plenary Lectures presented at the XIII International Conference on Computational Plasticity (COMPLAS 2015). URL: https://www.scipedia.com/public/Contents_2016c (cit. on p. 23).

[5] Jostein Bratlie. "Local refinement of GERBS surfaces with applications to interactive geometric modeling." In: *39th International conference applications of mathematics in engineering and economics AMEE13*. Ed. by Vesela Pasheva and George Venkov. Vol. 1570. AIP Conference Proceedings. AIP Publishing, 2013, pp. 18–25. DOI: 10.1063/1.4854738 (cit. on pp. 16, 17).

[6] Jostein Bratlie, Rune Dalmo, and Børre Bang. "Evaluation of smooth spline blending surfaces using GPU." In: *Curves and surfaces. 8th International Conference*. Ed. by Jean-Daniel Boissonnat et al. Vol. 9213. Lecture Notes in Computer Science. Springer, 2015, pp. 60–69. DOI: 10.1007/978-3-319-22804-4 (cit. on pp. 16–18).

[7] Tanita Brustad, Aleksander Pedersen, and Børre Bang. "A field study of sensors for winter road assessment." In: *Transportation Research Interdisciplinary Perspectives* 7 (Sept. 2020), p. 100206. DOI: 10.1016/j.trip.2020.100206 (cit. on pp. 24, 29, 46).

[8] Bruce Candy. *Metal detector: Basics and theory*. English. Minelab. Forthcoming (cit. on p. 27).

[9] Donald E. Carlucci and Sidney S. Jacobson. *Ballistics: Theory and Design of Guns and Ammunition*. 2nd. CRC Press, 2014. ISBN: 978-1-4665-6437-4 (cit. on p. 21).

[10] Juan Castro Palacio et al. "Using a smartphone acceleration sensor to study uniform and uniformly accelerated circular motions." In: *Revista Brasileira de Ensino de Física* 36 (June 2014), pp. 1–5. DOI: 10.1590/S1806-11172014000200015 (cit. on p. 43).

[11] Elaine Cohen, Tom Lyche, and Richard Riesenfeld. "Discrete B-Splines and Subdivision Techniques in Computer-Aided Geometric Design and Computer Graphics." In: *Computer Graphics and Image Processing* 14.2 (1980), pp. 87–111 (cit. on p. 41).

[12] Steven A. Coons. *Surfaces for Computer-Aided Design of Space Forms*. 545 Technology Square, Cambridge, Massachusetts 02139, 1967 (cit. on p. 11).

[13] J. A. Cottrell, T. J. R. Hughes, and Y. Bazilevs. *Isogeometric Analysis: Toward Integration of CAD and FEA*. 1st. Wiley Publishing, 2009. ISBN: 0470748737 (cit. on pp. 9, 42).

[14] National Research Council. *Expanding the Vision of Sensor Materials*. Washington, DC: The National Academies Press, 1995. ISBN: 978-0-309-05175-0. DOI: 10.17226/4782. URL: https://www.nap.edu/catalog/4782/expanding-the-vision-of-sensor-materials (cit. on pp. 23, 31).

[15] L. T. Dechevsky, B. Bang, and A. Lakså. "Generalized Expo-Rational B-Splines." In: *International Journal of Pure and Applied Mathematics* 57.6 (2009), pp. 833–872 (cit. on p. 11).

[16] L. T. Dechevsky, J. Gundersen, and N. Grip. "Wavelet compression, data fitting and approximation based on adaptive composition of Lorentz-type thresholding and Besov-type non-threshold shrinkage." In: *Large-Scale Scientific Computing 2009*. Ed. by Ivan Lirkov, Svetozar Margenov, and Jerzy Waśniewski. Vol. 5910. Lecture Notes in Computer Science. Springer, 2010, pp. 738–746 (cit. on p. 16).

[17] Lubomir T. Dechevsky, Arne Lakså, and Børre Bang. "Expo-Rational B-Splines." In: *International Journal of Pure and Applied Mathematics* 27.3 (2006), pp. 319–362 (cit. on p. 11).

[18] Lubomir T. Dechevsky and Peter Zanaty. "Beta-function B-spline smoothing on triangulations." In: 8650 (2013). Ed. by Atilla M. Baskurt and Robert Sitnik, pp. 9–23. DOI: 10.1117/12.2007681. URL: https://doi.org/10.1117/12.2007681 (cit. on p. 16).

[19] Lubomir T. Dechevsky and Peter Zanaty. "Smooth GERBS, orthogonal systems and energy minimization." In: *AIP Conference Proceedings* 1570.1 (2013), pp. 135–162 (cit. on pp. 13, 15).

[20] Jiansong Deng, Falai Chen, and Yuyu Feng. "Dimensions of spline spaces over T-meshes." In: *Journal of Computational and Applied Mathematics* 194.2 (Oct. 2006), pp. 267–283. ISSN: 0377-0427. DOI: 10.1016/j.cam.2005.07.009 (cit. on p. 10).

[21] Jiansong Deng et al. "Polynomial splines over hierarchical T-meshes." In: *Graphical Models* 70.4 (2008), pp. 76–86. ISSN: 1524-0703. DOI: http://dx.doi.org/10.1016/j.gmod.2008.03.001. URL: http:

//www.sciencedirect.com/science/article/pii/S1524070308000039 (cit. on p. 10).

[22] Tor Dokken, Tom Lyche, and Kjell Fredrik Pettersen. "Polynomial splines over locally refined box-partitions." In: *Computer Aided Geometric Design* 30.3 (2013), pp. 331–356. ISSN: 0167-8396. DOI: http://dx.doi.org/10.1016/j.cagd.2012.12.005. URL: http://www.sciencedirect.com/science/article/pii/S0167839613000113 (cit. on p. 10).

[23] J. Du, C. Gerdtman, and Maria Lindén. "Signal Processing Algorithms for Position Measurement with MEMS-Based Accelerometer." In: *16th Nordic-Baltic Conference on Biomedical Engineering*. Ed. by Henrik Mindedal and Mikael Persson. Cham: Springer International Publishing, 2015, pp. 36–39. ISBN: 978-3-319-12967-9 (cit. on p. 24).

[24] Jan Fagerberg, David C. Mowery, and Richard R. Nelson. "The Oxford handbook of innovation." In: Oxford University Press, 2006, p. 680. ISBN: 9780199286805 (cit. on p. 29).

[25] Paul de Faget de Casteljau. *Shape mathematics and CAD*. English language. Vol. 2. Mathematics and CAD. 120 Pentonville Road, London, N1 9JN: Kogan Page, 1986 (cit. on p. 31).

[26] Seth M. Feeman, Landon B. Wright, and John L. Salmon. "Exploration and evaluation of CAD modeling in virtual reality." In: *Computer-Aided Design and Applications* 15.6 (2018), pp. 892–904. DOI: 10.1080/16864360.2018.1462570 (cit. on p. 31).

[27] C. Giannelli, B. Jüttler, and H. Speleers. "THB–splines: The truncated basis for hierarchical splines." In: *Computer Aided Geometric Design* 29.7 (2012), pp. 485–498. DOI: 10.1016/j.cagd.2012.03.025 (cit. on p. 10).

[28] Georg Glaeser. "Innovations in Geometry." In: *Encyclopedia of Creativity, Invention, Innovation and Entrepreneurship*. Ed. by Elias G. Carayannis. New York, NY: Springer New York, 2013, pp. 1019–1025. ISBN: 978-1-4614-3858-8. DOI: 10.1007/978-1-4614-3858-8_462 (cit. on p. 29).

[29] Steven Glaser et al. "Sensor technology innovation for the advancement of structural health monitoring: A strategic program of US-China research for the next decade." In: *Smart Structures and Systems* 3 (Apr. 2007), pp. 221–244. DOI: 10.12989/sss.2007.3.2.221 (cit. on p. 31).

[30] Hector Gomez and Kristoffer G. van der Zee. "Computational Phase-Field Modeling." In: *Encyclopedia of Computational Mechanics Second Edition*. American Cancer Society, 2017, pp. 1–35. ISBN: 9781119176817. DOI: 10.1002/9781119176817.ecm2118 (cit. on p. 23).

[31] Tor-Morten Grønli et al. "Unveiling the Data Shadow: A Scalable Software Architecture for Public Health and Electronically Assessed Data (PHEAD)." In: *Norsk Informatik Konferanse (NIK) 2019* (2019) (cit. on p. 31).

[32] Birgitte Haavardsholm, Jostein Bratlie, and Rune Dalmo. "Surface deformation over flexible joints using spline blending techniques." In: *ICNPAA 2014 World Congress: 10th International conference on Mathe-*

matical Problems in Engineering, Aerospace and Sciences. Ed. by Seenith Sivasundaram. Vol. 1637. AIP Conference Proceedings. AIP Publishing, 2014, pp. 377–383. DOI: http://dx.doi.org/10.1063/1.4904602 (cit. on pp. 16, 17).

[33] Taisto Haavasoja, Juhani Nylander, and Pauli Nylander. "Experiences of Mobile Road Condition Monitoring." In: *Proceedings of SIRWEC 2012, Helsinki, Finland*. May 2012 (cit. on p. 26).

[34] Esraa El-hariri et al. "RoadMonitor: An Intelligent Road Surface Condition Monitoring System." In: vol. 323. Sept. 2014. DOI: 10.1007/978-3-319-11310-4_33 (cit. on p. 23).

[35] Erich Hartmann. "Parametric Gn blending of curves and surfaces Blending functions." In: *The Visual Computer - VC* 17 (Feb. 2001), pp. 1–13. DOI: 10.1007/PL00013398 (cit. on p. 15).

[36] T. J. R. Hughes, J. A. Cottrell, and Y. Bazilevs. "Isogeometric Analysis: CAD, Finite Elements, NURBS, Exact Geometry and Mesh Refinement." In: *Computer Methods in Applied Mechanics and Engineering* 194.39-41 (Oct. 2005), pp. 4135–4195. ISSN: 00457825. DOI: 10.1016/j.cma.2004.10.008 (cit. on p. 42).

[37] Kjetil André Johannessen, Trond Kvamsdal, and Tor Dokken. "Isogeometric analysis using LR B-splines." In: *Computer Methods in Applied Mechanics and Engineering* 269 (2014), pp. 471–514. ISSN: 0045-7825. DOI: https://doi.org/10.1016/j.cma.2013.09.014. URL: http://www.sciencedirect.com/science/article/pii/S0045782513002417 (cit. on p. 10).

[38] Manon Kok, Jeroen D. Hol, and Thomas B. Schön. "Using Inertial Sensors for Position and Orientation Estimation." In: *Foundations and Trends® in Signal Processing* 11.1-2 (2017), pp. 1–153. ISSN: 1932-8354. DOI: 10.1561/2000000094 (cit. on p. 24).

[39] Tatiana Kravetc. "Finite element method application of ERBS triangles." In: *Norsk Informatik Konferanse (NIK) 2019 - Open Journal Systems* (2019: Norsk Informatikkonferanse Oct. 2019) (cit. on p. 16).

[40] Jochen Kuhn and Patrik Vogt. "Analyzing spring pendulum phenomena with a smart-phone acceleration sensor." In: *The Physics Teacher* 50.8 (2012), pp. 504–505. DOI: 10.1119/1.4758162 (cit. on p. 43).

[41] A. Lakså. "Basic properties of Expo-Rational B-splines and practical use in Computer Aided Geometric Design." (Dr.philos.) PhD thesis. University of Oslo, 2007 (cit. on p. 12).

[42] A. Lakså, B. Bang, and L. T. Dechevsky. "Exploring Expo-Rational B-splines for Curves and Surfaces." In: *Mathematical methods for Curves and Surfaces*. Ed. by M. Dæhlen, K. Mørken, and L. L. Schumaker. Nashboro Press, 2005, pp. 253–262 (cit. on p. 11).

[43] Arne Lakså, Børre Bang, and Lubomir T. Dechevsky. "Exploring expo-rational B-splines for curves and surfaces." In: Preprint 2 (2004). ISSN 1504-4653, p. 11 (cit. on p. 15).

[44] Chris Lees. "Delivering and managing high productivity, low cost workplaces : A data driven perspective." In: *Corporate Real Estate Journal* 7.3 (2018), pp. 243–255. ISSN: 2043-9148. URL: https://www.ingentaconnect.com/content/hsp/crej/2018/00000007/00000003/art00006 (cit. on p. 32).

[45] "Advances in Robot Kinematics: Mechanisms and Motion." In: ed. by Jadran Lenarcic and Bernard Roth. 10th ed. Springer Netherlands, 2006, p. 500. ISBN: 978-1-4020-4941-5 (cit. on p. 30).

[46] Cornelie Leopold. "GEOMETRY CONCEPTS IN ARCHITECTURAL DESIGN." In: *12th International Conference on Geometry and Graphics* (Aug. 2006) (cit. on p. 30).

[47] G. G. Lorentz. *Bernstein Polynomials*. 2nd. Reprinted, 2012. Providence, Rhode Island: AMS Chelsea Publishing, 1986 (cit. on p. 31).

[48] Lufft. *MARWIS specifications*. (Accessed 2019-09-05). 2019 (cit. on p. 26).

[49] Lufft. *USER Manual MARWIS/StaRWIS*. (Accessed 2019-10-01). 2018 (cit. on p. 26).

[50] Lufft. *ViewMondo User's Manual*. (Accessed 2019-10-02). 2018 (cit. on p. 26).

[51] Sean Luke et al. "MASON: A Multiagent Simulation Environment." In: *Simulation* 81.7 (2005), pp. 517–527. ISSN: 0037-5497 (cit. on p. 42).

[52] T. Moguchaya et al. "Curve and surface fitting by wavelet shrinkage using GM-Waves." In: *Mathematical methods for Curves and Surfaces*. Ed. by M. Dæhlen, K. Mørken, and L. L. Schumaker. Nashboro Press, 2005, pp. 263–274 (cit. on p. 16).

[53] J.Cotrina Navau and N.Pla Garcia. "Modeling surfaces from meshes of arbitrary topology." In: *Computer Aided Geometric Design* 17.7 (2000), pp. 643–671. ISSN: 0167-8396. DOI: https://doi.org/10.1016/S0167-8396(00)00020-0. URL: http://www.sciencedirect.com/science/article/pii/S0167839600000200 (cit. on p. 11).

[54] J.Cotrina Navau and N.Pla Garcia. "Modelling surfaces from planar irregular meshes." In: *Computer Aided Geometric Design* 17.1 (2000), pp. 1–15. ISSN: 0167-8396. DOI: https://doi.org/10.1016/S0167-8396(99)00034-5. URL: http://www.sciencedirect.com/science/article/pii/S0167839699000345 (cit. on pp. 11, 15).

[55] Hans Olofsen. "Blending functions based on trigonometric and polynomial approximations of the Fabius function." In: *Norsk Informatik Konferanse (NIK) 2019 - Open Journal Systems* (2019: Norsk Informatikkonferanse 2019) (cit. on p. 15).

[56] Raqib Omer. "An Automatic Image Recognition System for Winter Road Condition Monitoring." In: UWSpace, 2011. URL: http://hdl.handle.net/10012/5799 (cit. on p. 23).

[57] Raqib Omer and Liping Fu. "An automatic image recognition system for winter road surface condition classification." In: *13th International IEEE*

Conference on Intelligent Transportation Systems (2010), pp. 1375–1379 (cit. on p. 23).

[58] A. Pedersen. "Arbitrary holes in surfaces using blending type spline constructions." In: 9th International Conference on Mathematical Methods for Curves and Surfaces (Tønsberg, Norway). Conference talk and abstract at 9th International Conference on Mathematical Methods for Curves and Surfaces. 2016 (cit. on p. 45).

[59] A. Pedersen. "Geometrical approach to a simple pendulum motion in 3D for large initial angles." In: *For review* (Apr. 2020) (cit. on pp. 24, 45).

[60] A. Pedersen. "Interactive modelling and simulation using blending techniques." In: *Norsk Informatikkonferanse - Open Journal Systems* (2015: Norsk Informatikkonferanse Oct. 2015) (cit. on p. 46).

[61] A. Pedersen. "Terrain level curves using blending splines." In: *Terrain level curves using blending splines*. 9th International Conference on Curves and Surfaces (Arcachon, France). Conference talk and abstract at 9th International Conference on Curves and Surfaces. 2018 (cit. on p. 45).

[62] A. Pedersen, J. Bratlie, and R. Dalmo. "Surface hole modeling using blending splines." In: Multiphysics 2014 (Sofia, Bulgaria). abstract issn:2409-1669/2409-7527. 2014 (cit. on p. 45).

[63] A. Pedersen, T.F. Brustad, and B. Bang. "Targeted sanding and its impact on heavy hauler pull force and surface friction." In: *For review* 17 (2019) (cit. on pp. 29, 46).

[64] A. Pedersen et al. "Alternative representation of railway track geometry." In: *International Heavy Haul Association* (2019) (cit. on p. 45).

[65] Aleksander Pedersen. "Altering Perceptions, Visualizing Sub-ground Metal Objects." In: *Emerging Science Journal* 4 (June 2020), pp. 205–213. DOI: 10.28991/esj-2020-01224 (cit. on pp. 24, 46).

[66] Aleksander Pedersen. "Shooting simulator." Faculty of Technology. MA thesis. Narvik University College, 2014 (cit. on pp. 17, 19).

[67] Aleksander Pedersen and Børre Bang. "Blending type spline constructions: A brief overview." In: *AIP Conference Proceedings* 1690 (Nov. 2015), p. 020001. DOI: 10.1063/1.4936679 (cit. on p. 46).

[68] Aleksander Pedersen, Jostein Bratlie, and Rune Dalmo. "Spline Representation of Connected Surfaces with Custom-Shaped Holes." In: *Large-Scale Scientific Computing*. Ed. by Ivan Lirkov, Svetozar D. Margenov, and Jerzy Waśniewski. Cham: Springer International Publishing, 2015, pp. 394–400. ISBN: 978-3-319-26520-9 (cit. on p. 45).

[69] Aleksander Pedersen and Tanita F. Brustad. "A Study on Hybrid Sensor Technology in Winter Road Assessment." In: *Safety* 6.1 (2020). ISSN: 2313-576X. DOI: 10.3390/safety6010017. URL: https://www.mdpi.com/2313-576X/6/1/17 (cit. on pp. 29, 46).

[70] Aleksander Pedersen, Rune Dalmo, and Jostein Bratlie. "Modeling terminal ballistics using blending-type spline surfaces." In: *ICNPAA 2014 World Congress: 10th International conference on Mathematical Problems*

in Engineering, Aerospace and Sciences. Ed. by Seenith Sivasundaram. Vol. 1637. AIP Conference Proceedings. AIP Publishing, 2014, pp. 796–803. DOI: http://dx.doi.org/10.1063/1.4904652 (cit. on p. 16).

[71] Ronnie J. Phillips. "Digital Technology and Institutional Change from the Gilded Age to Modern Times: The Impact of the Telegraph and the Internet." In: *Journal of Economic Issues* 34.2 (2000), pp. 267–289. DOI: 10.1080/00213624.2000.11506266 (cit. on p. 31).

[72] Einar Rasmussen. "Improved visuawlization of scalar data using interpolation." MA thesis. Narvik University College, 2006 (cit. on pp. 19, 20).

[73] Peter Rau. *User Manual - MARWIS App*. (Accessed 2019-10-02). 2017 (cit. on p. 26).

[74] Rhinoceros. *Rhinoceros - design, model, present, analyze, realize...* Rhino 6 product site. Feb. 2020. URL: www.rhino3d.com/ (cit. on p. 42).

[75] Andreas Schütte et al. "Numerical Simulation of Maneuvering Aircraft by Aerodynamic, Flight Mechanics and Structural Mechanics Coupling." In: *Journal of Aircraft* 46.1 (2009), pp. 53–64. DOI: 10.2514/1.31182 (cit. on p. 42).

[76] Thomas W. Sederberg et al. "T-splines and T-NURCCs." In: *ACM SIGGRAPH 2003 Papers*. SIGGRAPH '03. San Diego, California: ACM, 2003, pp. 477–484. ISBN: 1-58113-709-5. DOI: 10.1145/1201775.882295. URL: http://doi.acm.org/10.1145/1201775.882295 (cit. on p. 10).

[77] William A. Sethares. "The geometry of musical rhythm: what makes a "good" rhythm good?" In: *Journal of Mathematics and the Arts* 8.3-4 (2014), pp. 135–137. DOI: 10.1080/17513472.2014.906116 (cit. on p. 30).

[78] Ubejd Shala and Angel Rodriguez. "Indoor Positioning using Sensorfusion in Android Devices." In: (2011), p. 58 (cit. on p. 24).

[79] OBD Solutions. *STN1100 Family Reference and Programming Manual*. (Accessed 2019-10-21) https://www.scantool.net/downloads/98/stn1100-frpm.pdf (cit. on p. 26).

[80] OBD Solutions. *WHAT IS OBD?* Online. (Accessed 2019-10-21) https://www.obdsol.com/knowledgebase/on-board-diagnostics/what-is-obd/. 2019 (cit. on p. 26).

[81] SparkFun. *Getting Started with Walabot*. Online. (Accessed 2019-10-02) https://learn.sparkfun.com/tutorials/getting-started-with-walabot?_ga=2.140213947.929731503.1570004485-127684519.1570004485. 2018 (cit. on p. 27).

[82] Márta Szilvási-Nagy and Teréz P. Vendel. "Generating curves and swept surfaces by blended circles." In: *Computer Aided Geometric Design* 17.2 (2000), pp. 197–206. ISSN: 0167-8396. DOI: https://doi.org/10.1016/S0167-8396(99)00045-X. URL: http://www.sciencedirect.com/science/article/pii/S016783969900045X (cit. on p. 15).

[83] Teconer. *Winter maintenance of roads and runways*. (Accessed 2019-09-05). 2015 (cit. on p. 26).

[84] Jacinto Ulloa et al. "Phase-field modeling of fracture for quasi-brittle materials." In: *Underground Space* 4.1 (2019). Computational Modeling of Fracture in Geotechnical Engineering Part II, pp. 10–21. ISSN: 2467-9674. DOI: https://doi.org/10.1016/j.undsp.2018.08.002. URL: http://www.sciencedirect.com/science/article/pii/S2467967418300503 (cit. on p. 23).

[85] Patrik Vogt and Jochen Kuhn. "Analyzing free fall with a smartphone acceleration sensor." In: *The Physics Teacher* 50 (Mar. 2012), pp. 182–183. DOI: 10.1119/1.3685123 (cit. on p. 43).

[86] Patrik Vogt and Jochen Kuhn. "Analyzing simple pendulum phenomena with a smartphone acceleration sensor." In: *The Physics Teacher* 50.7 (2012), pp. 439–440. DOI: 10.1119/1.4752056 (cit. on p. 43).

[87] A.V. Vuong et al. "A Hierarchical Approach to Adaptive Local Refinement in Isogeometric Analysis." In: *Computer Methods in Applied Mechanics and Engineering* 200 (Dec. 2011), pp. 3554–3567. DOI: 10.1016/j.cma.2011.09.004 (cit. on p. 10).

[88] Walabot. *Walabot - Technical Brief*. (Accessed 2019-09-05). 2019 (cit. on p. 27).

[89] Qi Wang. "Expo-rational B-spline surfaces and simulation and visualization." MA thesis. Narvik University College, July 2009 (cit. on pp. 16, 18, 19).

[90] Hans-Jörg Wenz. "Interpolation of curve data by blended generalized circles." In: *Computer Aided Geometric Design* 13.8 (1996), pp. 673–680. ISSN: 0167-8396. DOI: https://doi.org/10.1016/0167-8396(95)00054-2. URL: http://www.sciencedirect.com/science/article/pii/0167839695000542 (cit. on p. 11).

[91] T. Wimalajeewa and S. K. Jayaweera. "Impact of mobile node density on detection performance measures in a hybrid sensor network." In: *IEEE Transactions on Wireless Communications* 9.5 (May 2010), pp. 1760–1769. ISSN: 1558-2248. DOI: 10.1109/TWC.2010.05.091012 (cit. on p. 43).

[92] Lexing Ying and Denis Zorin. "A Simple Manifold-Based Construction of Surfaces of Arbitrary Smoothness." In: *ACM Trans. Graph.* 23.3 (Aug. 2004), pp. 271–275. ISSN: 0730-0301. DOI: 10.1145/1015706.1015714 (cit. on pp. 11, 15).

[93] Youtube. *Walabot Programmable 3D Sensor*. Online videos. (Accessed 2019-10-03) https://www.youtube.com/channel/UCdQcnXMiEGizQvPODZIwvBA/videos. 2019 (cit. on p. 27).

[94] P. Zanaty. "Application of Generalized Expo-Rational B-splines in Computer Aided Design and Analysis." PhD thesis. University of Oslo, 2014 (cit. on p. 16).

Part IV

Appendix

Paper A

The included paper is a reprint of

Spline representation of connected surfaces with custom-shaped holes

Aleksander Pedersen, Jostein Bratlie and Rune dalmo
UiT The Arctic University of Norway
Large-Scale Scientific Computing 2015, Springer International Publishing, P394-400, ISBN 978-3-319-26520-9

A SPLINE REPRESENTATION OF CONNECTED SURFACES WITH CUSTOM-SHAPED HOLES

This is a reprint

Aleksander Pedersen, Jostein Bratlie and Rune Dalmo

Faculty of Engineering Science and Technology
UiT The arctic University of Norway
Norway

Abstract Compact surfaces possessing a finite number of boundaries are important for isogeometric analysis (IGA). Generalized expo-rational B-Splines (GERBS) is a blending type spline construction where local functions associated with each knot are blended by C^k-smooth basis functions. Modeling surfaces with custom-shaped boundaries, or holes, can be achieved by using certain features and properties of the blending type spline construction, including local refinement and insertion of multiple inner knots. In this paper we investigate representation of arbitrary inner boundaries on parametric surfaces by using the above mentioned blending type spline construction.

A.1 Introduction

The field of isogeometric analysis (IGA), introduced by Hughes et.al. in [11], is attempting to integrate finite element analysis (FEA) and computer aided design (CAD).

Polynomials on Bernstein form, B-splines in particular, are numerically more stable than polynomials on monomial form [9]. They can provide exact representations of elementary curves, surfaces and volumes. The non-uniform rational B-splines (NURBS) have been incorporated into the initial graphics exchange specification (IGES) and standard for the exchange of product model data (STEP) industry standards used in CAD. Spline based methods is one of the current approaches on IGA, attempting to bridge the gap from CAD to FEA. Some notable variants of spline based IGA include T-splines [15], PHT-splines [7], locally refined B-splines (LR B-splines) [8] and hierarchical B-splines [10, 16].

This study constitutes one part in a series of attempts to explore the use of blending type splines in the construction and analysis of iso geometry. In this article we address the use of tensor product boolean sum surfaces of Coons type [3] as local surface patches for the spline construction. Our main motivation is to explore how well we can control the shape of an internal hole, represented by a boundary curve, in a C^k smooth surface.

The following sections provide a brief overview of the GERBS surface construction, Coons patch and boolean sum surfaces followed by a description of our method before we present our results and finally give our concluding remarks.

A.2 The blending-type spline construction

Expo-rational B-splines (ERBS) were first introduced under this name in [6, 12]. The generalization of expo-rational B-splines (GERBS) appeared in [5]. Later, in [14, 13], the ERBS blending construction was presented in the framework of the B-spline recursion formula associated with the knots $(t_i)_{i=0}^{k+d}$:

$$B_{d,k}(t) = B \circ \omega_{d,k}(t) B_{d-1,k}(t) + (1 - B \circ \omega_{d,k+1}(t)) B_{d-1,k+1}(t),$$

where $\omega_{d,i}(t) = \frac{t-t_i}{t_{i+d}-t_i}$, $B_{0,i}(t) = \begin{cases} 1; & \text{if } t_i \le t < t_{i+1}. \\ 0; & \text{otherwise.} \end{cases}$

The degree $d = 1$ in the case of GERBS; moreover, B is a C^k-smooth blending function possessing the following set of properties:

1. $B : I \rightarrow I$ $(I = [0, 1] \subset \mathbb{R})$,
2. $B(0) = 0$,
3. $B(1) = 1$,
4. $B^{'}(t) >= 0$, $t \in I$.
5. $B(t) + B(1 - t) = 1$, $t \in I$.

The last property is optional and specifies point symmetry around the point $(0.5, 0.5)$, however, we assume this property in the present study.

In the present work we consider tensor product surfaces defined as

$$S(u, v) = \sum_{i=1}^{n} \sum_{j=1}^{m} \ell_{i,j}(u, v) B_{1,i}(u) B_{1,j}(v),$$

where $\ell_{i,j}(u, v)$ are *local surfaces* which are blended together by the C^k-smooth blending functions $B_{1,i}$ and $B_{1,j}$.

Local refinement by knot insertion for the blending construction was addressed in [2, 4]. Splitting the geometry, which can be achieved by using multiple inner knots in this case, is one form of editing which was first investigated in [1] as a technique for artistic editing where a method for creating holes in the geometry was presented.

One consequence of splitting by using multiple knots is that affine transforms can be applied to the local surface patches associated with the knots. Separating two connected double knots gives a geometric G^0 continuity of the construction, in the corresponding parametric direction, while maintaining the C^k mathematical smoothness. This follows as a consequence of the transfinite Hermite interpolation property at the knots, which in turn is due to the vanishing derivatives of the basis function at the knots.

Figure A.1 shows an example of how the blending construction can be split by using multiple knots which are moved away from each other, and how the parametric representation is still continuous.

Using double knots in both parametric directions splits the surface into four equal pieces. Each quadrangle has four local patches, pointing at a single patch, which represent a corner in the final surface. A geometric hole appears in the center of the surface since the four local patches in the center are pointing to a respective patch in a corner.

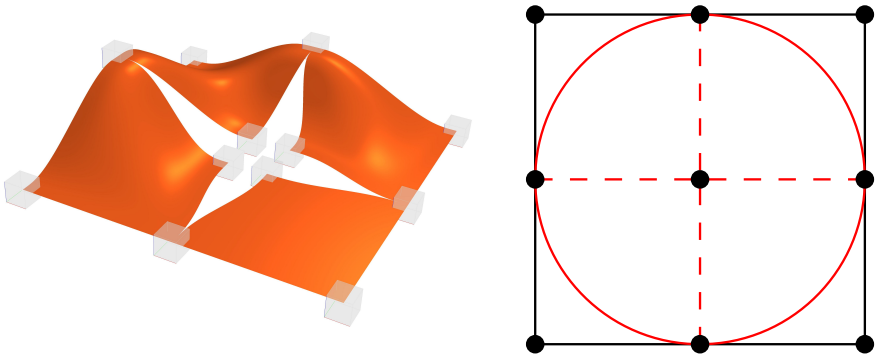

Figure A.1: A blending-type spline surface with multiple knots that are separated to generate a split (on the left) and the parametric representation of the same surface (on the right).

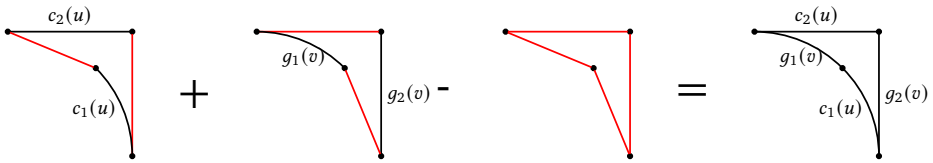

Figure A.2: The surfaces involved in a bilinear Coons patch construction. The red lines indicate linear segments between two nodes, and the black lines indicate the interpolated curves. Adding two ruled surfaces and subtracting a bilinear one yields the final Coons patch surface (right). From left to right: $L_1 + L_2 - L_3 = \ell$

A.3 Boolean sum surfaces

The Coons surface patch [3] is a surface segment bounded by four spatial curves that it interpolates to. Coons proposed using blending surfaces in [3]. Two ruled surfaces, where each of them interpolates two of the four boundary curves, are added together with this construction. A slope correction surface is subtracted to compensate for the curves which the ruled surfaces fail to interpolate.

Figure A.2 illustrates the components of a bilinear Coons patch defined by the boolean sum surface

$$\ell(u,v) = L_1(u,v) + L_2(u,v) - L_3(u,v),$$

where the ruled surface $L_1(u,v)$ interpolates the two boundary curves $c_1(u), c_2(u)$ but is linear along v, $L_2(u,v)$ interpolates $g_1(v), g_2(v)$ but is linear along u, and $L_3(u,v)$ is a bilinear slope correction surface matching the linear components of both $L_1(u,v)$ and $L_2(u,v)$.

A.4 Coons patches as local geometry

We propose using Coons patches as local surfaces in connection with double knots to obtain splits, or holes, with an arbitrary shape. The desired shape for the inner boundary can be described by curves which are interpolated by the Coons patch local surfaces. The only requirement for each quadrant is that they interpolate at the parametric central knot of every edge.

The initial shape of the resulting surface (before separating the multiple knots) will be preserved since the local patches that are blended together have exactly the same shape and since the desired geometric hole is constructed using the inner boundary curve.

As an experiment and proof of concept, we provide two surfaces. They are constructed from an inner and outer boundary curve. In both cases the outer boundary curve is a closed parametric rectangular curve. Both examples have uniform 3×3 knots vectors, where the middle knot is a double knot, in both parametric directions.

In the first example, shown on the left in Figure A.3, the inner boundary is a circular curve interpolating the outer boundary at the middle double knots. In the second example, shown on the right in Figure A.3, the inner boundary is a parametric ERBS-based free form blending-type spline curve interpolating the outer boundary curve at the middle knots.

A curve evaluated on the boundary of the two example surfaces is shown in Figure A.4 and a wireframe representation of the examples, showing the distribution of the parametric domain, is provided in Figure A.5. On both surfaces, $s(u, v)$ where $u, v \in [0, 2]$, the surface curve is evaluated along v for a fixed $u = 0.5$.

A.5 Concluding remarks

In both examples the middle knots on the boundary are equally distanced from both sides. We note that this is not a general requirement. Moreover, in both examples, a compact C^k-smooth tensor-product blending-type spline surface construction is created where the inner boundary curve limits a natural hole in the surface construction. Both constructions are exact constructions in the sense that the inner and outer boundary curves are interpolated. The construction is C^k everywhere and at the knots the smoothness depends on the local geometry. In the case where bilinear Coons patches are used as representation of the local geometry the smoothness is C^1. We note that in

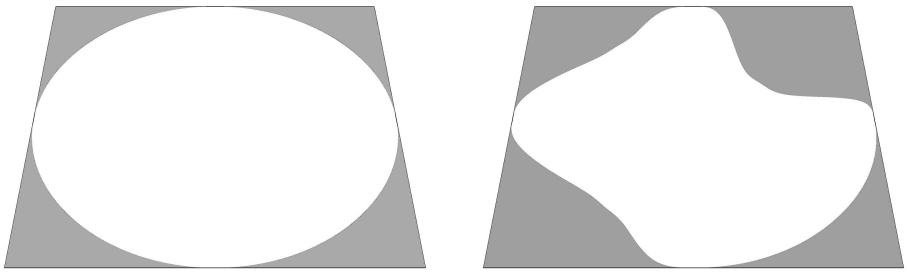

Figure A.3: The illustration shows the shaded version of the two example constructions. The surface on the left has a circular inner boundary while the one on the right has a free form ERBS-based inner boundary. Both inner boundary curves interpolate the outer boundary at the middle of the four edges.

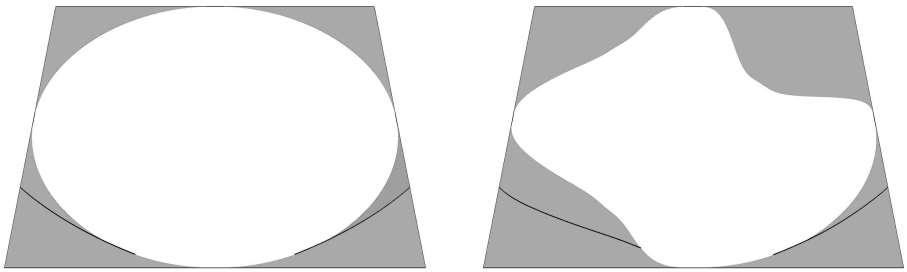

Figure A.4: The illustration shows a shaded version of the two example surface constructions, $S(u, v)$ where $u, v \in [0, 2]$, with a curve plotted in the parametric plane along v for a fixed $u = 0.5$. The surface on the left has a circular inner boundary while the one on the right has a free form ERBS-based inner boundary.

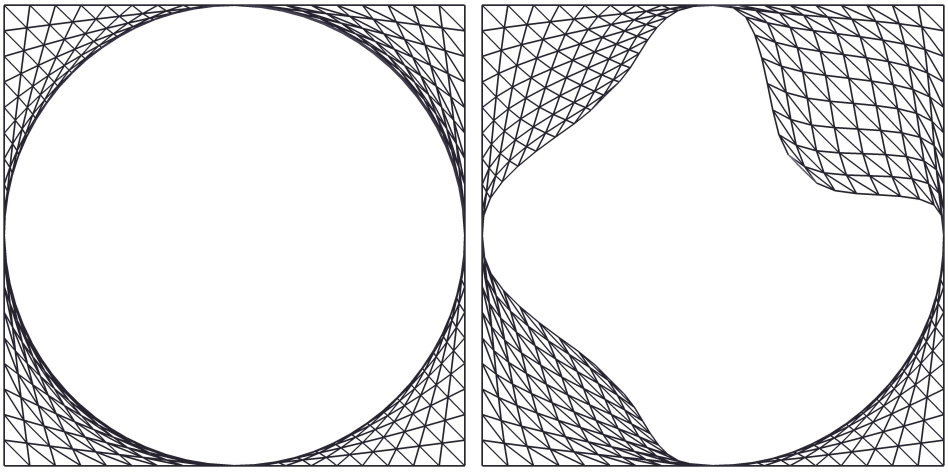

Figure A.5: The illustrations shows the tensor-product parameter grid distribution as wireframes of the two example constructions. The surface on the left has a circular inner boundary while the one on the right has a free form ERBS-based inner boundary. Both surfaces are sampled at 20×20 samples.

the case where bicubic blending would be used the construction would be C^2 at the knots. Further exploration is a topic for future work. All the while the construction has a natural inner hole represented by the inner boundary curve and is therefore G^0. The construction is also evaluable everywhere on the tensor-product parametric domain.

One expansion of this construction could be such that the inner and outer boundary curves do not interpolate at the boundary knots. Another interesting expansion could be to expand the construction into a three-tensor volumetric representation where the inner boundary would be a parametric surface.

Bibliography

[1] Kevin Moe Andresen. "Brukergrensesnitt for kunstnerisk design ved bruk av ERBS." MA thesis. Narvik University College, 2008 (cit. on p. 71).

[2] Jostein Bratlie. "Local refinement of GERBS surfaces with applications to interactive geometric modeling." In: *39th International conference applications of mathematics in engineering and economics AMEE13*. Ed. by Vesela Pasheva and George Venkov. Vol. 1570. AIP Conference Proceedings. AIP Publishing, 2013, pp. 18–25. DOI: 10.1063/1.4854738 (cit. on p. 71).

[3] Steven A. Coons. *Surfaces for Computer-Aided Design of Space Forms*. Project MAC-TR-41. Massachusetts, USA: Massachusetts Institute of Technology, 1967 (cit. on pp. 70, 72).

[4] Rune Dalmo. "Local refinement of ERBS curves." In: *39th International conference applications of mathematics in engineering and economics AMEE13*. Ed. by Vesela Pasheva and George Venkov. Vol. 1570. AIP Conference Proceedings. AIP Publishing, 2013, pp. 204–211. DOI: 10.1063/1.4854757 (cit. on p. 71).

[5] L. T. Dechevsky, B. Bang, and A. Lakså. "Generalized Expo-Rational B-Splines." In: *International Journal of Pure and Applied Mathematics* 57.6 (2009), pp. 833–872 (cit. on p. 70).

[6] Lubomir T. Dechevsky, Arne Lakså, and Børre Bang. "Expo-Rational B-Splines." In: *International Journal of Pure and Applied Mathematics* 27.3 (2006), pp. 319–362 (cit. on p. 70).

[7] Jiansong Deng, Falai Chen, and Yuyu Feng. "Dimensions of spline spaces over T-meshes." In: *Journal of Computational and Applied Mathematics* 194.2 (Oct. 2006), pp. 267–283. ISSN: 0377-0427. DOI: 10.1016/j.cam.2005.07.009 (cit. on p. 70).

[8] Tor Dokken, Tom Lyche, and Kjell Fredrik Pettersen. "Polynomial splines over locally refined box-partitions." In: *Computer Aided Geometric Design* 30.3 (2013), pp. 331–356. ISSN: 0167-8396. DOI: http://dx.doi.org/10.1016/j.cagd.2012.12.005. URL: http://www.sciencedirect.com/science/article/pii/S0167839613000113 (cit. on p. 70).

[9] R. T. Farouki and V. T. Rajan. "On the numerical condition of polynomials in Bernstein form." In: *Computer Aided Geometric Design* 4.3 (1987), pp. 191–216 (cit. on p. 70).

[10] C. Giannelli, B. Jüttler, and H. Speleers. "THB–splines: The truncated basis for hierarchical splines." In: *Computer Aided Geometric Design* 29.7 (2012), pp. 485–498. DOI: 10.1016/j.cagd.2012.03.025 (cit. on p. 70).

[11] T. J. R. Hughes, J. A. Cottrell, and Y. Bazilevs. "Isogeometric Analysis: CAD, Finite Elements, NURBS, Exact Geometry and Mesh Refinement." In: *Computer Methods in Applied Mechanics and Engineering* 194.39-41 (Oct. 2005), pp. 4135–4195. ISSN: 00457825. DOI: 10.1016/j.cma.2004.10.008 (cit. on p. 70).

[12] A. Lakså, B. Bang, and L. T. Dechevsky. "Exploring Expo-Rational B-splines for Curves and Surfaces." In: *Mathematical methods for Curves and Surfaces*. Ed. by M. Dæhlen, K. Mørken, and L. L. Schumaker. Nashboro Press, 2005, pp. 253–262 (cit. on p. 70).

[13] Arne Lakså. "Construction and properties of non-polynomial spline curves." In: *ICNPAA 2014 World Congress: 10th International conference on Mathematical Problems in Engineering, Aerospace and Sciences*. Ed. by Seenith Sivasundaram. Vol. 1637. AIP Conference Proceedings. AIP Publishing, 2014, pp. 545–554. DOI: http://dx.doi.org/10.1063/1.4904623 (cit. on p. 70).

[14] Arne Lakså. "ERBS-surface construction on irregular grids." In: *39th International conference applications of mathematics in engineering and economics AMEE13*. Ed. by Vesela Pasheva and George Venkov. Vol. 1570. AIP Conference Proceedings. AIP Publishing, 2013, pp. 113–120. DOI: 10.1063/1.4854749 (cit. on p. 70).

[15] Thomas W. Sederberg et al. "T-splines and T-NURCCs." In: *ACM SIGGRAPH 2003 Papers*. SIGGRAPH '03. San Diego, California: ACM, 2003, pp. 477–484. ISBN: 1-58113-709-5. DOI: 10.1145/1201775.882295. URL: http://doi.acm.org/10.1145/1201775.882295 (cit. on p. 70).

[16] A.V. Vuong et al. "A Hierarchical Approach to Adaptive Local Refinement in Isogeometric Analysis." In: *Computer Methods in Applied Mechanics and Engineering* 200 (Dec. 2011), pp. 3554–3567. DOI: 10.1016/j.cma.2011.09.004 (cit. on p. 70).

Paper B

The included paper is a reprint of

Alternative representation of railway track geometry

Aleksander Pedersen, Tanita Fossli Brustad, Børre Bang and Rune dalmo
Faculty of Engineering Science and Technology
UiT The Arctic University of Norway, Norway
International Heavy Haul Association 2019, In-Proceedings

B ALTERNATIVE REPRESENTATION OF RAILWAY TRACK GEOMETRY

This is a reprint

Aleksander Pedersen, Tanita Fossli Brustad, Børre Bang and Rune Dalmo

Faculty of Engineering Science and Technology
UiT The arctic University of Norway
Norway

Abstract Track geometry is important in the design, construction and maintenance of railways. Increasing comfort and faster travel times, as well as decreasing the amount of maintenance needed on railway tracks, are examples of criteria when rail geometry is constructed or modified. There are several existing methods and commercial tools available that can identify such criteria, such as lateral change of acceleration (LCA). By applying available new interpolation methods to represent the existing chain of curve elements in a railroad construction, we exploit the geometrical properties to study the positional and curvature continuity. In this paper we investigate the composition of curve segments that make up a railway track, and compare the original track geometry and a spline curve representation.

B.1 Introduction

Over the years railway geometry has changed in line with the development of trains and rail transport. Early railway tracks usually consisted of a connection of straight sections and circular arcs. With the low speed of trains and the wide radius of the circular sections, the transition between straight and circular sections was considered easy and safe with regards to the motion of the train [5], and was well within the scope of current surveying technologies at that time. When the evolution of railway tracks made the radius of the circular tracks smaller and the speed of trains increased, transitions became jerky and unpleasant, and sometimes even dangerous [5, 7]. This realization opened the door to easement curves, or transition curves as they are more known by, which made the transition from straight track to curved track safer and more comfortable even at higher speeds [5, 7, 8]. A well-known and much used transition curve is the clothoid curve [1, 6], although other curves, like the cubic parabola and lemniscate [8], were also utilized. For a long time the clothoid curve was a sufficient transition curve for railways, and still is today. However, with the introduction of the lateral change of acceleration (LCA) function [3] in the last quarter of the 20th century, new design criteria were introduced to improve vehicle-road properties in railway. The new criterion of the LCA showed that the high speed requirements in modern rail transport made the popular clothoid curve undesirable because of its discontinuity in LCA at the start and end. This has given rise to a new generation of transition curves [13, 10, 9, 11, 12] with performance superior to the clothoid curve when it comes to LCA. In this paper we consider a composition of curve elements making up a railway track and compare this geometry with a b-spline curve representation with regards to curvature and LCA. We are interested in finding alternative representations of transition curves, which improve the shortcomings of the clothoids, and propose the use of b-splines for this purpose. The railway geometry that we are using is a list of segments that constitutes the railway known as Ofotbanen, stretching from Narvik to the border of Sweden. The list consists of three different types of curves; lines, arcs and clothoids (euler spiral). Ofotbanen [2] is a railway line with a main traffic of 10-12 daily freight trains hauling iron ore from Sweden to Narvik. The line is also important for transporting goods by freight trains and there are two daily passenger trains. Ofotbanen was completed in 1902 and today's track follows that original track to a large extent. A fascinating fact about Ofotbanen, and one of the main reasons for choosing it in this research, is the variety of compositions of the segments, ranging from line-clothoid-arc to arc-clothoid-arc and also arc-clothoid-clothoid-arc. These combinations of curve segments in connection with the heavy load can be related to maintenance problems. We show some results in the comparison part of this paper.

B.2 Theory and method

Lateral change of acceleration

The lateral change of acceleration (LCA) is the change of the resultant acceleration occurring along the curve normal with respect to time. The function is expressed in [3] as

$$z = \frac{pv}{\sqrt{(u^2 + p^2)}}\left(3ka_t + v^2\frac{dk}{dl} - \frac{(kv^2u + gp)}{(u^2 + p^2)}\frac{du}{dl}\right),$$

where p is the horizontal width of the platform m, v is the velocity of the train $\frac{m}{s}$, u is the superelevation which is the elevation of the outer rail according to the inner rail m, k is the curvature along the curve $\frac{1}{m}$, a_t is the tangential acceleration $\frac{m}{s^2}$, and g is the gravity constant $9.81\frac{m}{s^2}$. When comparing curves with a basis in the LCA function, there are three criteria [9] that are used to compare them. The continuity of the LCA is the most important of the three criteria. This is because discontinuities (in the form of jumps) affect travel comfort and cause wear on wheels and rails. Any curve without discontinuity in LCA is considered superior to those that have discontinuities. If none of the curves have discontinuities, they are considered equivalent in regards to criteria 1, and criteria 2 has to be used. Criteria 2 compares the extreme value (largest absolute value) of the LCA function for each curve to a boundary value that it should be smaller than. Any curve satisfying this condition is superior to those that do not. If the curves are also equivalent after criteria 2, the third criteria can be considered. Criteria 3 looks at discontinuities in the form of breaks at the start and end of the transition curve. Any curve without breaks in the end points is superior to those that have breaks. In this work we have restricted the velocity in the LCA function so that it is constant. A constant velocity means that the LCA becomes a scaled version of the derivative of the curvature. This means that we can look at the curvature and the derivative of the curvature and get a good indication of the behavior in regards to LCA.

B-Splines

B-splines [4] are commonly used in computer representations of curves and surfaces. A parametric curve can be represented on b-spline form as

$$c(t) = \sum_{i=0}^{n} c_i B_i^d t,$$

where $B_i^d t$ are the Bernstein basis polynomials of degree d and the coefficients c_i are points defining a control polygon. One well known property of the cubic

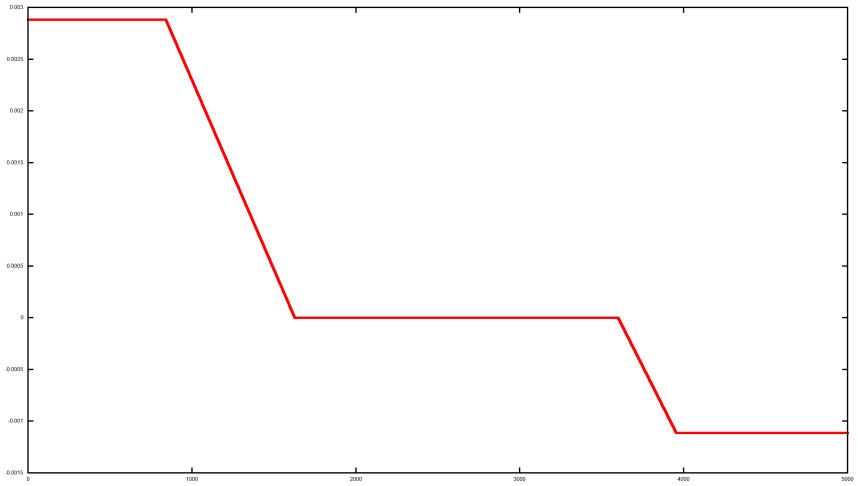

Figure B.1: Curvature plot of a simple segment curve. Consisting of 5 segments, arc-clothoid-line-clothoid-arc respectively.

B-spline is that it minimizes the second derivative. When the speed of the parameterization is constant, then the minimization property also applies to the curvature of the spline curve. As outlined above, the model of our railway curve consists of a composition of simple geometrical objects. The curvature of the straight line curve segments is zero, whereas the curvature of the circle arcs is constant. The change of curvature in clothoids is constant. This means that the curvature for the global, composite curve is C^0 continuous at the joints between the curve segments. An example of a curvature plot is shown in Figure B.1.

Method

We evaluated the original composite curve at selected points of interest (POI) to obtain data points. Then we approximated the data points with a cubic b-spline curve via solving a least squares problem, where the idea was to approximate straight lines and (parts of) circle arcs well, while leaving the approximation of transition curves to the "system". Finally, we evaluated the curvatures of the composite curve and the b-spline approximation curve, measured the differences and compared the results. The differences were measured in terms of mean squared error

$$MSE = \sum_{i=1}^{n} (c_i - s_i)^2, \tag{B.1}$$

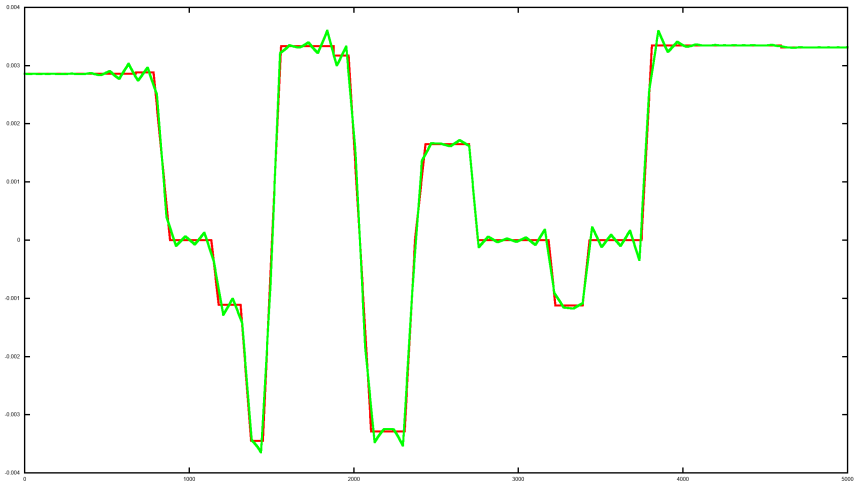

Figure B.2: Curvature comparison between segment curve (red) and b-spline (green) using uniform knotvector and sampling. Nr. Control points is 90.

where c_i and s_i are samples of the composite curve and the spline curve, and the maximum distance

$$MAX = max(c_i - s_i)^2. \tag{B.2}$$

B.3 Results

Here we give our results by showing how the proposed method performs when applied to a collection of representative curve segments. We experiment with varying the number of data points (samples), testing uniform and non-uniform samples, uniform and non-uniform spline knotvectors, and different numbers of spline coefficients. Graphs showing curvature- and difference plots are shown in Figures B.2 to B.5.

Table B.1 is showing how the different constructions compare to each other using a mean squared error estimate. MSE (B.1) is the average of the squares of errors. The Max value (B.2) is the largest distance between the two curves.

B.4 Analysis and discussion

The b-spline approximates the composite curve well, as expected, this is shown in Figure B.5 and Table B.1. By considering Figures B.2 to B.4 we observe that the

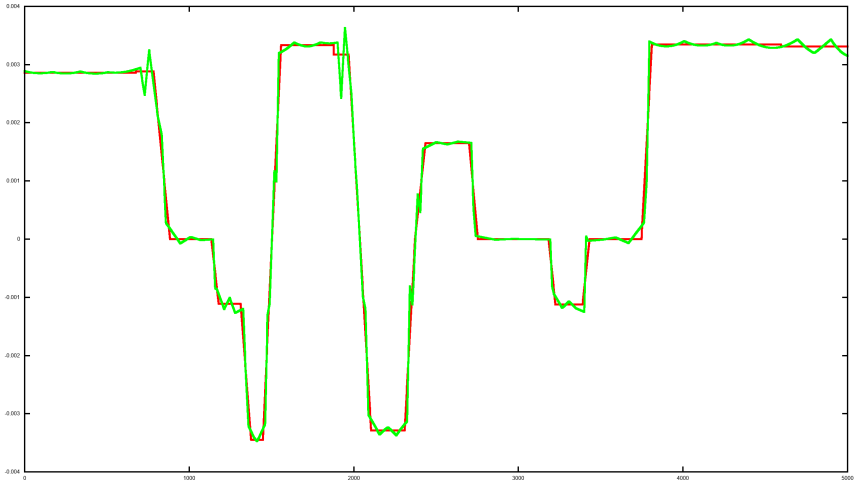

Figure B.3: Curvature comparison between segment curve (red) and b-spline (green) using non-uniform knotvector with 86 control points and 500 sampling size.

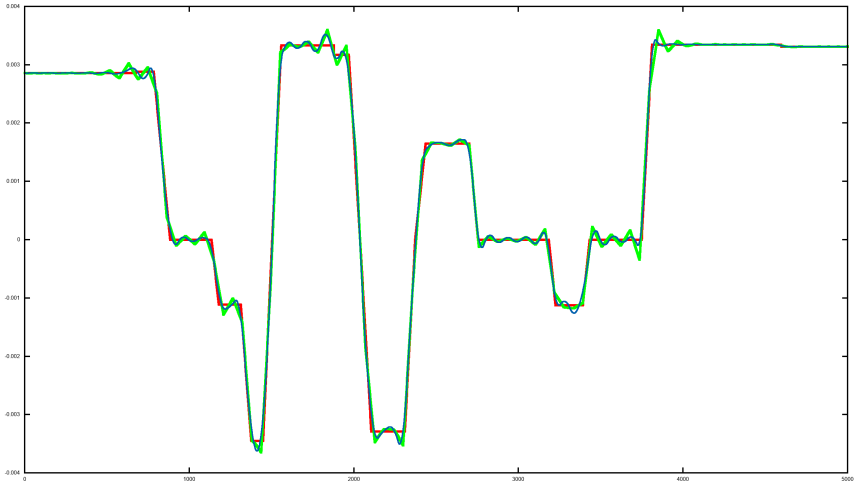

Figure B.4: Curvature comparison between segment curve (red) and both a 3rd (green) and 4th (blue) degree b-spline with uniform knotvector and sampling.

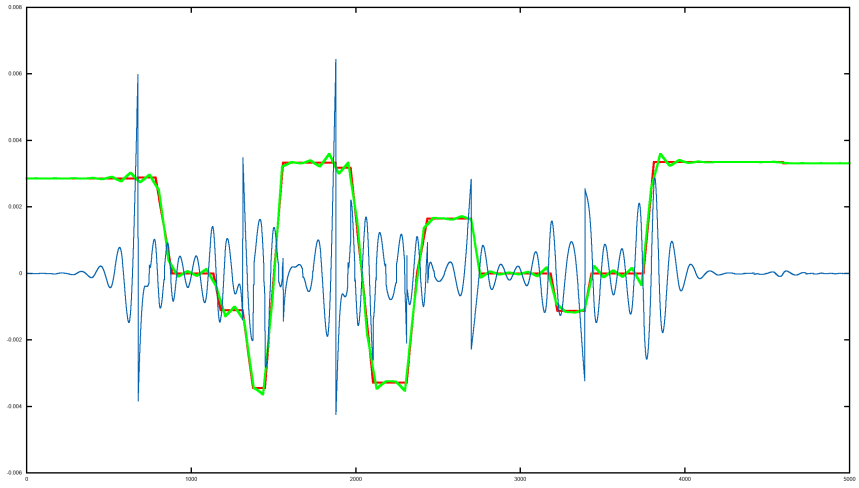

Figure B.5: Curvature plot against error distance between segment curve and b-spline with uniform knotvector and sampling. Segment curve (red), b-spline (green) and distance difference (blue).

Error measurements		
Distance error	Measurements	
	MSE	MAX
Uniform 30/500	0.180716	2.54563
Uniform 60/500	0.001348	0.01307
Uniform 300/500	0.000001	0.00330
Non-Uniform 31/500	0.263089	4.41375
Non-Uniform 58/500	0.002167	0.03209
Non-Uniform 85/500	0.000264	0.00408
Non-Uniform 274/2500	0.000001	0.00438

Table B.1: The distance error column is explaining the distribution of control points and sample points of the curve. Measurements are mean squared error and max distance between the two curves

curvature of the b-spline matches the curvatures of the straight line- and circular arc segments. However, we note that there are some wiggles in the graphs in those areas which are due to noise arising from the polynomial interpolation. Here we remark that this is expected, but the curvature numbers for the curve are so small that this noise is shown in the graphs. When comparing the graphs in Figures B.2 and B.3, made from a similar number of control points (90 vs. 86), we note that a non-uniform parameterization of the b-spline works better with respect to wiggles and smoothness in some areas than a uniform parameterization. The curvature plots for the b-spline curves indicate improved smoothness over the junctions when compared to the composite curve, as shown in Figures B.2 and B.3. Figure B.4 shows how the curvature of a quartic b-spline is smoother than the curvature of a cubic b-spline. With the same number of control points, the curve is also less wiggly.

B.5 Conclusion

The curvature of the proposed b-spline approximation does not vary linearly with arch length, as point-ed out in [14], however, this criterion is challenged with the advent of the LCA [3]. One possible application of this work is within maintenance and trying to reduce wear of the railway tracks. Alternative transition curves will influence the positioning of the railway. An improved curvature/LCA can possibly be achieved even with relatively small changes to the layout of the railway transition curve segments. Another possible application is within software for railway geometry construction. For future work we note that utilizing non-polynomial splines in the attempt to avoid oscillations near sharp edges would be interesting, and that a possible application to simulation and evaluation of ride comfort parameters based on relevant ISO standards (ISO 2631 etc.) could be considered.

B.6 Acknowledgements

The data used in this work is extracted from the Banenor database using Novapoint and helpful background information regarding “Ofotbanen” has been given by employees at Banenor. A special thanks to Ingeborg Tulluan, who was kind enough to extract the data needed in this work. Also, thanks to Bjørn Gunnar Larsen for information regarding wear and measurements for some parts of Ofotbanen.

Bibliography

[1] R.C. Archibald. "Euler Integrals and Euler's Spiral, Sometimes Called Fresnel Integrals and the Clothoide or Cornu's Spiral." In: *American Mathematical Monthly* 25 (1918), pp. 276–282 (cit. on p. 81).

[2] Banenord. *Ofotbanen*. Accessed: 2019-28-02. 2019. URL: https://www.banenor.no/Jernbanen/Banene/Ofotbanen/ (cit. on p. 81).

[3] O. Baykal. "On concept of lateral change of acceleration." In: *Journal of Surveying Engineering* 122.3 (1996), pp. 132–141 (cit. on pp. 81, 82, 87).

[4] C. De Boor. *A practical guide to splines*. Vol. 27. 1. Springer-Verlag New York, 1978, p. 348. ISBN: 978-0-387-95366-3 (cit. on p. 82).

[5] J Glover. "Transition Curves for Railways." In: *Proc. Inst. C.E* 140 (1900) (cit. on p. 81).

[6] A. L. Higgins. "The Transition Spiral and Its Introduction to Railway Curves with Field Exercises in Construction and Alignment, Constable: London." In: (1921) (cit. on p. 81).

[7] E Horsburg. "The Railway Transition Curve." In: *Proceedings of the Royal Society of Edinburgh* 32 (1913), pp. 333–347 (cit. on p. 81).

[8] A. W. Miller. "The transition spiral." In: *Australian Surveyor* 7(8) (1939), pp. 518–526 (cit. on p. 81).

[9] E Tari. "New curve trends in alignment design." PhD thesis. Istanbul Technical University. Institute of Science and Technology, Istanbul, Turkey., 1997 (cit. on pp. 81, 82).

[10] E Tari. "Spline as a Route Element. On The Use of Computer in Civil Engineering." In: *Proc 5th Symp* (1996) (cit. on p. 81).

[11] E Tari. "The new generation transition curves." In: *The Bulletin of the Istanbul Technical University* 54.1 (2004), pp. 35–41 (cit. on p. 81).

[12] O Tari E.& Baykal. "A new transition curve with enhanced properties." In: *Canadian Journal of Civil Engineering* 32.5 (2005), pp. 913–923 (cit. on p. 81).

[13] O Tari E.& Baykal. "A new transition curve." In: *Proc Symp 27-29 September, 1st Turkish-German Joint Geodetic Days* (1995), pp. 107–119 (cit. on p. 81).

[14] D. S. Walton D.J. & Meek. "Clothoidal Splines." In: *Comput. & Graphics* 14 (1990), pp. 95–100 (cit. on p. 87).

Paper C

The included paper is a reprint of

Geometrical approach to a simple pendulum motion in 3D for large initial angles

Aleksander Pedersen
Faculty of Engineering Science and Technology
UiT The Arctic University of Norway, Norway
Submitted for review

C GEOMETRICAL APPROACH TO A SIMPLE PENDULUM MOTION IN 3D FOR LARGE INITIAL ANGLES

This paper is submitted for review.

Aleksander Pedersen

Faculty of Engineering Science and Technology
UiT The arctic University of Norway
Norway

Abstract Geometrical interpretations can provide insight into the modeling of dynamics, both simple and advanced problems. The pendulum motion problem has been well studied on many occasions and can provide excellent textbook examples of dynamics. In this paper we present a new approach solving the simple pendulum motion in 3D for large initial angles. A geometrical approach using a Taylor expansion series using two well known equations of motion on vector form to model the pendulum trajectory on a sphere shell is presented. The results are compared with an exsiting method, and both visual and numerical results are presented showing the period of each experiment for a set of oscillations.

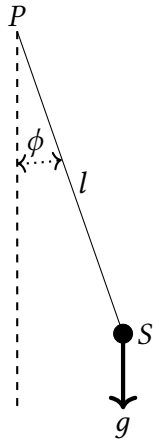

Figure C.1: Simple pendulum setup, with only the gravitational force acting on the pendulum body.

C.1 Introduction

The motion of a pendulum provides excellent textbook examples in both advanced and introductory courses in universities and is one of the most studied problems which, even today, provides insight into dynamics. There are a vast amount of pendulum problems, ranging from ballistic pendulums to double, inverted and Foucault. A comprehensive composition of these articles can be found in [6], which contains a bibliography from four journals devoted to teaching physics and general science. A simple pendulum is described as a rigid body attached to a frictionless pivot point with a massless string, as in Figure C.1. The motion of a pendulum can be shown, if the initial amplitude angle is sufficiently small, by

$$\phi(t) = \phi_0 \cos(\omega t),$$

where $\phi(t)$ is the angle at a given timestep, ϕ_0 is the initial angle and $\omega = \sqrt{\frac{g}{l}}$ is the frequency of the motion with g as the gravity constant and l is the length of the string, as seen in Figure C.1. The angle is always given as a counterclockwise value with zero at pendulum rest. The period of the simple pendulum (harmonic oscillator equation) with the exact expression is also known as a complete elliptic integral of the first kind [1]:

$$T = \left[2\pi\sqrt{\frac{l}{g}}\right]\left\{\frac{2}{\pi}\int_0^{\pi/2}\frac{d\phi}{\sqrt{1-k^2 sin^2\phi}}\right\}, \tag{C.1}$$

where $k = sin(\phi_m/2)$, ϕ_m is the maximum angular displacement. For small initial angular amplitudes, (C.1) reduces to the familiar equation for the pendulum

period

$$T = 2\pi\sqrt{\frac{l}{g}}.$$

In the existing literature there are several contributions with respect to period approximations given simplifications for (C.1). Problems related to large amplitudes for the simple pendulum have already been extensively discussed in existing literature, with contributions such as linearization of the simple pendulum for any amplitude [9], complex trajectories of simple pendulums [3], approximation for the large-angle simple pendulum period [2] and simple formulas for the large-angle pendulum period [7].

This paper treats the pendulum motion using a Taylor expansion series of both the second equation of motion (C.2) and the kinematic equation (C.3). When utilizing the two equations for motion in combination with a geometrical mean, we can describe the pendulum trajectory. We present a method for representing the motion of a simple pendulum using simplified models that approximate the nonlinear dynamical system in $\mathbb{R}^3$ for large initial amplitudes.

C.2 Preliminaries

The pendulum sphere, with position and derivatives following the arc trajectory is constructed using a basis that is analogous to Hamiltonian systems. Such systems model numerous problems in physics, mechanics, fluid dynamics, etc.

1. Hamiltonian matrices have found various applications in settling important issues in systems and control.

2. A given matrix Θ is Hamiltonian if it satisfies $\Theta^T J\Theta = J$ where $J = \begin{bmatrix} 0_{nxn} & I_n \\ -I_n & 0_{nxn} \end{bmatrix}$ and where I is the identity matrix.

For the simplified model we consider here, torsion, control and disturbance forces, and moments are ignored. Our simplified method is compared to a solution using a numerical method to solve the differential equation

$$mL\frac{\mathrm{d}^2\phi}{\mathrm{dt}^2} = -mg\sin(\phi),$$

with respect to large initial amplitudes, where m is the mass, $L = l$ is the arm length, g is gravity constant and ϕ is the amplitude angle. The simple

pendulum setup can be seen in Figure C.2.

C.2.1 Simplified pendulum motion

The simplified pendulum motion can be described, when the time-step dt is sufficiently small, using linear steps for which the acceleration is treated as constant. From standard literature the equations of motion are defined [5] and the second equation of motion

$$s = s_0 + v_0 t + \frac{1}{2} a t^2, \tag{C.2}$$

is valid when the acceleration is constant. This formula describes a linear step using the initial velocity and contribution from acceleration during a time-step. The kinematic equation describing the velocity based on the acceleration during a time-step and initial velocity

$$v = v_0 + at, \tag{C.3}$$

is defining the change of velocity.

In our case we are using vectors and a Taylor expansion series of (C.2) and (C.3) which yields

$$\begin{aligned} \Delta\vec{v} &= \vec{a}\Delta t + \frac{1}{2}\vec{a}'\Delta t^2 + \frac{1}{6}\vec{a}''\Delta t^3 + \frac{1}{24}\vec{a}'''\Delta t^4, \\ \Delta\vec{s} &= \vec{v}\Delta t + \frac{1}{2}\vec{a}\Delta t^2 + \frac{1}{6}\vec{a}'\Delta t^3 + \frac{1}{24}\vec{a}''\Delta t^4, \end{aligned} \tag{C.4}$$

respectively. Where $\vec{v} = \vec{v}_{prev} + k\Delta\vec{v}$, where $0 \leq k \leq \frac{1}{2}$. In the following study $k = \frac{1}{2}$ and a difference plot is presented in the results. In both equations we are using four terms, since the terms after become close to zero, $\frac{1}{120}\Delta t^5 = e^{-12} \approx 0$ where $\Delta t = 0.016$ seconds, and can be seen as noise in comparison to the four contributing terms.

C.3 Method

The equations of motion used in this paper (C.2) and (C.3) both require a constant acceleration and the motion is constrained to a straight line. In our case a linearization of a non-linear problem is utilized and the Taylor expansion series are valid.

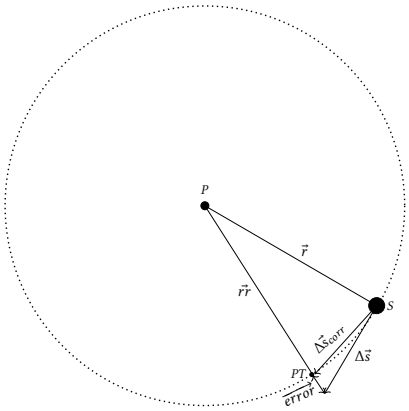

Figure C.2: The pendulum setup seen from the Y-plane intersection. The gravitational force is the only contributing force on the pendulum sphere S. With respect to the linearization of equations mentioned earlier, the step vector $\Delta\vec{s}$ is calculated using (C.4). The string $\vec{r}$ is the vector from the sphere to the pivot center P, $|\vec{r}|$ is the arm length for further use. $\vec{rr}$ is the new string vector for the next position after error correction, that is from the pivot P to PT.

C.3.1 Geometrical interpretation

The geometrical interpretation of a simple pendulum trajectory in $\mathbb{R}^3$ is that the shell of a sphere, and the intersection curve between the sphere and the Y-plane yields a simple pendulum trajectory in $\mathbb{R}^2$, which is illustrated in Figure C.2. For further calculations and notations, this paper is set in an affine space where the functions are point or vector valued elements in $\mathbb{R}^3$.

For further use, note the variables $\vec{G}, \vec{V}, \vec{R} \in \mathbb{R}^3$, where

$$\begin{aligned}\vec{G} &= [0, 0, -g],\\ \vec{V} &= [v_x, v_y, v_z],\\ \vec{R} &= \frac{\vec{r}}{|\vec{r}|},\end{aligned}$$

where $\vec{r} = S - P$ is the vector between the pivot point and the sphere center point, then $|\vec{r}| = l$. The total acceleration of the pendulum system is then

$$\vec{a} = \vec{G} - \langle \vec{G}, \vec{R} \rangle \vec{R} - \frac{\vec{V}^2}{|\vec{r}|}\vec{R},$$

where $\vec{G} - \langle \vec{G}, \vec{R} \rangle \vec{R}$ (Figure C.3) represents the acceleration contribution from gravity normal to the direction of the arm, and $\frac{\vec{V}^2}{|\vec{r}|}R$ (Figure C.4) denotes the inwards acceleration parallel to the direction of the arm. For the first case, the

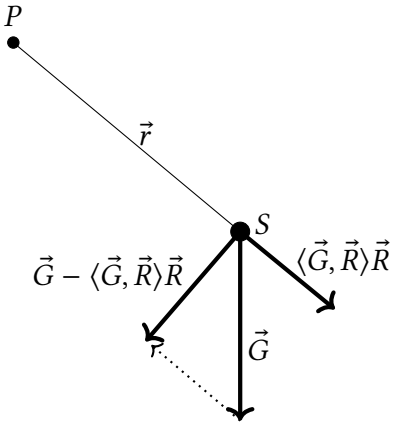

Figure C.3: Explanation of gravity contribution

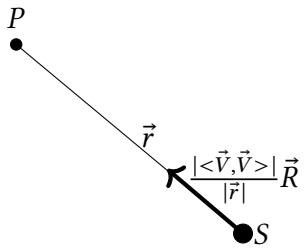

Figure C.4: Explanation of inward acceleration from circular motion

acceleration is calculated based on gravity. There are two initial conditions for the system, amplitude angle and starting velocity. We can easily check if (C.5) holds for some special cases, for instance, when $\vec{V}_0 = [0, 0, 0]$ and $\theta = 90°$ in the xy-plane, the only contribution is $\vec{a} = \vec{G} = [0, 0, -g]$.

$$\vec{a} = \vec{G} - \overbrace{\langle \vec{G}, \vec{R} \rangle \vec{R}}^{=0} - \frac{\overbrace{\vec{V}_0^{\,2}}^{=0}}{|\vec{r}|} \vec{R} \,. \tag{C.5}$$

All variables are either positions or vectors, and for every time-step we calculate the pendulum velocity generated by gravity and previous time-step information. Since the method requires a linear step, we have to restrict the time-step ($\Delta t < \epsilon$) and both the velocity and distance calculations are close to linear. In our case we have applied the constraint $\Delta t \leq 0.016$s, which corresponds to 60 calculations per second in our simulation framework.

$\hat{a}$	$\vec{a}$	$\vec{a}$	$\vec{a}$
o	$\hat{a}'$	$\vec{a}'$	$\vec{a}'$
o	x	$\hat{a}''$	$\vec{a}''$
o	x	x	$\vec{a}'''$

$\xrightarrow{Pre-evaluation}$

$\hat{a}$	$\vec{a}$	$\vec{a}$	$\vec{a}$
$\hat{a}'$	$\hat{a}'$	$\vec{a}'$	$\vec{a}'$
$\hat{a}''$	$\hat{a}''$	$\hat{a}''$	$\vec{a}''$
$\hat{a}'''$	$\hat{a}'''$	$\hat{a}'''$	$\vec{a}'''$

Table C.1: The table on the left hand side illustrates the three calculation steps (green) needed to obtain the third derivative, and as a correction step they are pre-evaluated. The table on the right hand side illustrates variables after obtaining the starting conditions for the system and we no longer have 0 and temporary values x. When the three steps are completed, (C.6) will be valid.

From (C.4) we need to know the derivatives of the total acceleration:

$$\vec{a}' = \frac{\hat{a} - \vec{a}}{\Delta t}, \quad \vec{a}'' = \frac{\hat{a}' - \vec{a}'}{\Delta t}, \quad \vec{a}''' = \frac{\hat{a}'' - \vec{a}''}{\Delta t}. \tag{C.6}$$

The variables $\hat{a}$, $\hat{a}'$, $\hat{a}''$ are denoting the values of the previous steps. A complete set of derivatives, requires using at least three initial steps as shown in Table C.1.

C.3.2 Error correction

Based on the proposed method, we realize that the linear step $\Delta\vec{s}$ will introduce an error to the system. This is compensated for by computing an error correction distance from the center of the sphere to the radius $|\bar{r}|$ of the motion which corresponds to the point PT in Figure C.2. The induced error has to be corrected by calculating the correct Δs and also the loss or gain of energy in this correction. The distance $\Delta\vec{s}_{corr}$ is then calculated

$$PT = P + \vec{r}\vec{r}\frac{|\vec{r}|}{|\vec{r}\vec{r}|}, \quad \Delta\vec{s}_{corr} = PT - S.$$

After calculating the new and corrected step $\Delta\bar{s}_{corr}$, it is necessary to correct the velocity based on the energy formulation $E_T = E_K + E_P$. E_T is the total energy contribution from kinetic E_K and potential E_P. The total energy before $E_T b$ and after $E_T a$ correction is calculated and the current velocity of the system is adjusted as follows

$$\vec{V}_{corr} = e_f \cdot \vec{V}, \quad e_f = \frac{E_{Tb}}{E_{Ta}}. \tag{C.7}$$

$\vec{V}_{corr}$ is the new velocity after correction and $\vec{V}$ is velocity we already have after $\Delta\vec{v}$ is added. Based on the distance and energy correction, there is a loss

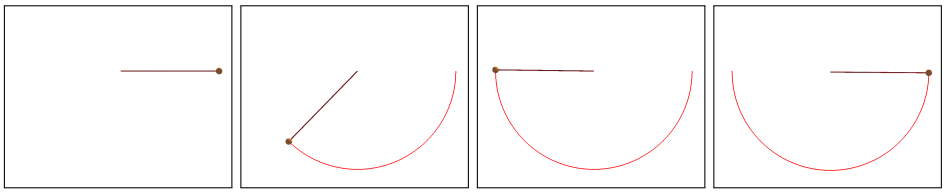

Figure C.5: Simulated pendulum motion using the simplified method proposed here. The trajectory and position of the pendulum sphere at four different timesteps.

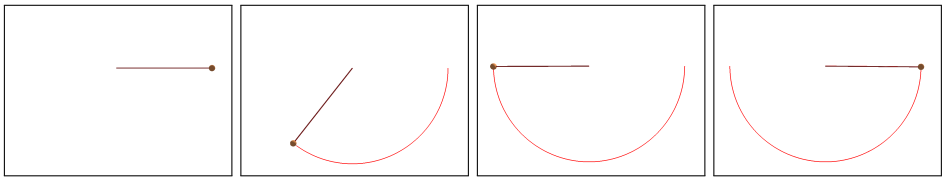

Figure C.6: Simulated pendulum motion using the numerical integration method Runge-Kutta. The trajectory and position of the pendulum sphere at four different time-steps.

or gain of energy after every correction step, which corresponds to e_f being close to $\epsilon < 1.0 < \epsilon$, and the velocity changes after the correction step to make up for the change in energy in the next calculation step.

C.4 Results

The method proposed here is a form of a predictor corrector method, which is usually applied to the partial differential equation to be solved by correcting the predicted values. In this case we assume that the position should be on the sphere shell, and are predicting both the step and velocity based on (C.4), which is close to the solution, but an error correction step is still required to take into account energy loss and adjust the velocity accordingly. The trajectory for a simple pendulum sphere attached at a pivot point is visualized in Figures C.5 and C.6. The two sets of figures represent our simplified geometrical approach to the solution by Runge-Kutta to solve the partial differential equation. Both methods compare and have exactly the same positions and period independent of initial amplitude angle. In Table C.2 we present a comparison of periods at selected initial angles, including large angles above 100°.

In the graphs presented in Figure C.7, the relation between both solutions is shown for various initial angles. The ratio between the two solutions is, in this case, off by one time-step, hence, the difference by 0.048 sseconds. The offset introduced here is caused by the method, which requires previous steps

Period for number of oscillations				
RK4 90°	Geo 90°	RK4 135°	Geo 135°	RK4-Geo
0	0	0	0	0
1.712	1.664	2.64	2.592	0.048
3.456	3.408	5.296	5.248	0.048
5.2	5.152	7.952	7.904	0.048
6.944	6.896	10.608	10.56	0.048
8.688	8.64	13.264	13.216	0.048
10.432	10.384	15.92	15.872	0.048

Table C.2: Table showing the different periods using Runge Kutta 4 and the geometrical approach. The last column, Rk4-Geo, is to show that the difference is constant.

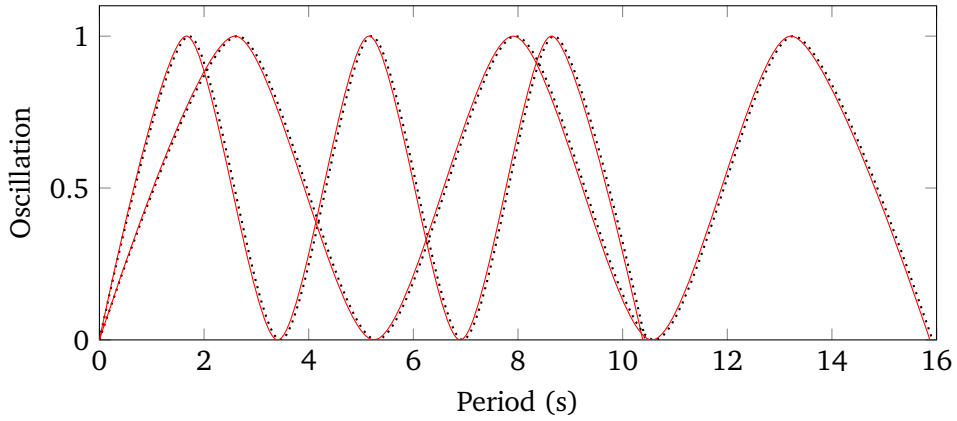

Figure C.7: Period comparison for initial angles of 90° and 135°. Black dotted line is the solution using Runge Kutta 4, Red curve is the solution using geometrical approach. The graph plots the three first oscillations.

in order to both calculate and correct the next step, and we are then behind by one step.

From Equation (C.4) we are using the velocity contribution $\vec{v} = \vec{v}_{prev} + k\Delta\vec{v}$. By comparing the energy correction difference using $k = 0, \frac{1}{3}, \frac{1}{2}$, we show that they are all close to 1, but the best value seems to be $k = \frac{1}{3}$ which corresponds to the green curve shown in Figure C.8. The graph presents the error correction for one complete oscillation with an initial angle of 135°.

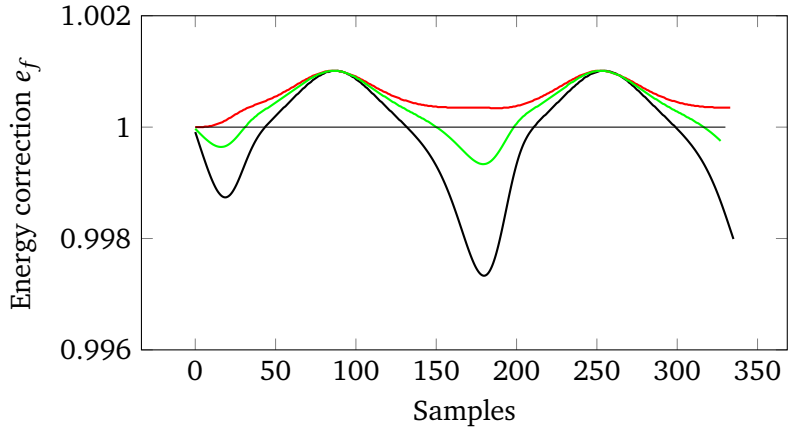

Figure C.8: Graph showing the energy correction term e_f from Equation (C.7) as a result of varying the velocity contribution using $\vec{v} = \vec{v}_{prev} + k\Delta\vec{v}$. $k = 0$ is the black curve, $k = \frac{1}{3}$ is the green curve and $k = \frac{1}{2}$ is the red curve. In the present study, k has been set to $\frac{1}{2}$

C.5 Conclusion

In this paper we have used a Taylor series expansion of two well-known equations for motion and derived a system which approximates the simple pendulum motion. We have compared our method to a numerical solution of a partial differential equation describing the simple pendulum motion for large initial amplitudes, addressed in Table C.2 and Figure C.7. Table C.2 and Figure C.7. An energy correction difference was presented in Figure C.8 using two different approaches for calculating the velocity contribution. This measurement was conducted using an initial angle of 135°. There are in general two states worth mentioning here, the maxima and minima. The maxima corresponds to where the velocity is greatest (the bottom point of the pendulum motion) and the minima is when the pendulum is changing direction (the top of the trajectory at the initial angle). From the three values of k tested in this work, we conclude that the best solution is when the area is smallest, hence, $k = \frac{1}{3}$ provides a best approximation of the new velocity. The solution shows promising results and for further validation we have employed a change in the data, where we have replaced the gravity vector with acceleration data gathered from a smart phone application. Initial tests shows pendulum motions with friction from the air drag as well as loss of energy from the friction in the string attached to the pendulum and a pivot point. For research and development purposes we have created a prototype simulation framework that includes the smart phone application for recording sensor data. The simulation framework contains solutions for the previously mentioned simple pendulums. The presented method is evaluated

with respect to applications, where the acceleration is represented using sensor data. The relation of simplicity between our construction and models for reverse engineering of physics and mechanics equations from sensor measurements is apparent and connected. Papers where reverse engineering in physics and mechanics problems are investigated can be found in [10, 11, 8, 4].

Bibliography

[1] Gregory Baker, James Blackburn, and Kenneth Krane. *The Pendulum: A Case Study in Physics*. Vol. 59. July 2006. DOI: 10.1063/1.2337835 (cit. on p. 91).

[2] Augusto Beléndez et al. "Approximation for a large-angle simple pendulum period." In: *European Journal of Physics* 30 (Feb. 2009). DOI: 10.1088/0143-0807/30/2/L03 (cit. on p. 92).

[3] Carl Bender, Darryl Holm, and Daniel Hook. "Complex Trajectories of a Simple Pendulum." In: *J. Phys. A* 40 (Sept. 2006), pp. 81–90. DOI: 10.1088/1751-8113/40/3/F01 (cit. on p. 92).

[4] Juan Castro Palacio et al. "Using a smartphone acceleration sensor to study uniform and uniformly accelerated circular motions." In: *Revista Brasileira de Ensino de Física* 36 (June 2014), pp. 1–5. DOI: 10.1590/S1806-11172014000200015 (cit. on p. 100).

[5] Glenn Elert. *The Physics Hypertextbook*. Online. https://physics.info/motion-equations/. 1998-2020 (Accessed 2020-31-03) (cit. on p. 93).

[6] Colin Gauld. *Pendulums in the Physics Education Literature: A Bibliography*. Vol. 13. 2004, pp. 811–832. DOI: 10.1007/s11191-004-9508-7 (cit. on p. 91).

[7] Richard Kidd and Stuart Fogg. "A simple formula for the large-angle pendulum period." In: *The Physics Teacher* 40 (Feb. 2002), pp. 81–83. DOI: 10.1119/1.1457310 (cit. on p. 92).

[8] Jochen Kuhn and Patrik Vogt. "Analyzing spring pendulum phenomena with a smart-phone acceleration sensor." In: *The Physics Teacher* 50.8 (2012), pp. 504–505. DOI: 10.1119/1.4758162 (cit. on p. 100).

[9] Mario Molina. "Simple Linearizations of the Simple Pendulum for Any Amplitude." In: *The Physics Teacher* 35 (Oct. 1997). DOI: 10.1119/1.2344777 (cit. on p. 92).

[10] Patrik Vogt and Jochen Kuhn. "Analyzing free fall with a smartphone acceleration sensor." In: *The Physics Teacher* 50 (Mar. 2012), pp. 182–183. DOI: 10.1119/1.3685123 (cit. on p. 100).

[11] Patrik Vogt and Jochen Kuhn. "Analyzing simple pendulum phenomena with a smartphone acceleration sensor." In: *The Physics Teacher* 50.7 (2012), pp. 439–440. DOI: 10.1119/1.4752056 (cit. on p. 100).

Contribution D

This appendix contains three conference talks with unpublished extended material

Blending spline applications

Aleksander Pedersen
Faculty of Engineering Science and Technology
UiT The Arctic University of Norway, Norway

D.1 - Surface construction with arbitrary inner and outer boundaries, Multiphysics 2014, Sofia, Bulgaria, Abstract issn 2409-1669/2409-7527

D.2 - Heat diffusion problem, 9th International Conference on Mathematical Methods for Curves and Surfaces, Tønsberg, Norway, Conference talk

D.3 - Terrain and level curves, 9th International Conference on Curves and Surfaces, Arcachon, France, Conference talk

D BLENDING SPLINE APPLICATIONS

Conference talks and contributions

Aleksander Pedersen

Faculty of Engineering Science and Technology
UiT The arctic University of Norway
Norway

Abstract This section consist of contributions from conference talks and abstracts with preliminary paper material.

D.1 Surface construction with arbitrary inner and outer boundaries

This section is an extended part of the contribution included as Appendix A. The construction presented in this section is extending the previous construction with both inner and outer boundaries from arbitrary curves. Terminal ballistics is described as the behavior of a projectile at the end of its travel and how it affects the target, with a wide variety of phenomena such as perforation of a target material. Creating realistic models with effects of terminal ballistics can be challenging, and surface perforation by projectile interaction usually depends on a detailed case study. The problem can be grouped into two parts; (a) realistic representation of the material in terms of geometry, and (b) realistic simulation of the effects of terminal ballistics onto the target material.

Non-uniform rational B-splines (NURBS) have become the de-facto standard for the representation of models within the field of computer-aided design (CAD). However, finite elements analysis (FEA) has been a much more common building block in models for simulations and numerical computations of partial differential equations (PDEs). Isogeometric analysis (IGA) was introduced by Hughes et.al. [10] as an attempt to bridge the gap between the two paradigms. The main goal with IGA is to use a common representation for CAD and FEA, without the need to convert between different representations. Several spline based methods [6, 7, 8, 14, 15] are among the present approaches on IGA.

D.1.1 Surface modeling

Terminal ballistics describes the regime that a projectile enters at the conclusion of its flight. Examples of such regimes are provided in Figure D.1.

Taking target penetration as an example of terminal ballistics, the theoretical models for target penetration will have to be explored, depending on the materials and surface properties. Furthermore, the individual penetration theories have to be solved and computed separately; there are several different models just for the case of penetration and perforation of metals, not to mention composite structures and soils or fluids. As a basic example, we mention that S. Jacobson [3] refined the concept that there are different energy relationships for plugging and piercing:

$$E_{plug} = force \cdot distance \approx \pi \cdot dt \cdot Y_s \cdot t,$$

$$E_{piercing} = Y_{flow} \cdot V \approx \frac{\pi d^2}{4} \cdot t \cdot Y_{flow},$$

where Y_s is the shear yield strength of the material, V is the volume of the

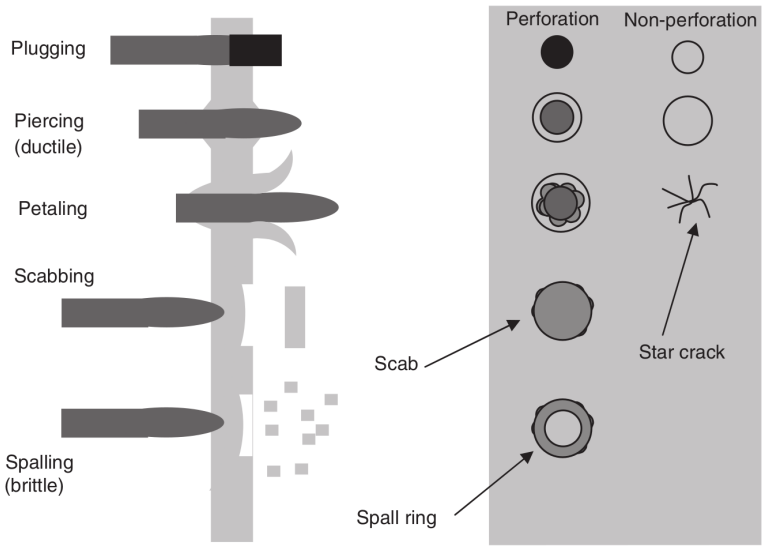

Figure D.1: Image from ballistics: theory and design of guns and ammunition [4]: Illustrating some of the different target failure modes

plug, and Y_{flow} is the flow or plastic yield stress of the target material.

In this section we consider the geometry of a thin ductile surface after it has undergone projectile piercing. The purpose is to illustrate examples of how the geometry could be shaped when applying calculations. The example considered here is a thin plate deformation, and, to simplify the problem, there is only a deformation on the plate itself; i.e. the bullet is not deformed and its mass is preserved. In Appendix A we proposed a construction using the blending method to represent effects of terminal ballistics on a target with constraints as outlined in the previous sections.

For the extended version we present here, the underlying geometric construction is Coons surface patches as local coefficients illustrated in Appendix A, Figure A.2.

D.1.2 Results

The resulting surface using the above construction has both inner and outer boundaries which is specified by the blending construction. Two examples from Appendix A using the method to represent inner holes in a tensor product surface as illustrated in Figure A.3 are extended with an outer boundary as shown in Figures D.2 to D.4.

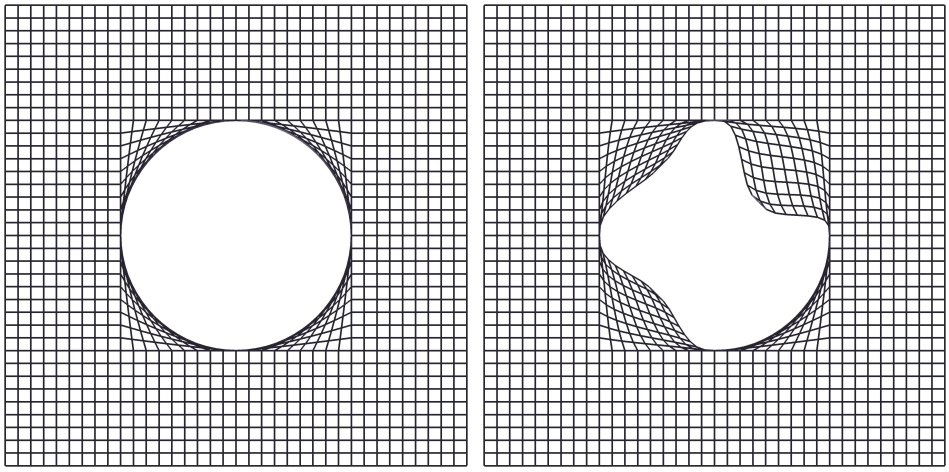

Figure D.2: An illustration showing the parametric domain of a surface construction limited by an inner and outer global boundary curve. The surface is constructed using Coons patches as local coefficients. Each Coons patch is constructed using the boundary curves, which are subcurves of the inner and outer global boundary curves. Figure on the left hand side; The inner boundary curve is a circle. Figure on the right hand side; The inner boundary curve is a free form blending-type spline curve.

Figure D.2 shows the parametric lines for two examples of inner boundary curves, using the proposed method.

Figure D.3 shows a single continuous parametric line (shown in red) in the parametric domain.

D.1.3 Conclusion

We have demonstrated the representation of custom-shaped surface holes, defined as boundary curves using a blending type spline construction. The proposed method appears to be a promising alternative representing effects of terminal ballistics, at least for the simplified models of thin plate deformation considered in this work. We regard the use of Boolean sum local surfaces in this construction as an alternative to trimmed curves, which can be found in most CAD applications. Benefits of the proposed method when compared to NURBS are increased control and precision when shaping the boundary curves. This follows from the combination of using local functions as spline coefficients and the transfinite Hermite interpolation property, which states that the positions and all existing derivatives of the local functions are interpolated by the global spline construction at the knots. The construction presented in this section and those in Appendix A are types of local surface constructions that have

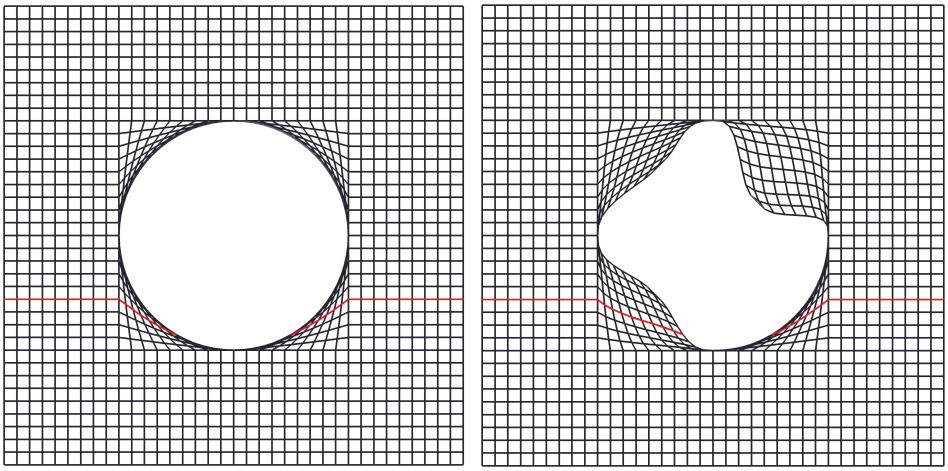

Figure D.3: Even though the geometry is discontinuous e.g. G^0, the domain is complete and we illustrate a single continuous parametric line $u = [0, 1]$ in $v = 0.367$.

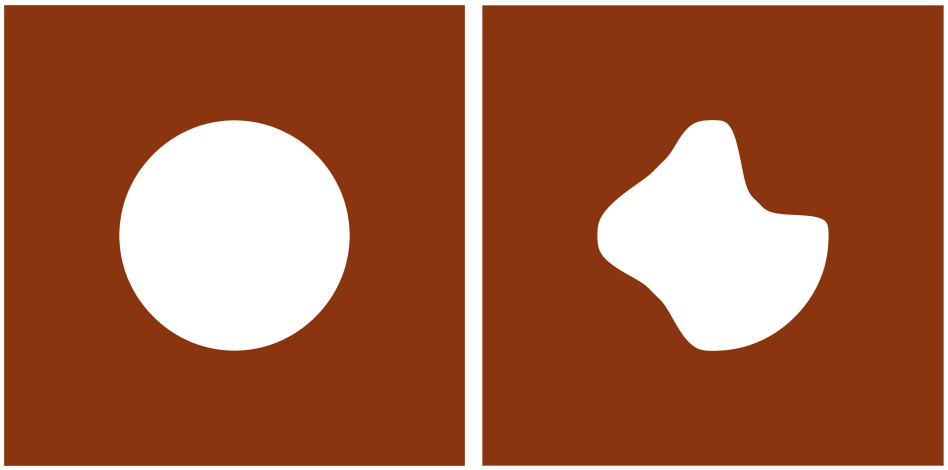

Figure D.4: An illustration showing a shaded version of Figure D.2. The local geometry is constructed using Coons patches from local curve segments on the two global boundary curves. Construction of the inner hole is made possible by inner double knots pointing to subcurves from an implicit inner boundary limiting the hole. On left hand side; The inner boundary curve is a circle. On right hand side; The inner boundary curve is a free form blending-type spline curve.

properties making them interesting and suitable for simulations as an attempt at Isogeometric analysis (IGA).

D.1.4 Future work

Modeling the rotational energy of a projectile affecting a target by applying affine transformations on local surfaces could reveal potential simple solutions and should be investigated further. Another topic for future work is to extend the method to a tensor product of higher dimension than the two dimensional problem considered here.

D.2 Heat diffusion problem

The work done in this section was presented at the Mathematical Methods for Curves and Surfaces conference in 2016 [12].

D.2.1 From previous contribution

In Appendix A and Section D.1 we were exploring modeling using a blending type spline construction. By employing knot insertion we can create geometry with discontinuities, e.g. holes, that can be deformed in such a way that they represent penetration/perforation of a surface subjected to forces caused by bending or projectile interaction. One possible application area is to model heat transfer problems where we have both inner and outer boundaries in the geometry. In [12] we were discussing preliminary results and tests using the blending construction with the following partial differential equation

$$\frac{\partial u}{\partial t} = \alpha \nabla^2 u = \alpha \left(\frac{\partial^2 u}{\partial x^2} + \frac{\partial^2 u}{\partial y^2} \right),$$
$$u(x, y, 0) = t_0,\ u(0, y, t) = u(a, y, t) = T_l,\ u(x, 0, t) = u(x, b, t) = 0.$$

Solving the heat diffusion equation we used two approaches, both constructed using the following central finite difference scheme:

$$T_{i,j}^{k+1} = T_{i,j}^{k} + \triangle t \alpha \left(\frac{T_{i,j+1}^{k} + T_{i+1,j}^{k} - 4T_{i,j}^{k} + T_{i-1,j}^{k} + T_{i,j-1}^{k}}{h^2} \right), \tag{D.1}$$

where $h = \mathrm{d}x \cdot \mathrm{d}y = 1$ and $\triangle t \alpha = 1$, and

$$T_{i,j}^{k+1} = T_{i,j}^{k} + \triangle t \alpha \left(\frac{T_{i,j+1}^{k} + T_{i+1,j}^{k} - 4T_{i,j}^{k} + T_{i-1,j}^{k} + T_{i,j-1}^{k}}{h^2} \right), \tag{D.2}$$

where $h = \mathrm{d}x \cdot \mathrm{d}y \neq 1$ and $\frac{\triangle t \alpha}{h^2} = [0.1, 0.3]$.

The employed blending type construction can be seen in Figure D.6 where we have two surface constructions illustrating circular inner and outer boundaries. For this special case where we are visualizing the heat transfer, we are using the constuction consisting of straight lines as outer boundary, but circular inner hole. The global surface shown in Figure D.5 illustrates how the Coons [5] local surfaces are constructed using spatial boundary curves.

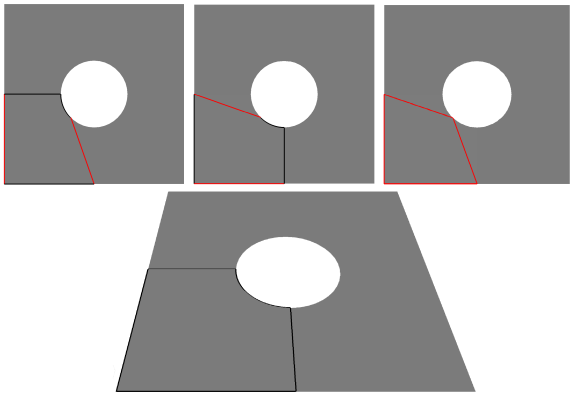

Figure D.5: Showing the four spatial curves (marked in red) used to create the Coons surface in the bottom part. Coons construction is taking the sum of the two first curves (fig 1 and fig 2) and subtracting the total product (fig 3) resulting in outlined quarter of the bottom surface.

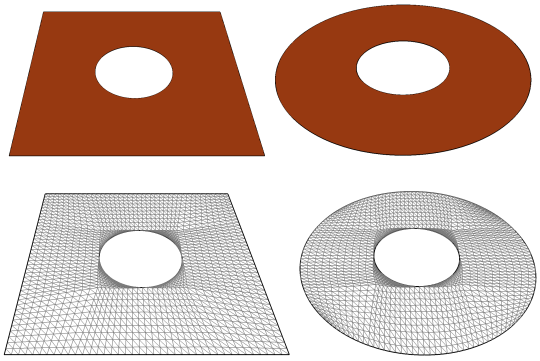

Figure D.6: The illustration on the left hand side has a fixed outer boundary and a circular inner boundary. The illustration on the right hand side shows the construction using circular inner and outer boundaries.

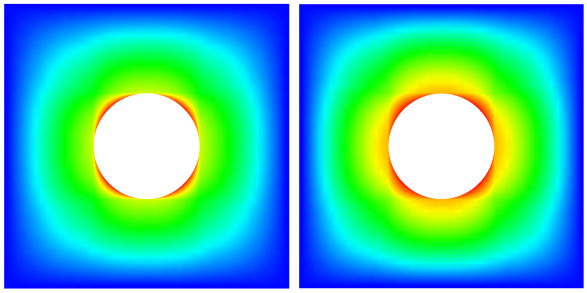

Figure D.7: Solution based on the central finite difference method used to solve the partial differential (D.2.1). The figure on the left is a regular case with $dx = dy = 1$. The figure on the right is using the second method(some correction is applied), where the parameterization is taken into consideration as dx & dy

D.2.2 Results/examples

The preliminary study demonstrated promising results and an illustration of the heat diffusion problem on the previously mentioned construction using (D.1) and (D.2). The heat transfer at a specific timestep is shown in Figure D.7. The difference shown in Figure D.7 is a result on the two different parameterizations introduced in (D.1) and (D.2).

D.2.3 Concluding remarks

In this work we presented preliminary results using a blending type spline construction in the context of a heat diffusion problem. The geometry and analysis based on the discrete form of (D.2.1) are presented as a visualization shown in Figure D.7. The technique presented here is not using the same basis functions solving the partial differential equation as for the geometry, but still yield interesting properties with respect to discontinuous geometry and visualizations.

D.2.4 Future work

Using a blending type spline construction in the context of partial differential equations shows promising applicable areas as well as properties suitable for visualization and analysis that should be investigated further. The initial work forms a basis with elements found in the context of IGA.

D.3 Terrain and level curves

The work done in this section was presented at the Curves and Surfaces conference in 2018 [13]. In this work we explored different constructions for terrain approximation using a blending type spline construction. In addition, level curves (intersection curves) have been investigated and two terrain generation methods have been proposed. The representation of the Earth's surface in digital form, digital terrain model(DTM) can be useful when studying properties for applications. Level curves [1] is one of several possible ways to describe the properties of terrain. Other methods have been investigated previously, such as radial basis functions [11], digital elevation model (DEM) from contours [9], and piecewise optimal triangulations on data [2]. The data (points) used for all constructions are gathered from www.hoydedata.no [16], which offers elevation data and presents a point-cloud. The pointcloud we used in this work consists of several million points, but for this construction we are interested in point data representing the ground. A view of the point-cloud represented with ranging colors based on the z-value is shown in Figure D.8 (top illustration). The scope of this contribution can be summarized as follows:

- Terrain construction using a subset of the scattered point-cloud (ground only)
- Triangulate the given point-cloud using Delaunay triangulation
- For visualization purposes, only a part of the triangulated terrain is used.
- Create a blending spline surface given two different constructions
- Create level curves using an intersection algorithm on a parametric surface

D.3.1 Surface construction

The total size of the point-cloud used was 2.2M points (lidar point-cloud $P_c(X, Y)$) and the triangulated terrain surface used only a portion of the total size; 11217 points. We present two surface constructions approximating the triangulated surface for a given section. Both surfaces are tensor product surfaces, but are constructed using two different schemes.

A. Tensor product surface 1 (Figure D.11).

    1. The points used in this construction are obtained by evaluating the triangulated surface on a uniformly distributed grid, which is a

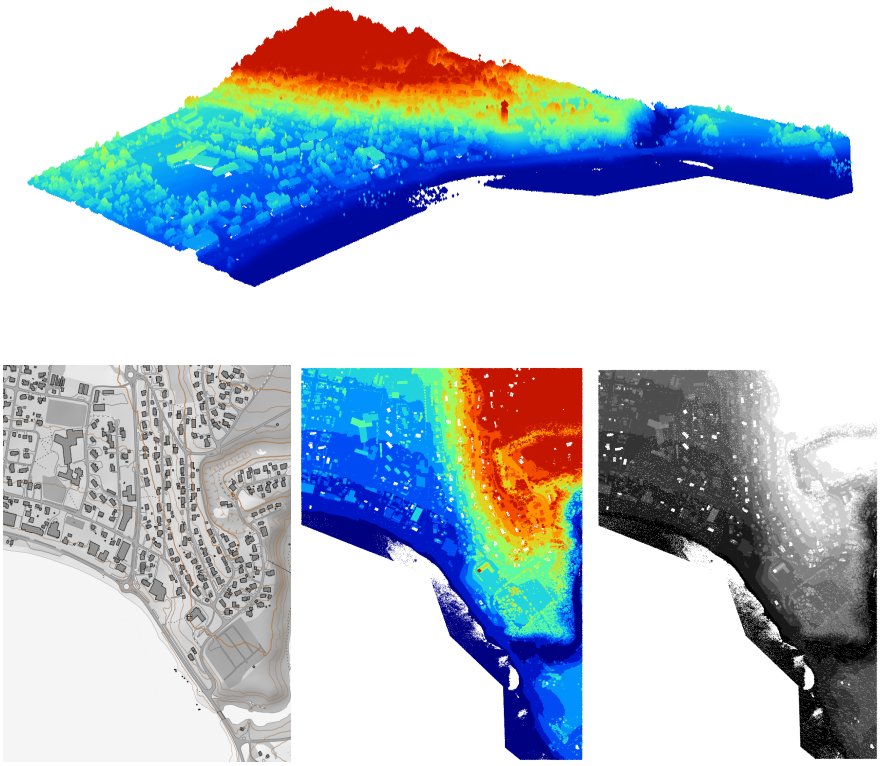

Figure D.8: Here we show the pointcloud data used in this contribution, where: Top: 3D view of lidar pointcloud colored using z-value, Bottom Left: Structural view, Center: Color seen from above Right: Grayscale seen from above

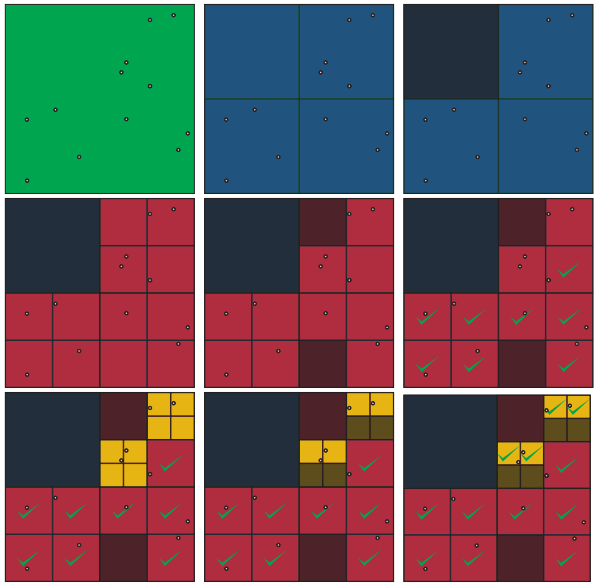

Figure D.9: Here we illustrate the region subdivision; finding points inside a given region by dividing every section containing more than 1 point into 4 smaller regions.

subset $S_{x,y} \in P_c(X, Y)$. The total number of points is 735 for $S_{x,y}$.

2. The points obtained after evaluation are used for the blending type spline construction.

3. The local surface coefficients for this tensor product surface are constructed by Hermite interpolation of the positions (points) and the respective derivatives obtained by divided differences for the total set of points.

B. Tensor product surface 2 (Figure D.12).

1. The space containing all points are separated into regions(grid). Each region represents a box containing zero or more points D.9.

2. For every box we calculate the average height of all containing points and create a horizontal plane within the bounds of each box, similar to a voxel construction. If a box/region does not contain any points, the closest valid neighbor is chosen.

3. The blending type spline construction is then using each of the horizontal planes as local surface coefficients.

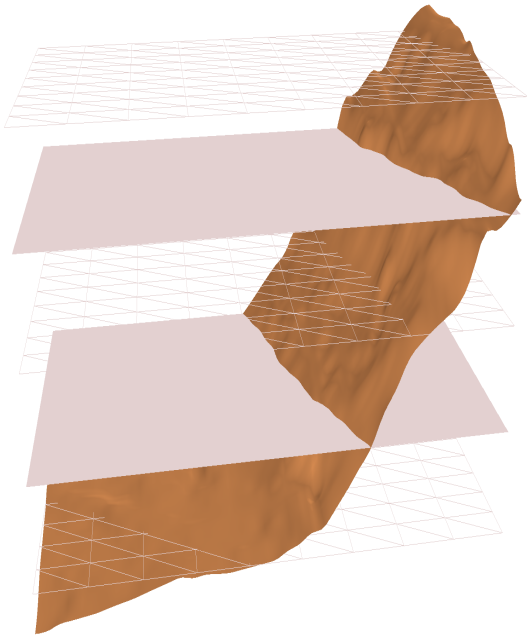

Figure D.10: This illustration shows the horizontal intersection planes for given z-values.

D.3.2 Level curves

The surface level curves are constructed using two intersection algorithms, one triangle based and one using evaluation of the tensor product surface in u and v directions. The level curve is generated by intersecting the constructed surface with horizontal planes along the z-axis, as shown in Figure D.10.

D.3.3 Results

The resulting tensor product surface using the first construction (A. from Section D.3.1) is shown in Figure D.11. This construction uses Bezier surfaces of second degree as local coefficients which leads to a smooth terrain surface. Comparing this construction to the triangulated reveal areas prone to bigger differences. Such areas are located where the steepness of the triangulated surface exceeds a certain angle. For planar sections the two surfaces almost coincide.

The resulting tensor product surface using the second construction (B. from Section D.3.1) is shown in Figure D.12. This construction is based on horizontal planes evaluated at equidistant samples along each direction for a region. Since these planes are horizontal and not inclined in any direction, the resulting surface will have "jumps" where the steepness exceeds a certain angle. This

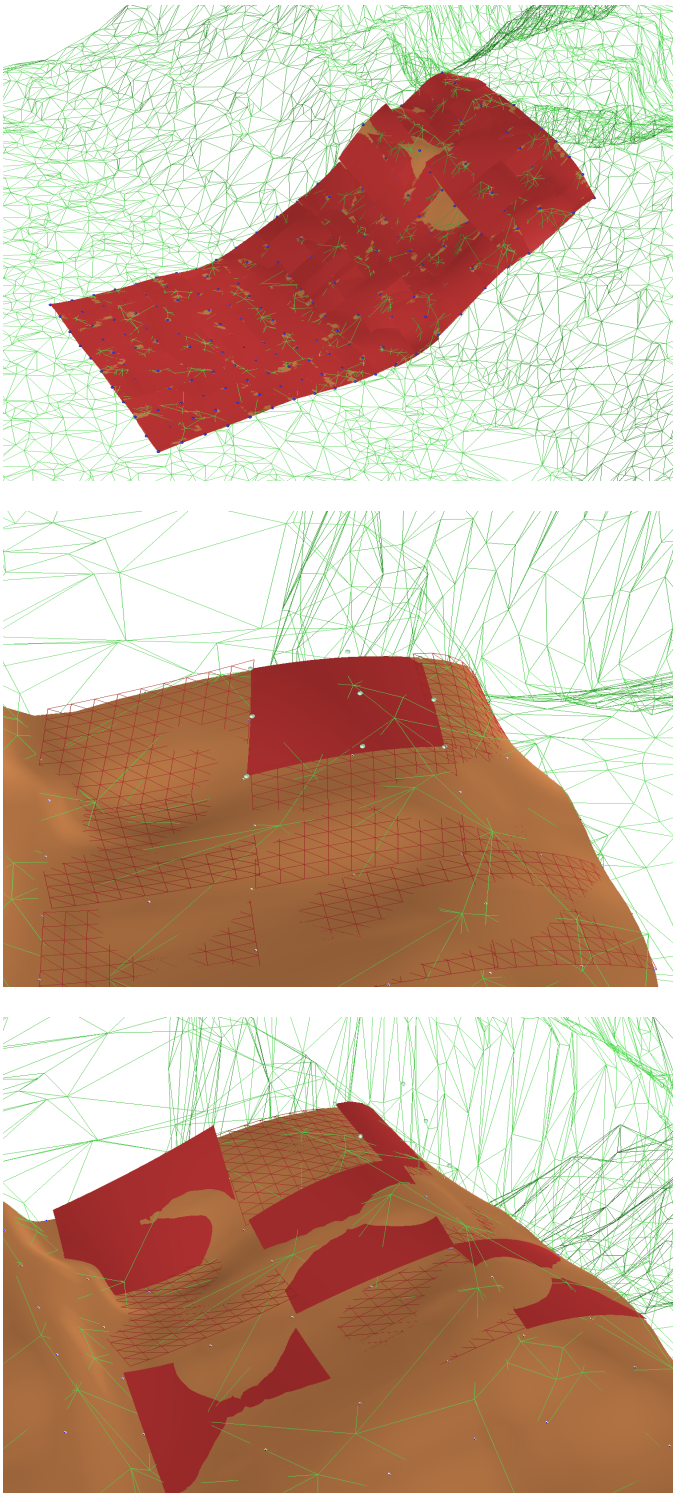

Figure D.11: The three figures presented here show the tensor product surface from construction (A.). The local surfaces are shown in red, where the control points for each local surface are shown using green spheres. The local surfaces used here are Bezier surface constructions.

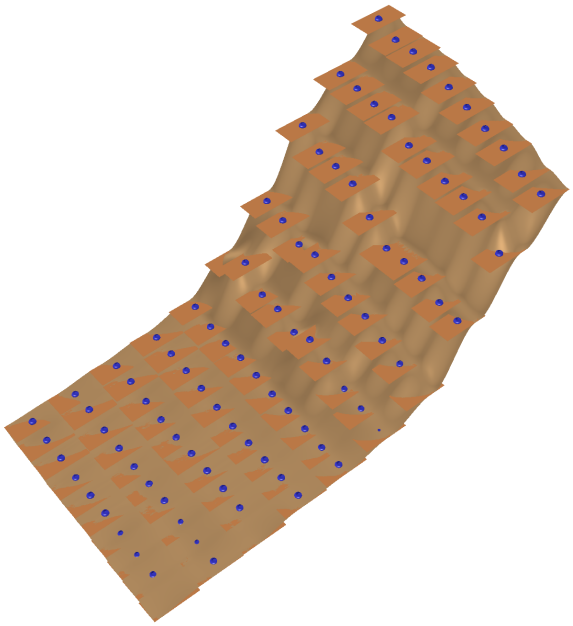

Figure D.12: The illustration presented here shows the tensor product surface from construction (B.). The local horizontal planes are shown in beige where the center point has a blue sphere.

construction also has high accuracy for planar sections.

Using the two different algorithms for constructing level curves by intersecting the surface construction (A. and B. from D.3.1) with horizontal planes we present the results as shown in Figure D.13. The intersection algorithm used here are only valid within certain conditions and are not suited for multi-intersection joints and crossing paths.

A visualization of the three surfaces, triangulated and the two tensor surface constructions are illustrated in Figure D.14. The preliminary analysis based on visual confirmation shows that the two constructions both indicate well the resulting terrain, with some areas prone to lower precision. As described earlier, the second construction will have higher error estimates when the terrain inclination exceed a certain angle.

An error difference between the two tensor product surfaces compared to the triangulated surface is shown in Figure D.15.

D.3.4 Concluding remarks

In this section we presented two different constructions for terrain generation by interactive modeling using a blending type spline construction where properties such as level curve information is included. An initial error estimate

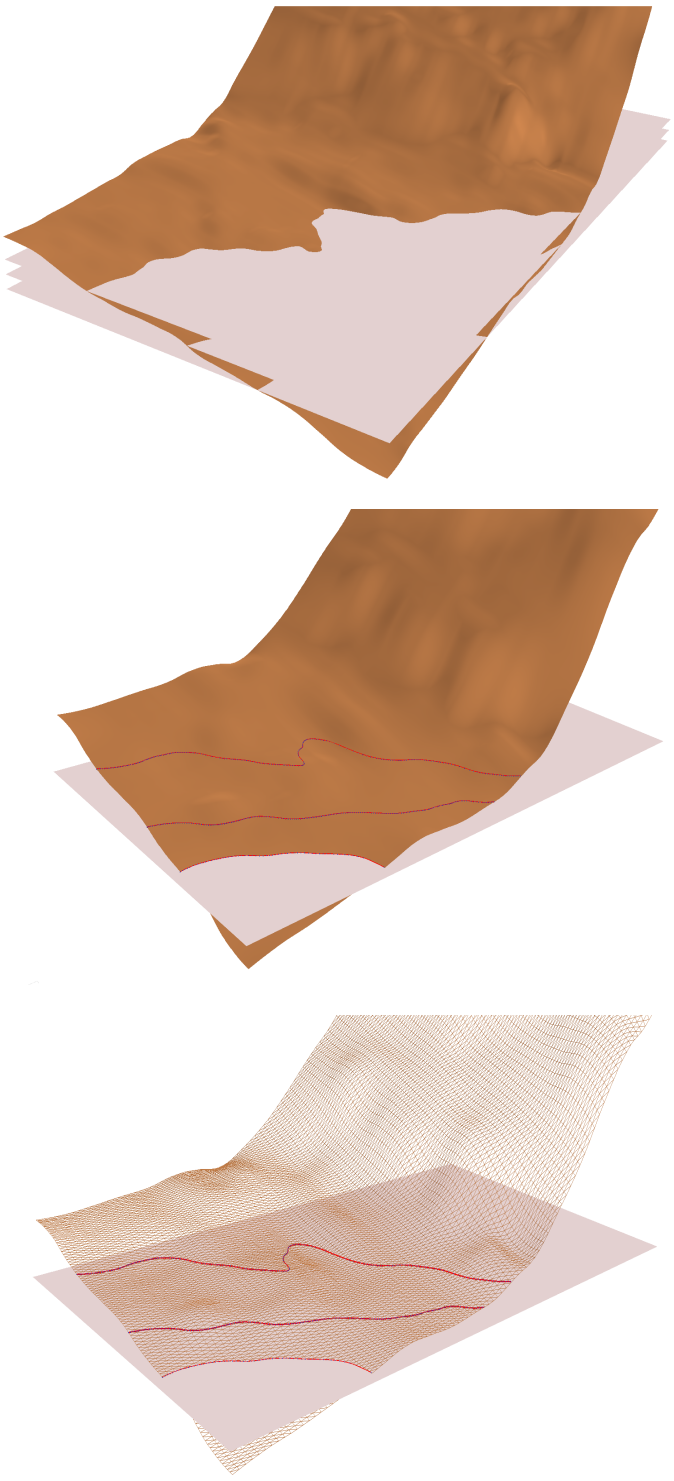

Figure D.13: The intersection algorithms generate level curves which are illustrated here as curves. The intersection is performed using horizontal planes at given z-values and the surface construction (A.) previously mentioned in Section D.3.1

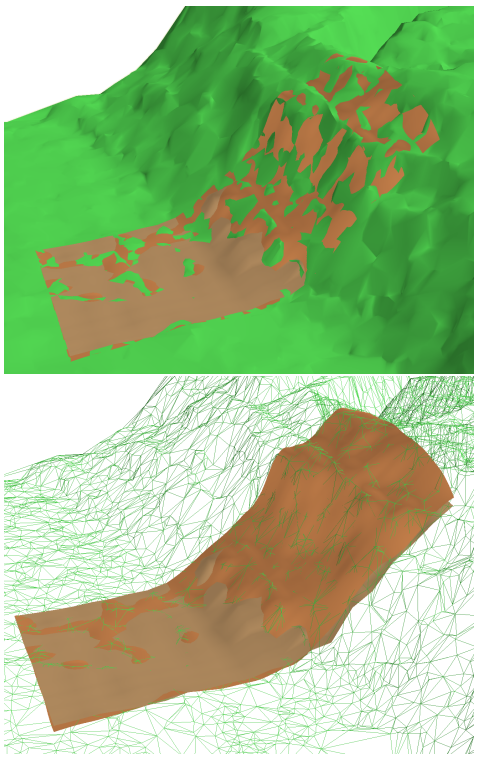

Figure D.14: Here we show a comparison of the three surfaces against each other. The green surface is the triangulated surface, brown color represents the surface construction from (A.) and the beige color represents the surface construction from (B.)

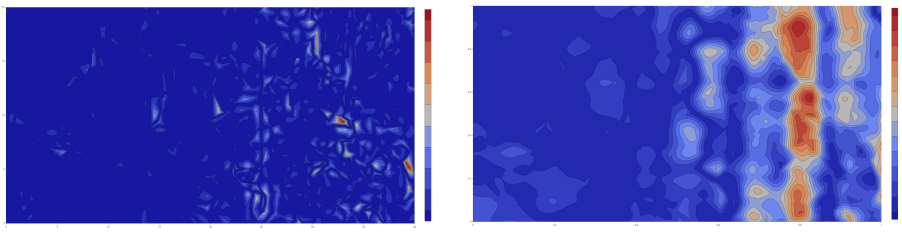

Figure D.15: Initial comparison between the two surface constructions (A. and B.) using a difference plot against the triangulated surface. (A.) is shown on the left. (B.) is shown on the right.

is presented using a difference plot (height difference) between each of the two surface constructions against the triangulated surface. Based on the error estimate we can conclude that both constructions have areas which are prone to bigger differences, but the first construction has a higher accuracy than the second method. The two intersection algorithms both generate level curves for given horizontal intersection planes. The accuracy between both algorithms has not been studied in the current work.

D.3.5 Future work

For future reference, a surface construction using level curves as input for local coefficients in the blending type spline construction should be investigated. Application areas where level curve information and interactive terrain geometry are suitable should be explored, with focus towards areas such as path planning and grids (pipelines, power, roads). The editing properties of the constructions presented here should present interesting properties when investigating terrain prone to flooding, avalanches, snow and wind. Another topic for future applications is seafloor modeling with focus towards platforms and bridge planning. Based on the initial assessment of the surface constructions, an interesting topic for the second construction would be to use inclined planes instead, describing position and tangent to the triangulated surface at the center point.

Bibliography

[1] Luis Gerardo de la Fraga Abigail Martinez Rivas. "Terrain Reconstruction from Contour Maps." In: *Proceedings of the 14th International Congress on Computing (CIC2005)* (2005) (cit. on p. 112).

[2] Martin Bertram et al. "Piecewise optimal triangulation for the approximation of scattered data in the plane." In: *Computer Aided Geometric Design* 17.8 (2000), pp. 767–787. ISSN: 0167-8396. DOI: https://doi.org/10.1016/S0167-8396(00)00026-1. URL: http://www.sciencedirect.com/science/article/pii/S0167839600000261 (cit. on p. 112).

[3] Donald E Carlucci and Sidney S Jacobson. *Ballistics: theory and design of guns and ammunition*. 2nd. Broken Sound Parkway: CRC Press, 2010 (cit. on p. 104).

[4] Donald E. Carlucci and Sidney S. Jacobson. *Ballistics: Theory and Design of Guns and Ammunition*. 2nd. CRC Press, 2014. ISBN: 978-1-4665-6437-4 (cit. on p. 105).

[5] Steven A. Coons. *Surfaces for Computer-Aided Design of Space Forms*. Project MAC-TR-41. Massachusetts, USA: Massachusetts Institute of Technology, 1967 (cit. on p. 109).

[6] Jiansong Deng, Falai Chen, and Yuyu Feng. "Dimensions of spline spaces over T-meshes." In: *Journal of Computational and Applied Mathematics* 194.2 (Oct. 2006), pp. 267–283. ISSN: 0377-0427. DOI: 10.1016/j.cam.2005.07.009 (cit. on p. 104).

[7] Tor Dokken, Tom Lyche, and Kjell Fredrik Pettersen. "Polynomial splines over locally refined box-partitions." In: *Computer Aided Geometric Design* 30.3 (2013), pp. 331–356. ISSN: 0167-8396. DOI: http://dx.doi.org/10.1016/j.cagd.2012.12.005. URL: http://www.sciencedirect.com/science/article/pii/S0167839613000113 (cit. on p. 104).

[8] C. Giannelli, B. Jüttler, and H. Speleers. "THB–splines: The truncated basis for hierarchical splines." In: *Computer Aided Geometric Design* 29.7 (2012), pp. 485–498. DOI: 10.1016/j.cagd.2012.03.025 (cit. on p. 104).

[9] Michael B. Gousie and Wm. Randolph Franklin. "Constructing a Dem from Grid-based Data by Computing Intermediate Contours." In: *Proceedings of the 11th ACM International Symposium on Advances in Geographic Information Systems*. GIS '03. New Orleans, Louisiana, USA:

ACM, 2003, pp. 71–77. ISBN: 1-58113-730-3. DOI: 10.1145/956676.956686 (cit. on p. 112).

[10] T. J. R. Hughes, J. A. Cottrell, and Y. Bazilevs. "Isogeometric Analysis: CAD, Finite Elements, NURBS, Exact Geometry and Mesh Refinement." In: *Computer Methods in Applied Mechanics and Engineering* 194.39-41 (Oct. 2005), pp. 4135–4195. ISSN: 00457825. DOI: 10.1016/j.cma.2004.10.008 (cit. on p. 104).

[11] C. Rabut (Eds.) L.L. Schumaker A. Cohen. "Numerical techniques based on radial basis functions." In: *Curve and Surface Fitting: Saint-Malo 1999* (1999) (cit. on p. 112).

[12] A. Pedersen. "Arbitrary holes in surfaces using blending type spline constructions." In: 9th International Conference on Mathematical Methods for Curves and Surfaces (Tønsberg, Norway). Conference talk and abstract at 9th International Conference on Mathematical Methods for Curves and Surfaces. 2016 (cit. on p. 109).

[13] A. Pedersen. "Terrain level curves using blending splines." In: *Terrain level curves using blending splines*. 9th International Conference on Curves and Surfaces (Arcachon, France). Conference talk and abstract at 9th International Conference on Curves and Surfaces. 2018 (cit. on p. 112).

[14] Thomas W. Sederberg et al. "T-splines and T-NURCCs." In: *ACM SIGGRAPH 2003 Papers*. SIGGRAPH '03. San Diego, California: ACM, 2003, pp. 477–484. ISBN: 1-58113-709-5. DOI: 10.1145/1201775.882295. URL: http://doi.acm.org/10.1145/1201775.882295 (cit. on p. 104).

[15] A.V. Vuong et al. "A Hierarchical Approach to Adaptive Local Refinement in Isogeometric Analysis." In: *Computer Methods in Applied Mechanics and Engineering* 200 (Dec. 2011), pp. 3554–3567. DOI: 10.1016/j.cma.2011.09.004 (cit. on p. 104).

[16] Kartverket - www.kartverket.no. *Høydedata - Vis hele Norge*. https://hoydedata.no/LaserInnsyn/. 2018 (Accessed 2018-06-26) (cit. on p. 112).

Paper E

The included paper is a reprint of

Targeted sanding and its impact on heavy hauler pull force and surface friction

Tanita Fossli Brustad, Aleksander Pedersen and Børre Bang
Faculty of Engineering Science and Technology
UiT The Arctic University of Norway, Norway
Submitted for review

E TARGETED SANDING AND ITS IMPACT ON HEAVY HAULER PULL FORCE AND SURFACE FRICTION

This paper is submitted for review

Tanita Fossli Brustad, Aleksander Pedersen and Børre Bang

Faculty of Engineering Science and Technology
UiT The arctic University of Norway
Norway

Abstract Road conditions during wintertime in northern Norway frequently cause problems for heavy haulers transporting goods. The trucks often experience difficulties when traveling uphill or downhill because of snowfall and ice formation, which again constitutes a safety risk and a nuisance for other road users. In this paper we have conducted a series of field tests where we investigated the impact of targeted sanding on a heavy hauler with focus on self-help, pull force and road friction.

E.1 Introduction

Wintertime in the northern parts of Norway offers many challenges within traffic and transport. Access to main roads and well-maintained roads decreases the further north you get. Road conditions during the winter can vary from day to day, and may deteriorate considerably at short notice due to ice formation and snowfall. Ice formation on certain parts of the road reduces the friction significantly, which again increases the risk of accidents [1, 3, 7, 12]. A well known problem during the winter months is connected to trucks (heavy haulers) transporting goods. These trucks often experience difficulties when travelling uphill or downhill, because of snow and ice, causing safety risks for other drivers and leading to roads being closed over a period of time [4]. Since northern Norway has a limited amount of roads leading to key cities in the region, trucks blocking roads are a complication for other road users, who will have to wait for the roads to be reopened or use detours that might add several hours to the trip. Part of a solution to this problem is to make it easier for the drivers to help themselves in certain situations. For example, driving uphill can be complicated if the friction on the road surface is low. Low friction can lead to a lack of wheel grip with trucks "spinning" on the spot unable to get up the hill, either because they had to stop unexpectedly, or because the hill is too steep in relation to the friction. A way of increasing the friction is to spread sand [11] in the areas where the wheels are (targeted sanding) so that the truck can get passed the problem zone without having to block the road and wait for help. Autoline AS [2] has created a device that makes it possible for truck drivers to turn on automatic targeted sanding on their own without leaving the cab of the truck. This gives drivers the ability to help themselves in some cases where they otherwise would have had to wait for rescue. Using targeted sanding as a self-aid for trucks may lead to cost reductions in winter maintenance and decrease negative environmental effects [5, 8] since only small areas of the road are sanded. As a part of the WiRMa project and in collaboration with Autoline AS and Nord-Norsk Trafikksenter AS we have conducted a number of field tests connected to the Autoline targeted sanding device and the impact this has on pull force of a heavy hauler.

E.2 Method

In this study a field test was performed to look at changes in pull force, before and after targeted sanding, for a heavy hauler pulling a trailer on a snow covered flat surface with a friction of 0.24. The friction on the test surface was measured with a Teconer RCM-411 [9] and the pull force was measured with a weight attached between the truck and the trailer. The experiments were done in order to observe the impact targeted sanding would have on a

heavy hauler with focus on the force it was able to pull a trailer with. The field tests were performed at Nord-Norsk Trafikksenter in Finnsnes in Troms and Finnmark, Norway, in -14 degrees Celsius on a clear winter day. Truck driving during the tests was performed by John-Egil Bustamo, and driving with friction measurement was done by Aleksander Pedersen and Børre Bang. The

Figure E.1: The truck and trailer used in the experiments.

truck used in the experiment was a Scania with a weight of 20 tons towing a trailer weighing 20 tons, see figure E.1. This was a standard truck setup from Nord-Norsk Trafikksenter used in education and license purposes. The weight used to measure the pull force was a Dynafor LLX2 digital load indicator 10 tons + 13.5 tons shackles [10] and it was connected as can be seen in figure E.2. The experiments were performed by locking the wheels on the trailer and moving the truck forward with increasing torque and accelerator deployment until the truck wheels lost grip, while collecting pull force data from the weight. A more detailed description of the setup is included in figure E.3. The device used for sanding was a sand spreader developed by Autoline AS, which is a box filled with gravel, mounted in front of the drive wheels of the truck. The box is operated from the cab and releases a small amount of gravel at a fixed interval while running. The process can be seen in figure E.4. Experiments were performed before and after sand spreading. Three tests were carried out without sand and two with sand. The two tests after sanding had to be terminated before reaching maximum pull force due to safety issues. Nonetheless, interesting results were obtained. To compare the results before and after sanding, graphs of the pull force were created and a visual comparison of the numbers was carried out. The graphs were also compared to an exponential function ($y = ae^x$, $a \neq 0$) that is based on regression of the data set.

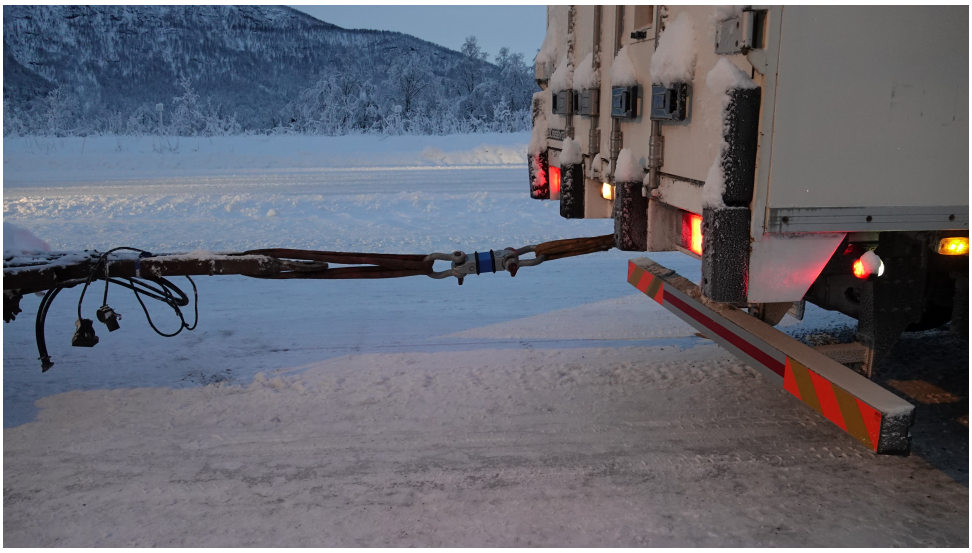

Figure E.2: Connection of the weight between the truck and the trailer.

E.3 Results and discussion

The result from all five experiments can be seen in Figure E.5. The first three spikes are measurements before sanding and the two last spikes are after sanding. From the figure it can be observed that the results from the tests before sanding are similar with a small decrease in maximum pull force. The decrease in maximum pull force may come from the fact that the experiments are done in the same spot, leading to a decrease in friction after each run. The two results after sanding was, as mentioned in Appendix E.2, terminated before reaching a maximum pull force. This is easy to see from the graph where one of the tests is almost equal to the results before sanding. However, in the last measurement a significant increase in pull force is obtained where the tests were run over a longer period of time prior to termination. In order to compare the results before and after sanding the authors selected one experiment from each and compared the graphs up until maximum pull force. The chosen experiments were the first and the last from Figure E.5, as shown in Figure E.6. From the plots in this figure it can be seen that the maximum weight measured from experiments 1 and 5 is 4222 kg and 6334 kg, respectively. This means that there is an increase in maximum pull force of over 2000 kg after sanding compared to before for this specific test case. The interesting part about the previous results is what happens along the curves towards maximum force, i.e. how the curves are developing. When comparing with an exponential regression curve, dotted lines in Figure E.6, one notices that the blue curve is a lot steeper than the red curve. Using regression to find the closest match for the data set by an exponential function, the following functions are obtained:

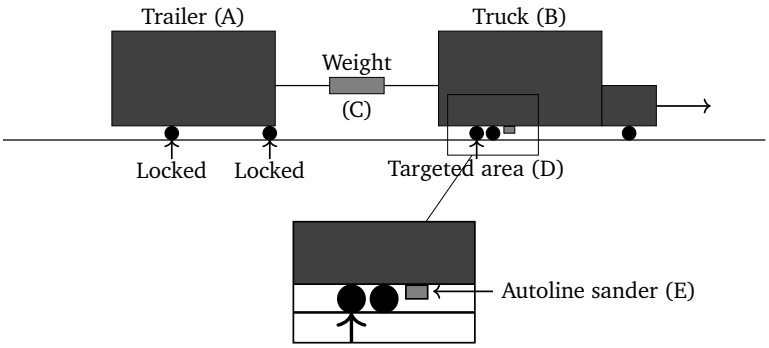

Figure E.3: The experiment setup: Trailer (A) wheels are locked. A weight (C) is attached between the trailer (A) and the truck (B). Truck (B) is trying to move forward with increasing throttle until the wheels loose grip at targeted area (D). The Autoline sander (E) is only used in two of the experiments, to measure the difference in pull force w/wo sanding.

Figure E.4: The Autoline sander in action.

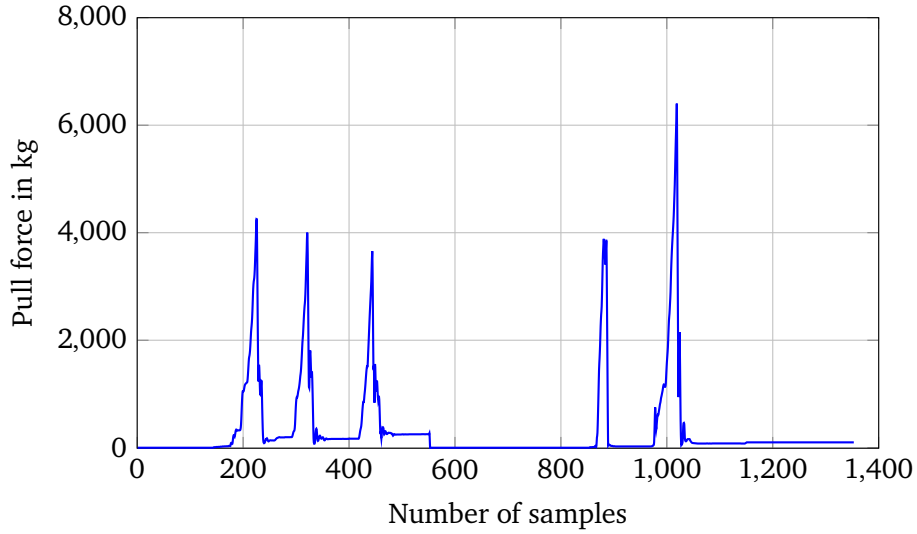

Figure E.5: The output pull force in kg (y-axis) from the weight at 0.25 s (4 Hz) intervals, from start at sample n=0 and end n=1400 (x-axis). The spikes represent the five experiments, the first three before sanding and the last two after sanding.

$$\begin{aligned} Y_1 &= 265.68e^{0.2977x}, R^2 = 0.8921, \\ Y_2 &= 190.67e^{0.2854x}, R^2 = 0.9675, \\ Y_1^{'} &= 79.093e^{0.2977x}, \\ Y_2^{'} &= 54.417e^{0.2854x}, \end{aligned} \tag{E.1}$$

where Y_1 and Y_2 correspond to the blue and red dotted lines in Figure E.6. The scaled derivative plot of $Y_1^{'}$ and $Y_2^{'}$ are shown in figure E.7, and as is seen, the increase is around 500-600 kg/s for the last experiment compared to 300-400 kg/s for the first experiment. Since both graphs have a good match with an exponential function, see R^2 in (E.1), we know that they both grow rapidly and if we look at the development 1-2 seconds later, keeping in mind that the test after sanding were terminated prematurely for safety reasons, the force would be doubled or even tripled. The main result here is that the targeted sanding works well, and will increase the friction of the surface significantly compared to a non sanded surface. Based on the graphs and the maximum forces obtained, an increase in friction can be estimated by computing the ratio of the two results

$$\frac{6334kg}{4222kg} \approx 1.50,$$

which corresponds to more than 50% increase in friction. Based on the data obtained from other sensors, the average friction coefficient was about 0.24

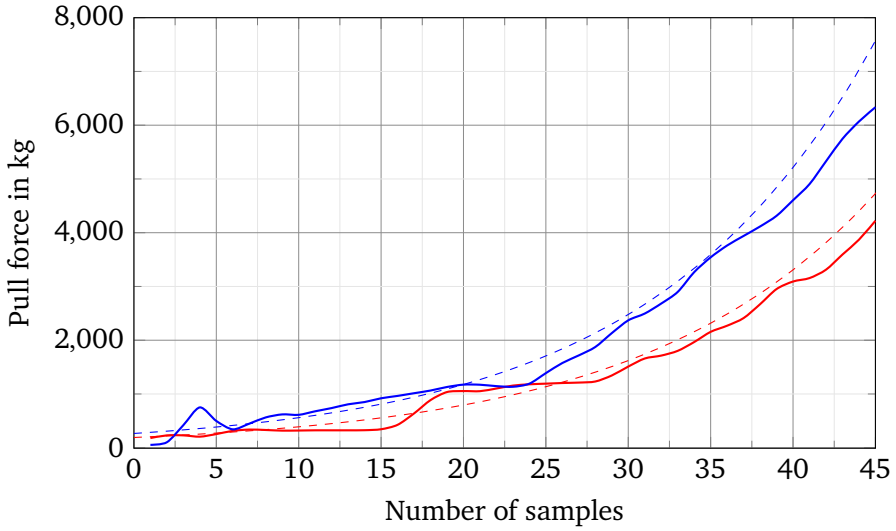

Figure E.6: The pull force (y-axis) up until maximum force (x-axis) from the first (red) and last (blue) experiments with associated exponential regression curves in stapled lines, see Y_1 and Y_2 in (E.1).

before sanding, and after sanding it could be estimated to 0.48 in this particular case, which is within the expected range (0.3 - 0.5) [6] for a sanded snow/ice road.

E.4 Conclusion

A field test was performed with five experiments to look at the impact targeted sanding would have on heavy hauler driving on winter roads. The tests were focused around the possible pull force of the truck before sanding compared to after sanding. A limited number of experiments were made over the course of one day in stable winter conditions of -14 degrees Celsius. This of course limits the collected data to a specific situation and will only give an implication of the sanding effect. However, based on the gathered results a conclusion can be made that targeted sanding is effective with regards to friction and pull force on certain road conditions, since it increases the friction on the road in the considered area, giving the truck better grip. The results show an increase of about 2000 kg in maximum pull force, and also revealed some interesting outcomes regarding the development of the derivative/slope of the force, where we see a time dependent increase in pull force that is much higher after sanding compared to before. For future work it would be ideal to do more field tests under varying conditions and expand the number of parameters measured during the tests, in order to be more confident in the obtained

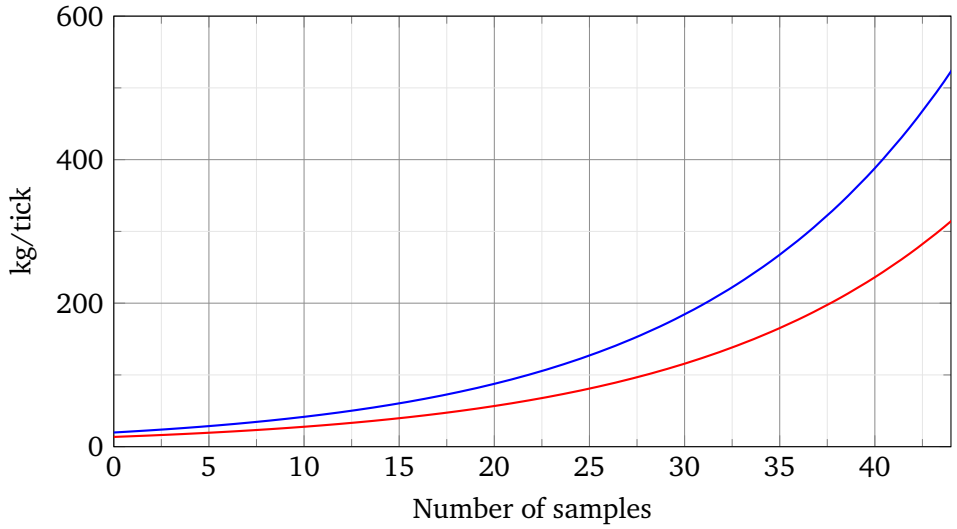

Figure E.7: Data plot of the derivative of the pull force from the first (red) and last (blue) experiments in figure E.6. This is a measure of kilogram per tick, and not per second. Each tick is 0.25 seconds.

results. Measured time dependent values for torque on the driving wheels together with accelerator and power values would be of interest. Lastly, road condition monitoring equipment will, in the near future, be able to classify, and possibly give standardized friction estimates. This would open up possibilities for predictions usable in route planning for heavy haulers, with and without vehicle mounted sand spreaders.

E.5 Acknowledgement

This research was partially financed by the Interreg-Nord project “WiRMa”, project ID 20201092. The authors would like to give special thanks to Autoline AS with John-Egil Bustadmo for his ideas, good discussions, and providing the support making this experiment possible, and also thanks to Nord-Norsk Trafikksenter AS for excellent service at their track facilities.

Bibliography

[1] Jean Andrey, Brian Mills, and Jessica Adams. *Weather Information and Road Safety*. Aug. 2001 (cit. on p. 125).

[2] Autoline AS. *Autoline*. 2017 (Accessed 2019-03-05). URL: http://www.autoline.no/About-us (cit. on p. 125).

[3] Daniel Eisenberg and Kenneth E. Warner. "Effects of Snowfalls on Motor Vehicle Collisions, Injuries, and Fatalities." In: *American Journal of Public Health* 95.1 (2005), pp. 120–124 (cit. on p. 125).

[4] J Granlund and P Thomson. *Traffic safety risks with EU tractor-semitrailer rigs on slippery roads*. HVTT14: International Symposium on Heavy Vehicle Transport Technology, 14th, 2016, Rotorua, New Zealand. 2016 (cit. on p. 125).

[5] Christer Johansson, Michael Norman, and Lars Gidhagen. "Spatial & temporal variations of PM10 and particle number concentrations in urban air." In: *Environmental Monitoring and Assessment* 127.1 (Apr. 2007), pp. 477–487 (cit. on p. 125).

[6] Alex Klein-Paste and Bård Nonstad. *Lærebok Drift og vedlikehold av veger*. Tech. rep. STATENS VEGVESENS RAPPORTER Nr. 365 Chapter 12. Vegdirektoratet - Trafikksikkerhet, miljø- og teknologiavdelingen - Vegteknologi, 2015 (cit. on p. 130).

[7] Keith K. Knapp, Dennis Kroeger, and Karen Giese. *Mobility and safety impacts of winter storm events in a freeway environment*. Tech. rep. Iowa State University. Center for Transportation Research and Education, 2000 (cit. on p. 125).

[8] Kaarle J. Kupiainen et al. "Size and Composition of Airborne Particles from Pavement Wear, Tires, and Traction Sanding." In: *Environmental Science & Technology* 39.3 (2005), pp. 699–706 (cit. on p. 125).

[9] Teconer. *Winter maintenance of roads and runways*. http://www.teconer.fi/en/winter.html. 2015 (Accessed 2019-03-05) (cit. on p. 125).

[10] Tractel. *Dynafor LLX2*. https://www.tractel.com/us/series.php?id_serie=7. 2019 (Accessed 2019-03-05) (cit. on p. 126).

[11] Torgeir Vaa. *Implementation of New Sanding Method in Norway*. Sixth International Symposium on Snow Removal and Ice Control Technology. 2004 (cit. on p. 125).

[12] Carl-Gustaf Wallman and Henrik Åstrøm. *Friction measurement methods and the correlation between road friction and traffic safety : A literature review*. Tech. rep. 911A. Swedish National Road and Transport Research Institute, 2001 (cit. on p. 125).

Paper F

The included paper is a reprint of

Altering perceptions, visualizing sub-ground metal objects

Aleksander Pedersen
Faculty of Engineering Science and Technology
UiT The Arctic University of Norway, Norway
Emerging Science journal, Vol 4, No 3 (2020), DOI 10.28991, P 205-213

F ALTERING PERCEPTIONS, VISUALIZING SUB-GROUND METAL OBJECTS

This is a reprint

Aleksander Pedersen

Faculty of Engineering Science and Technology
UiT The arctic University of Norway

Abstract Smart phones and sensor technology represent a key part of everyday life and are being used in areas such as safety, training, health care, etc. Utilizing an array of internal sensors and a metal detector requires an evaluation of the precision of the measurements and performance reviews. Metal detectors are versatile, with uses in healthcare as well as recreational, but a common issue often seen in the proprietary equipment is bad presentation of data. Usually the user interface is just numbers on a display, simplified graphs or sounds. By combining smartphone sensors with a metal detector and a custom mount we model a mapping between the virtual and physical model, a digital twin. In this paper we are utilizing the computing capabilities of a smartphone and employing visualization techniques not possible by partial information. In addition, we present an improved graphical user interface without any proprietary accessories. For this purpose, preliminary case studies are included as a part of a prototype in development.

F.1 Introduction

What we have seen in the recent years is an increased usage of sensors and sensor technology in all parts of life. For instance, smart technology (houses and cities), health care applications [8] where among things, actuators and advanced communication technologies have created environments in patients home without the need of expensive healthcare facilities [1] and rehabilitation of patients [3], tracking and industry [11], and monitoring in sports applications [10].

A metal detector is a versatile device, with uses ranging from recreational to healthcare and food industry as well as robotics. Finding foreign metallic particles in food products [14] is crucial for good quality and better food safety assurance. Searching for foreign metallic objects for Ingestion in pediatric emergency [9] and in advanced robotics using Bluetooth to control a metal detector robot [2].

The most common device is the smart phone, with many applications utilizing the different built in sensors, some of which are used for exercising, gaming, etc. Another application area is to use external devices connected to the smart phone. In this work we combined the common sensors of a smart phone with the applications of a metal detector. To the best of our knowledge, there are no commercially available applications connecting an external metal detector to a mobile phone. What already exits are very specific and proprietary products. The provided simple user interfaces such as display, or headphones connected by Bluetooth or cable are optional accessories. By expanding the magnetic information collected by a search coil, with geometry from sensor information such as compass, gyro and accelerometer, we can generate informative plots that provide insight not gained from search coil sounds and classification alone.

The main purpose of this work is to construct a custom hybrid setup which combines the standard output of a metal detector with the sensors and computing capabilities of off-the-shelf smartphones, into simple algorithms which can replace today's proprietary solutions. A secondary part has been to find a way to visualize the data on a smartphone screen concisely. From the tools available today we know that improvements can be made, and especially on the presentation given by the metal detector setup. The presentation is usually just numbers on a display, some simplified graphs or a sound(pitch) stating the depth and type of material reflected. Combination of information can be used to either provide new insights not possible by partial information or make a toolset that make certain operations easier.

F.2 Components

The two main components of the custom setup are the metal detector and a smartphone. The smartphone is presumed attached to the metal detector in a fixed orientation. Throughout this work we consider the mount fixed along the handle of the metal detector with the screen pointing up towards the user. Additionally, the smartphone frame is considered fixed with respect to the search area plane, see Figure F.1.

F.2.1 Metal detector

In principle the functional parts of a metal detector consists of two coils, a search coil and a detector coil as well as a set of control logic. The search coil generates an electromagnetic field, and the detector receives the replicated field generated by the metallic objects, Eddy currents [4]. The output from the metal detector is then transferred to the control logics which emits an audio signal indicating the type of material. The audio signal can then be recorded and used for analysis purposes.

F.2.2 Smartphone components

The metal detector has its own control logic, and by adding an extra layer of information using built in sensors such as

1. Accelerometer
2. Gyroscope
3. Rotation vector (attitude composite sensor)
4. Microphone

For the simplest motion-based representation, the accelerometer is used to detects movement changes in x, y, and z-axis. The gyroscope is used for orientation by measuring the rate of rotation for the three-coordinate axis. The rotation vector is an attitude composite sensor reporting the orientation relative to an East-North-Up coordinate frame by integrating the underlying accelerometer, magnetometer and gyroscope readings. The microphone has its own reporting mechanism which can be invoked using the android library.

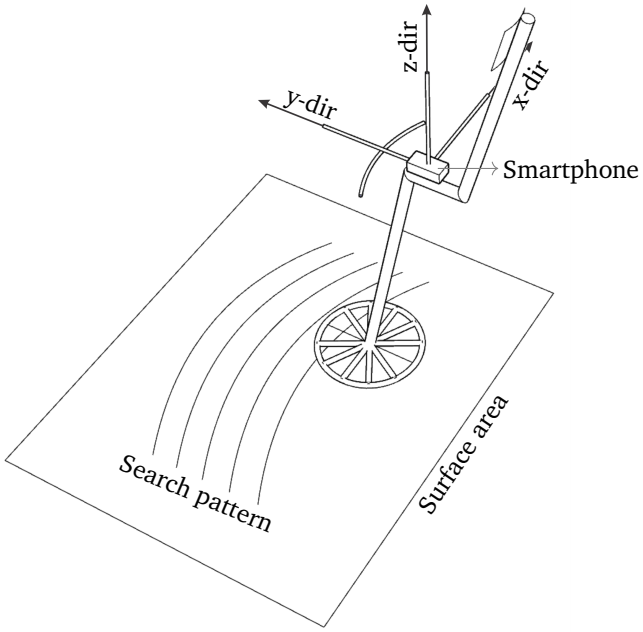

Figure F.1: Illustration of the custom mount attaching the phone to the metal detector with the axes aligned with the metal detector frame.

F.2.3 Frame representation

The metal detector and smartphone are modeled as a digital twin, where the components digital orientation are represented using a spatial 3-component frame following a right-hand system [16]. The phone frame is fixed, that is, the z-axis is aligned with the detector pointing upwards. The y-axis is aligned with the forward direction of the handle. The x-axis is orthogonal to the y- and z-axis, pointing towards the right.

F.3 Digital twin

To calibrate the smartphone sensors, we utilize an experiment which calibrates the phone sensors with an approximated pendulum motion. The x-axis is deciding the search pattern going from side to side when sweeping the metal detector over a surface area. The commercial device is replaced by a custom prototype based on a smart phone, shown in Figure F.2. The metal detector is a DEUS XP Metal detector [6]. The custom mount is a Celestron NEXYZ 3-AXIS Universal Smartphone Adapter [5].

(a) Setup from the side

(b) Setup from the front

Figure F.2: The commercial device is replaced by a custom prototype based on a smart phone. The metal detector is a DEUS XP Metal detector [6]. The custom mount is a Celestron NEXYZ 3-AXIS Universal Smarthphone Adapter [5].

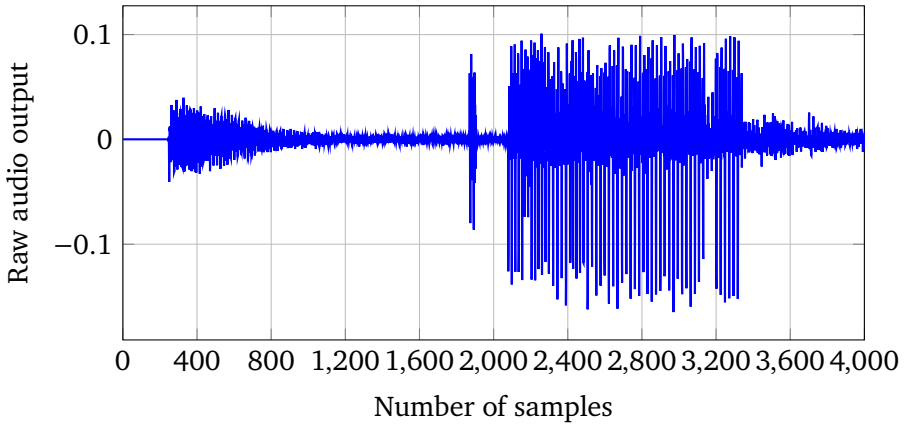

Figure F.3: Raw output from the metal detector using the phone as a recording device. Not processed with FFT

F.4 Results

The sound emitted from the metal detector is recorded on the smart phone and analyzed by performing frequency analysis. From this we can say something about the object or objects that are in the scope of the metal detector. The plot of a raw audio sample is shown in Figure F.3. The audio was sampled using a part of the android API called AudioRecord. AudioRecord is configured to use a 16 bit mono channel at a frequency of 12kHz. This audio data is then being processed using Fast Fourier transform (FFT). The result is a multi-resolution analysis with equally distributed bands of 256 samples.

Distributed over the whole spectrum, this gives $\frac{12000Hz}{256samples} = 46,875\frac{Hz}{sample}$. We can now compute the frequency for each amplitude in the graph, seen in Figure F.4. By using the mapping from sample index to frequency as we described above, the "beep" signal sound from the metal detector can be detected.

Two bands are illustrated in Figure F.5, showing a specific pattern emitted (left-hand side) and a signal containing noise only (right-hand side).

F.4.1 Visualization and processing algorithm

The visualization consist of a two step algorithm, where the coloring follows a straightforward conversion from the pre-processed sound signal to a HSV

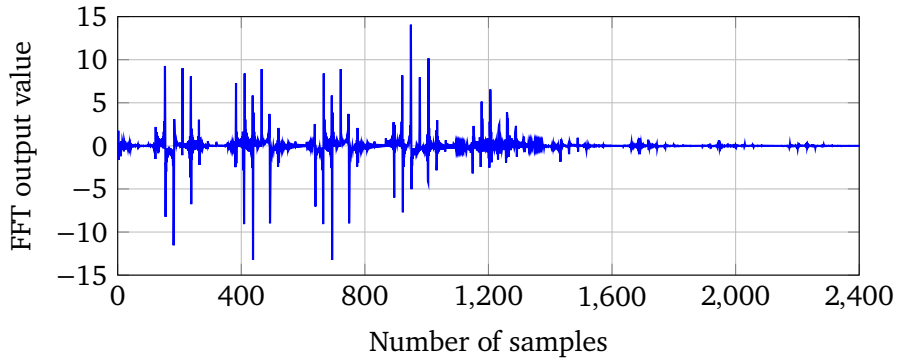

Figure F.4: The graph presented here is the FFT processed audio from a recorded session using the sound output from the metal detector.

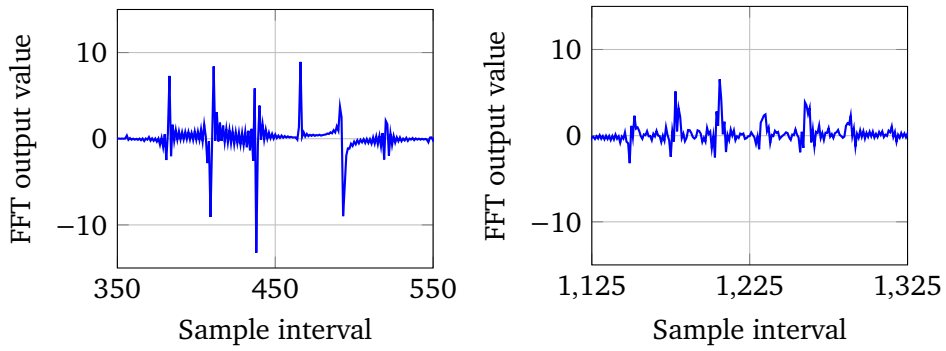

Figure F.5: The two graphs presented here is two subsets of the graph in Figure F.4. Both graphs are presenting different patterns obtained from two sample intervals $[350, 550]$ and $[1125, 1325]$ respectively.

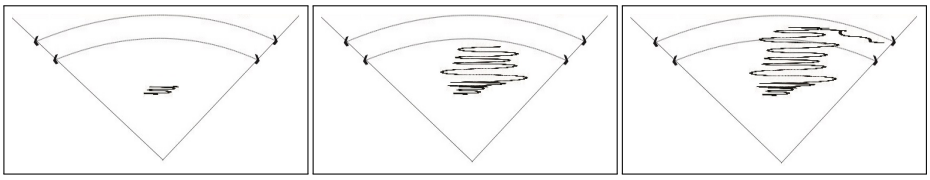

Figure F.6: The preliminary movement testing with positions drawn on a canvas for visualization purposes

(Hue, Saturation, Value) color model

$$\begin{aligned} h &= \frac{i_{nr}}{512} \cdot 360, \\ s &= 1, \\ v &= 1 - \frac{j_{fft}}{j_{max}} \cdot 0.5, \end{aligned} \tag{F.1}$$

where i is the sample index nr between $[0, 512]$ and $h \in [0, 360]$. Saturation is set to a constant value 1 and the j_{fft} is the processed sound signal value divided on the max peak value, j_{max} mapping the total value v between $[0.5, 1.0]$. The HSV color model produces a color representing the sound signal as shown in Figure F.8.

The second step of the algorithm is drawing the movement pattern on a canvas where the colors are based on the combination of a frequency band analysis and time dependent intensity accumulation as follows

$$\left.\begin{array}{l} \text{Induction} \longrightarrow \text{Sound vs. time} = (dB, t) \\ \text{Movement} \longrightarrow \text{Accel} + \text{Gyro} = (x, y, t) \end{array}\right\} \Rightarrow (x, y, color).$$

The process of combining the frequency analysis with the movement pattern in the prototype application follows the evaluation scheme seen in Figure F.7. The result is on the right-hand side where the sweeping motion is colored.

F.4.2 Mapping and deviation

The detector sweeping motion differs depending on the search state, where the angle changes as follows

1. General sweep $\longrightarrow [80, 120]^\circ$.
2. Targeted sweep $\longrightarrow [40, 80]^\circ$.
3. Pinpoint sweep $\longrightarrow [10, 40]^\circ$.

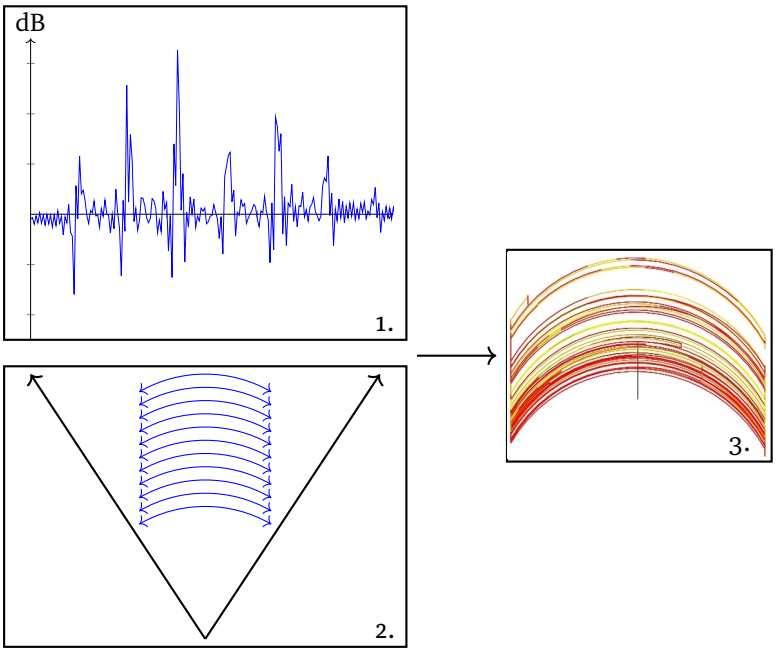

Figure F.7: The illustration here provides a visual presentation of the algorithm, consisting of: 1. The frequency analysis from the signal acquired, 2. The movement pattern captured, 3. The resulting visualization using an algorithm with 1. and 2. as arguments generating a colored trajectory following an arc.

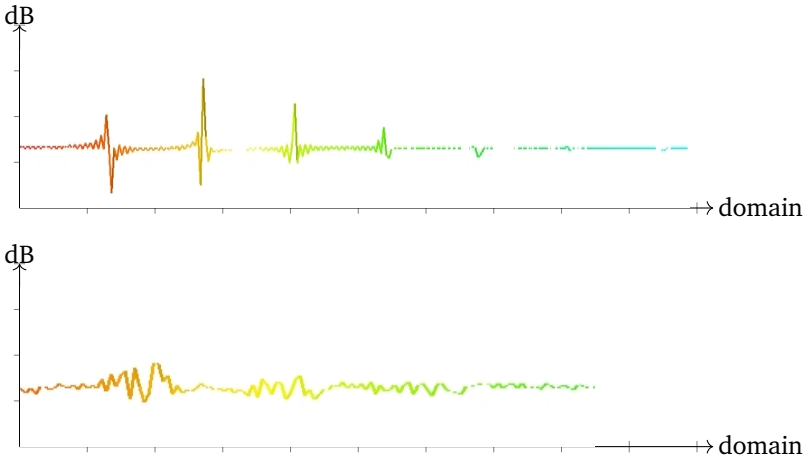

Figure F.8: Sound signal after fft and coloring from (F.1). Both figures represent the frequency domain separated into blocks. That is, the frequency from 0-12000hz is separated into 256 blocks after fft is performed. Figure on the top illustrates the signal from a specific material. Figure on the bottom illustrates the signal containing noisy data, which has been scaled in order to illustrate the noise better.

Sweep type	Screen l_c	Ground l_c
General 100°	1396px	104.7cm
Targeted 60°	837px	62.8cm
pinpoint 25°	349px	26.2cm

Table F.1: Curve length between the screen and ground using (F.2) with r fixed to 800px on the screen and 60cm on the ground

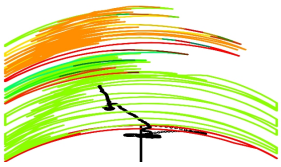

Figure F.9: Visualization of the three sweep types Table F.1. The sweep types are identified by the higher density of points in certain areas. Twice on the left bearing we see higher densities, which are a combination of targeted and pinpoint sweep. The colors are only present for visualization purposes.

Accuracy between screen dimension and ground measurement is calculated using curve length l_c (length of a complete sweep)

$$l_c = 2\pi r \frac{\theta}{360°}, \tag{F.2}$$

where θ is the sweeping angle. A test case visualizing the three states can be seen in Figure F.9.

The curve length ratio from Table F.1 is

$$\frac{l_{c,screen}}{l_{c,ground}} = \frac{1396px}{104.7cm} = 13.33px/cm. \tag{F.3}$$

Since the mapping is a relative correlation between the physical space and the digital twin, see Figure F.10, the ratio is an error estimate describing limitations of the current setup. With other words, the obtainable accuracy is $1.3px$ for every $1mm$ on the ground using the current algorithm and mapping.

Illustration of a test case where the average position values are visualized is shown in Figure F.11. These positions show the tendency of the metal detector movement. Next we calculate the standard deviation model as follows

$$\sigma = \sqrt{\frac{1}{N}\sum_{i=1}^{N}(x_i - \bar{x})^2},$$

where N is equal to the number of values in the total dataset, x_i is the value of the current index and $\bar{x}$ is the average value of the total data-set. The presented

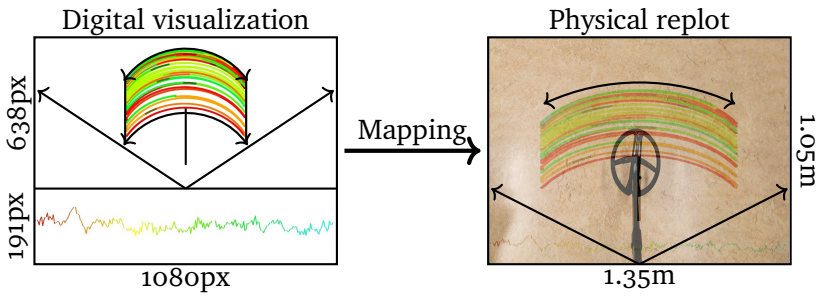

Figure F.10: The mapping between screen drawing resolution and the actual ground size measured from the metal detector

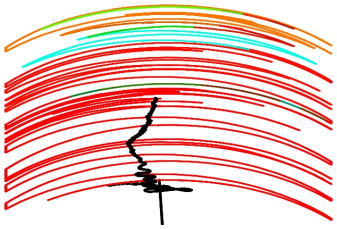

Figure F.11: Visualization of a general sweeping motion with the average position values painted in black. The black trajectory is calculated using a moving average of the positions during a test case.

model is in this case used to estimate the deviation away from the average positions, hence, the graph in Figure F.13 shows the tendencies around the average positions. Since the outward position is changing slowly based on the back and fort motion of the metal detector, it is similar to a linear development. The sweeping motion on the other hand are prone to higher values in the start, since we are in the general sweep phase. The curve is flattening out towards the area where we are pinpointing, and hence, we have a higher point density.

F.4.3 Error estimation

Precision on stability of sensor technology has been thoroughly researched in for instance [13, 7, 15, 12]. However, the canvas is graphical approximation using position and coloring of pixels, therefor the visualization will introduce errors which are not taken into account in the present study. Figure F.6 is illustrating the movement trajectory drawn on the canvas without any processing, i.e. smoothing or pathing. There are limitations of the current framework, where for instance the sweeping motion is only valid when standing still and the trajectory calculated is only from the device itself. The curve length mapping ratio shown in (F.3), was calculated ($13.33 px/cm$) and Table F.1 is estimating

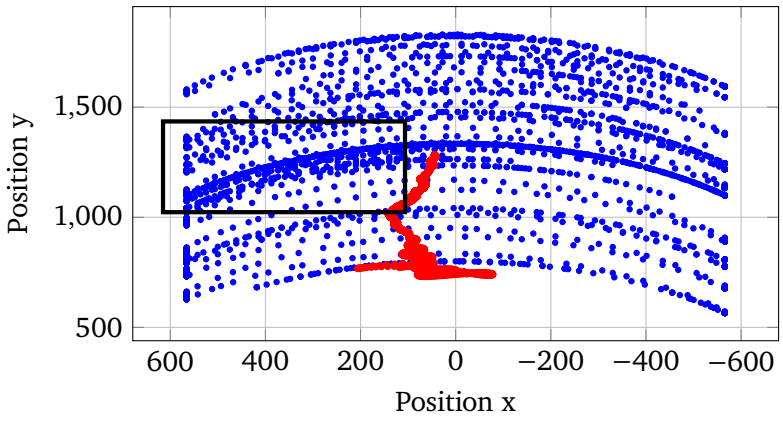

Figure F.12: The graph plots the positions before using the visualization algorithm, that is, we show the movement intensity by point density. The red dots are the average values. The tendency towards the left on the red dots are explained by the greater amount of positions toward the left area, shown in the black rectangle.

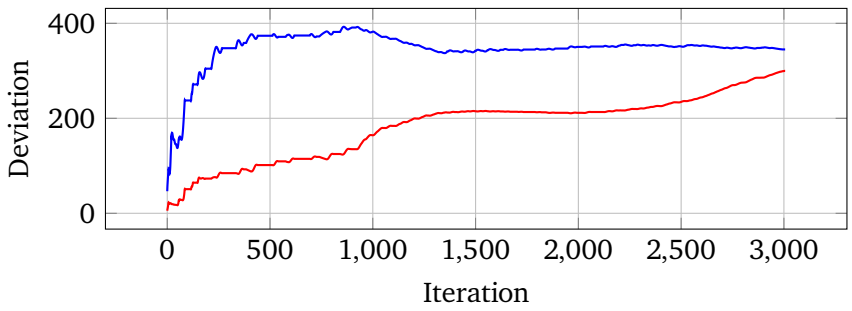

Figure F.13: This graph is plotting the standard deviation in x-direction (blue) and y-direction (red). Since the deviation calculation is using a continuous average, calculating the deviation every time a movement is detected, we expect the x-direction to flatten out towards the center of the motion and the y-direction to be close to linear.

the obtainable accuracy of the current implementation. Stability of sensor technology, implementation of motion tracking and user movement restrictions will influence the precision of the total system. When performing a sweep, such as the data shown in Figure F.12, the three states have different error ratios and calculating the standard deviation shown in Figure F.13, we are able to trace where the error ratio is at a maximum. The general sweep is going to have the biggest deviation, and by narrowing the sweep angle we achieve increased accuracy. The deviation is showing a higher precision (less turbulent) when the system is run longer and we are using the pinpointing sweep state. Since the values of sweeping is higher than the back and fort motion, the y-axis deviation for back and forth motion is close to linear.

F.5 Concluding remarks

Starting the development of a prototype application and implementing a multi-sensor system using the built-in sensor in a mobile phone, such as accelerometer, gyroscope, sound(microphone) and a metal detector, requires some extensive testing where we measure the outputs of the non-calibrated sensors. This is done in order to both properly calibrate the sensors, but also to know what to expect and include in the prototype application. Since the signal and component magnitudes can differ and the receiving signal can be weak depending on the depth to the object, a thorough analysis is required. The coloring scheme used for visualization purposes uses a signal that needs pre-processing, e.g., filtering or smoothing. We present a custom setup using a metal detector with an off-the-shelf smartphone creating a digital twin. We have created a tool for interactively modeling the inputs and visualize the information, and the canvas drawing is analogous to sketching indentation clues on a paper using an object beneath.

F.6 Future comments

For future development the signal wave lengths should be analyzed and using the signal amplitude, a better accuracy pinpointing the location of an object should be obtainable. The current implementation does not allow for the user change orientation during a sweep, and for future reference, the solution for this problem could be in generating reference points on the ground. The reference points can generate a stable ground-frame, which enables the user to rotate freely and change orientation during a recording.

Bibliography

[1] George Vasilev Angelov et al. "Healthcare Sensing and Monitoring." In: *Enhanced Living Environments: Algorithms, Architectures, Platforms, and Systems*. Ed. by Ivan Ganchev et al. Cham: Springer International Publishing, 2019, pp. 226–262. ISBN: 978-3-030-10752-9. DOI: 10.1007/978-3-030-10752-9_10 (cit. on p. 136).

[2] Ananya Bhattacharyya. "Bluetooth Controlled Metal Detector Robot." In: *ADBU Journal of Electrical and Electronics Engineering (AJEEE)* 1.1 (2017), pp. 1–5. ISSN: 2582-0257. URL: http://journals.dbuniversity.ac.in/ojs/index.php/AJEEE/article/view/562 (cit. on p. 136).

[3] Paolo Bonato. "Advances in wearable technology and applications in physical medicine and rehabilitation." In: *Journal of NeuroEngineering and Rehabilitation* 2 (1 2005). DOI: https://doi.org/10.1186/1743-0003-2-2 (cit. on p. 136).

[4] Bruce Candy. *Metal detector: Basics and theory*. English. Minelab. Forthcoming (cit. on p. 137).

[5] Celestron. *Optics and special mounts*. Accessed (2020-03-06). 2020. URL: https://www.celestron.com/products/nexyz-3-axis-universal-smartphone-adapter (cit. on pp. 138, 139).

[6] XP Detectors. *XP Metal Detectors - A new adventure*. Accessed (2020-03-06). 2020. URL: https://www.xpmetaldetectors.com/metal-detector/deus/ (cit. on pp. 138, 139).

[7] J. Du, C. Gerdtman, and Maria Lindén. "Signal Processing Algorithms for Position Measurement with MEMS-Based Accelerometer." In: *16th Nordic-Baltic Conference on Biomedical Engineering*. Ed. by Henrik Mindedal and Mikael Persson. Cham: Springer International Publishing, 2015, pp. 36–39. ISBN: 978-3-319-12967-9 (cit. on p. 145).

[8] I. Paramonov E. Stankevich and I. Timofeev. "Mobile Phone Sensors in Health Applications." In: *12th conference of fruct association* 12 (2012), pp. 136–141 (cit. on p. 136).

[9] Hazwani Binte Hamzah et al. "Handheld Metal Detector for Metallic Foreign Body Ingestion in Pediatric Emergency." In: *The Indian Journal of Pediatrics* 85.8 (2018), pp. 618–624. ISSN: 0973-7693. DOI: 10.1007/s12098-017-2552-5 (cit. on p. 136).

[10] David Harrison, Nadarajah Mani, and Gobinath Aroganam. "Review on Wearable Technology Sensors Used in Consumer Sport Applications." In: (Special Issue on Wearable Wireless Sensors 2019). DOI: https://doi.org/10.3390/s19091983 (cit. on p. 136).

[11] Soojin Cho & Hongki Jo & Shinae Jang & Jongwoong Park & Hyung-Jo Jung & Chung-Bang Yun & Billie F. Spencer & Jr. and Ju-Won Seo. "Structural Health Monitoring of a Cable-Stayed Bridge Using Smart Sensor Technology: Deployment and Evaluation." In: *Smart Structures and Systems* 6 (July 2010). DOI: 10.12989/sss.2010.6.5_6.439 (cit. on p. 136).

[12] J.D. Hol M. kok and T.B. Schon. "Using Intertial Sensors for Position and Orientation Estimation." In: *Foundations and Trends in Signal Processing* 11 (2017), pp. 1–153 (cit. on p. 145).

[13] Zhizhong Ma et al. "Experimental Evaluation of Mobile Phone Sensors." In: (June 2013). DOI: 10.1049/ic.2013.0047 (cit. on p. 145).

[14] Joanna Trafialek, Sylwia Kaczmarek, and Wojciech Kolanowski. "The Risk Analysis of Metallic Foreign Bodies in Food Products." In: *Journal of Food Quality* 39.4 (2016), pp. 398–407. DOI: 10.1111/jfq.12193 (cit. on p. 136).

[15] F. Frisk U. Shala and K. Klonowska. *Indoor Positioning using Sensor-fusion in Android Devices*. 2011 (cit. on p. 145).

[16] G. Watson. *Right Hand Rule for Cross Products*. Accessed (2020-03-22). 1998. URL: http://www.physics.udel.edu/~watson/phys345/Fall1998/class/1-right-hand-rule.html (cit. on p. 138).

Paper G

The included paper is a reprint of

A preliminary study on hybrid sensor technology in winter road assessment

Aleksander Pedersen and Tanita Fossli Brustad
Faculty of Engineering Science and Technology
UiT The Arctic University of Norway, Norway
Safety Journal, Vol 6, No 1, 17 pages

G A PRELIMINARY STUDY ON HYBRID SENSOR TECHNOLOGY IN WINTER ROAD ASSESSMENT

This is a reprint

Aleksander Pedersen and Tanita Fossli Brustad

Faculty of Engineering Science and Technology
UiT The arctic University of Norway
Norway

Abstract Road conditions during the winter months in Nordic countries can be highly unstable. Slippery roads combined with heavy haul traffic and ordinary road users can create dangerous, even lethal situations if road maintenance is unsuccessful. Accidents and critical road conditions may lead to blocked roads, putting strain on a limited number of main roads in many regions, and may, in the worst case, isolate areas entirely. Using sensors in winter road assessment has been a popular topic for over 20 years. However, with today's developments connected to smaller and cheaper sensors, new opportunities are presenting themselves. In this paper we perform preliminary experiments on a variety of sensors, both commercial and experimental, in order to evaluate their benefits in possible hybrid sensor technology, which can give a more complete characterization of the road surface than what is possible from just one sensor. From the collected data and visual analysis of the results, the idea of a hybrid sensor seems promising when considering the differences in the tested sensors and how they might complement each other.

G.1 Introduction

Transportation of raw material, goods, and people is a constantly growing factor in the Nordic countries. With this growth a significant increase in semi-trailers for long haul has been observed where research states that many of them are a safety risk on slippery winter roads [5]. In order to meet the current and future industry's needs with accessible and, more importantly, safe roads the pressure on successful winter road maintenance is high. Research shows that winter road maintenance is crucial for maintaining safe roads [4]. Knowing when and where critical conditions occur and improving risk assessment, can increase the efficiency of maintenance personnel (saving money), and can be used to warn road users of potential risks (increasing safety). The limited number of main roads, combined with long distances between key cities in the Nordic countries, makes the road network vulnerable. Critical road conditions can lead to closed roads, which again can lead to areas being isolated over prolonged periods of time. With today's developments connected to faster transfer speed of data, smaller and cheaper sensors, and a focus on smart environments, new opportunities are presenting themselves in winter road maintenance. The new popular area within the winter road assessment research field is that of hybrid measurements with transmission of information to neighboring vehicles or to road side servers [18, 19]. Hybrid measurements are becoming more and more recognized as a method that can give better overall information on road conditions, often with already available data, compared to lone sensors. This can be seen in recent research, for instance, in [9] where in-car sensor data is incorporated into weather forecast models to improve road weather forecasts, in [17] where a neural network is employed to develop a surface friction prediction model based on historical data from an optical sensor, or in [10] where acoustic measurements and machine learning algorithms are combined to classify dry, damp, and wet road surfaces.

The research and experiments performed in the paper are a part of the Winter Road Maintenance project (WiRMa project). In the project, partners from Norway, Sweden, and Finland conducted research and demonstrated profitable, industrial, and network based systems for decision support in winter road maintenance. The project vision is to demonstrate a viable winter road maintenance decision-support system (DSS) using novel technologies for ambitious ideas by

- Combining measurement techniques for improved icing measurements.
- Collecting, communicating and crunching road weather, vibration and road surface condition (snow, ice, wet, slush etc.) and indirect friction information from vehicles.

- Improving forecasts and nowcasts based on vehicle observations.

- Visualizing the information to be used as a DSS in winter road maintenance.

The specific motivation surrounding this work was connected to one of the work packages in the project, work package 4 - Winter road condition information. The overall aim of the work package was to investigate the possibility of combining new direct and indirect sensing methods together with known optical sensors to provide a more complete characterization of the road surface (hybrid measurement techniques) by turning vehicles into mobile monitoring stations. Currently, such development is on-going in the automotive industry, but that industry is very closed and the data gathered from modern vehicles is not available for winter road maintenance purposes. Additionally, the data available from vehicles is not based on continuous measurements at that point in time, as for example, slipperiness information is available only when ABS, ESP, or similar are engaged. Mobile systems with continuous measurements will play an important part in monitoring road conditions in Nordic countries and in tackling problems related to making road infrastructure maintenance decisions at the right time. As of now there is simply not enough data and information available to handle maintenance properly on roads that are subject to harsh conditions and long distances.

Based on the motivations and aims of the WiRMa project, the aim of this paper was to select and test a number of sensors to look at the possibility of equipping vehicles with hybrid measurement technology, in order to improve the risk assessment of roads in arctic conditions. The motivation behind this was to increase safety and accessibility for road users during the unpredictable winter months, and help maintenance personnel assess maintenance needs. As a final comment, it is important to remember that sensors will always only be a tool in decision support but ultimately the safety depends on the drivers' behavior of perceiving the sensor alerts, since this is considered to be one of the influential factors in reducing accidents [3]. In this paper the process and initial results of using certain sensors in winter road assessment are described. The process included the choices made in selecting sensors (both commercial and experimental), methods for collecting and storing data, and how the measurements were analyzed. The presented results are our initial experience with measurement data and the sensor's behavior, including a discussion where the data is analyzed and compared, in relation to reliability, similarity, and usefulness.

G.2 Preliminaries

This section gives a preliminary overview of some of the commercial sensors known in winter road assessment, and gives examples of the possibilities connected to experimental sensors within the field.

G.2.1 Commercial sensors

When it comes to sensors created for winter road assessment, two categories exist; stationary and mobile. In this paper the focus is on mobile sensors and four optical sensors have been considered; The Road Condition Monitor 411 (RCM411) [7], Mobile Advanced Road Weather Information Sensor (MARWIS) [12], MetRoadMobile [13], and Road Eye [11]. These sensors measure the reflected light, from a light source illuminating the road, and analyze the data to classify the surface conditions. The Directorate of Public Roads [22] also uses mobile sensors, but with different measuring types; retardation (deceleration) meter, continuous friction measurement using a mobile wagon attached to the car with either one or two friction wheels, or handheld friction meters. The friction wheels used in Norway are produced by ViaFriction [25], and the Directorate of Public Roads uses two different types, the Road analyzer and recorder 5 (RoAR5) [24] and OSCAR [23]. OSCAR is the most reliable of all the friction meters used by the Directorate of Public Roads.

G.2.2 Experimental sensors

In addition to the sensors that have been specifically created for winter road assessment, experimental sensors, including cameras, have dominated the research field for many years. Four examples showing the variety of experimental sensor types during the last three years (2017-2019) follow. In [14], Pan et al. applied a pre-trained convolutional neural network to automatically detect road surface conditions based on camera images. Hou et al. created a system called VehSense [8] that combined a smartphone and OBD-II data to detect vehicle skidding. Microphones, together with neural networks were presented in [15] as a way of detecting road surface wetness. Finally [6] combined piezoelectric and optical sensors to classify road conditions and measure ice/water thickness. These four examples express only a fragment of the creativity and possibilities within the field of road condition assessment, four additional examples [28, 2, 16, 26] may be of interest.

G.3 Method

This section describes the choice of sensors used in the experiments, both commercial and experimental. In addition, the placement of the sensors on the vehicle is shown, an overview is given of how the data for each sensor was collected and stored, and lastly, an explanation is given of how the data was evaluated.

G.3.1 Choice of commercial sensors

Based on the project description, one of the key aspects was to assess road condition using measurement techniques. Initially, when we became part of the project, two sensors were already bought and ready to use; RCM411 and MARWIS. The next step was to assemble and test these on a vehicle. Previously we were discussing four different optical sensors, but since two sensors were already at our disposal and we knew that they are commercially available, with extensive support, there was no need to buy any new equipment initially. In addition, the Road Eye sensor was to be used in another work package in the project, so naturally two different sensors were chosen for this work package. Another reason for choosing RCM411 and MARWIS was because they measure a range of variables, unlike Road Eye and MetRoadMobile which only measure one and two variables, respectively. Both RCM411 and MARWIS are used specifically for measurements on roads, and the Directorate of Public Roads has tested them. As a result, these two commercial sensors are in a much higher price range than the experimental sensors, but more reliable and suited for their specific purpose.

G.3.2 Choice of experimental sensors

The main attributes, in our opinion, which the experimental sensors should possess are: a low price, a reasonable size, should complement the commercial sensor in a beneficial way, and, preferably, be available on the market in some form. Taking these attributes into account, as well as the research done in the literature cited in section G.2.2, the main experimental sensor of choice ended up being a Walabot radar [27], with the supplementary selections of vehicle data (OBD data), video, sound, and smartphone sensors.

The Walabot radar is a pocket-sized 3D imaging sensor that uses radio frequency technology to illuminate the area in front of it and sense the returning signals. The sensor supports short range scanning and distance scanning, with the possibility to extract 3D image data, 2D image slices, raw signals, and the sum of raw signals in an image (image pixel energy).

The reason for choosing the Walabot sensor is its small size and low cost, as well as it being a radar. This is of interest since radar technology has not been tested extensively for winter road assessment, which in theory it should be suited for given that radar is not dependent on sight, being less affected by snowy or foggy conditions where, for instance, optical sensors have a problem. So since the commercial sensors of choice were both optical sensors, a radar sensor should compliment these sensors in a beneficial way. The other supplementary selections were chosen because of the simplicity to obtain the data, and because they give a variety of information that the other sensors do not give. Vehicle data is already measured by the car and is easily acquired by an OBD adapter (we chose a second generation adapter, OBD-II [20, 21]). As for the other data, most people today carry around a smartphone that can both record sound and video, in addition to having a number of other incorporated sensors.

G.3.3 Sensor placement on the vehicle

Figure G.1 shows the placement of the four main sensors (RCM411, MARWIS, Walabot, and OBD-II) on the car. The RCM411 sensor was mounted on the tow ball pointing at the right wheel track, the MARWIS sensor was secured with a rack to the truck bed pointing at the center of the road behind the vehicle, the Walabot sensor was attached below the back left passenger door pointing straight down at the wheel track, and the OBD-II adapter was plugged into the adapter inside the car. All these sensors had their fixed placement through-out the study, except for the Walabot, where various placements were considered before choosing the above described place. The sensors not mentioned here were not part of the main setup, but rather mounted and tested at small intervals under chosen conditions. This included a microphone attached at various places to the dashboard, and a smart-phone attached to a phone mount on the dashboard used as a dashcam to capture video of the road in front (which included sound from inside the car). In addition, the dashcam phone also utilized several in-house applications for different sensor measurements.

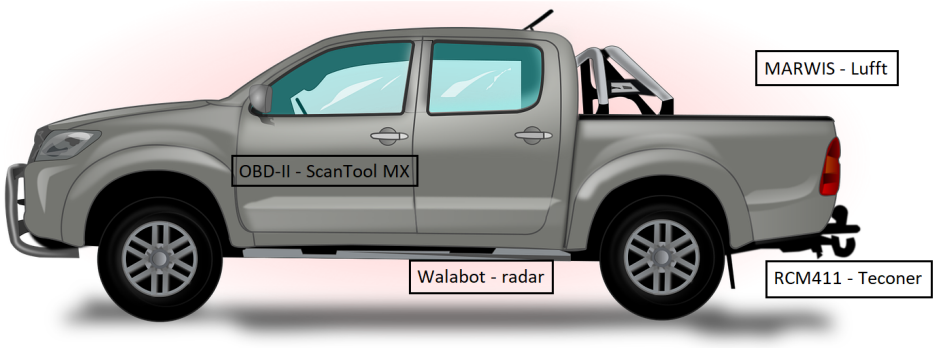

Figure G.1: Placement of the sensors on the car. Image by OpenClipart-Vectors from Pixabay.

G.3.4 Data collection and storage

The data collection and storage were different for each individual sensor. A description follows on the methods used for collecting and storing data for each sensor. As an overall storage place for all the sensor data in all experiments, and to ensure easy access and sharing, Box [1] was used.

The RCM411 sensor transferred data to a mobile phone using Bluetooth, which then communicated it to selected servers created specifically for RCM411 sensor data. The servers make it possible to see real-time updates on surface conditions online at `https://roadweather.online`, and download data (in comma-separated values files) from the sensor one owns. Since the online application already existed, was simple to use, and stored the data intuitively, this became the method used for collecting and storing data. In addition, the files from `https://roadweather.online` were downloaded and stored in Box.

The MARWIS sensor was compatible with two existing smartphone applications, one of which had equivalent functions as the RCM411 application, the MARWIS App. This app had just like the RCM411 application, no internal storage capability and only an option to communicate with a remote server, that required login information that we opted not to use since downloading raw data seemed impossible. Using the browser application ViewMondo, the data from MARWIS is visually good, but there were no tools available for converting the processed data back into a raw format. The other application, ConfigTool, was a configuration tool that included a collection of the different sensor variables with an associated visualization. ConfigTool also had an option to save the data to an .xml file in the internal storage. Since this was the only suitable option, we initially decided to store the data in this format. All the measurement data from the sensor was communicated to the phone using

Bluetooth, and the ConfigTool files were uploaded to Box.

The Walabot sensor was run from a Raspberry Pi where data was collected and stored, initially. The Raspberry Pi ran a C++ program that collected 4-5 measurement every second from the Walabot, and saved them in comma-separated values files (csv files). In order to prevent large data loss, in case of an interrupted connection, a new file was created after a given time interval, storing the data in multiple files instead of just one. Then, after ending a test-run the data was assembled into one file and stored in Box.

The vehicle data (OBD data) was collected from the vehicle through an OBD adapter (OBD-II) that extracted data from the vehicle and made it available via Bluetooth on a smartphone app. The app lets one select which variables OBD-II should extract from the vehicle, where the possible choices depend on the model and type of vehicle involved. From the app csv files were available for download, and the downloaded files were then stored in Box.

G.3.5 Measurement analysis

In order to evaluate the sensors, in a winter road assessment perspective, the following characteristics were examined and analyzed: possible data from the sensors, reliability of the sensors (including existing software), collection and storage experience, and test-run results. Example data from each sensor has been presented and discussed with a focus on relevance in winter road assessment. The reliability of the sensors, including any available software, has been considered and evaluated based on our experience when testing them. Both the reliability and experiments presented in this paper are preliminary results recorded when exploring and configuring this type of hybrid setup with multiple sensors and devices being run simultaneously. The collection and storage methods, chosen above, have been analyzed in regards to fulfilling the task we initially needed it to fulfill. Lastly, the initial test-run results have been analyzed with visual comparison by observing the differences between two graphs against each other. For the RCM411 sensor, a consistency test was performed to evaluate the stability of the sensor, while for MARWIS and Walabot, a comparison against RCM411 data was made.

Evaluation criteria		Criteria description
Sensor variables:	**S1.**	Number of relevant variables
	S2.	Variable relevance (High, Medium, Low, Exp (Experimental))
Reliability:	**R1.**	Reliability in the initial connection (High, Medium, Low)
	R2.	Reliability during measurements (High, Medium, Low)
	R3.	Reliability of the software (High, Medium, Low)
Data collection and storage:	**D1.**	Format of the collected data
	D2.	Assembly of files required (Yes, No, On stop (If the car power is turned off))
	D3.	Storage (Local, Online, Both)
Test-run results	**T1.**	Initial conclusion of the comparisons

Table G.1: Description of the evaluation criteria.

G.4 Results and discussion

This section includes the results of the initial tests of the three sensors: RCM411, MARWIS, and Walabot, with a discussion connected to the evaluation methods described in section G.3.5. In addition the supplementary sensors are considered with focus on our experience when using them, and a possible hybrid technology is discussed.

G.4.1 RCM411

This section describes the sensor variables available from the RCM411 sensor, gives a discussion on the reliability of the sensor based on our experience, and comments on the collection and storage of the data. In addition a consistency test of the variables: friction, surface temperature, and road state (defined here as road surface condition), is shown.

Sensor variables

The RCM411 sensor offers a range of different variables from the measurements. In the case of winter road assessment the most interesting are: friction, road state, air temperature, surface temperature, and water layer thickness. For the road state a number in the range 1-6 is given where 1 = Dry, 2 = Moist, 3 = Wet, 4 = Slush, 5 = Ice, and 6 = Snow. Figure G.2 shows three examples of extracted data from the RCM411.

Reliability

The RCM411 sensor was one of the most reliable sensors, in this initial study, in regards to uptime. Through the experiments the sensor did not once experience

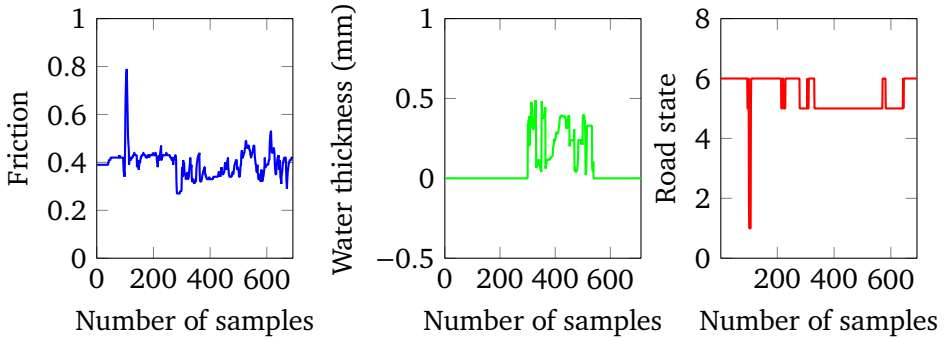

Figure G.2: Three of the possible data types that can be extracted from the RCM411. Left: Friction. Middle: Water thickness. Right: Road state.

disconnection problems or lose data during a run. The sensor was easy to mount on the vehicle and establishing a connection to a smartphone was painless. To us, the online resource showing real-time updates is dependable and useful, expressing the variables friction, water thickness, air temperature, and road temperature as a graph, and road state by adding color to the traced path.

Data collection and storage

The data collection and storage from the RCM411 sensor, via the online webpage, worked. One csv file was created for each run, with measurements taken once every second, and by logging into our account, the files, sorted by date and time, were easily downloaded. Since there was only one measurement per second from the sensor during the test-runs, the created files were not overly large and were well suited for analysis, even for runs lasting more than an hour.

Consistency test

The initial test-run of the RCM411 sensor was a consistency test where a decided track was driven twice in order to observe the similarities between the two runs. A comparison was made between three variables; friction, surface temperature, and road state, in order to evaluate the consistency of the measurements. The plots of the frictions can be seen in Figure G.3, surface temperatures in Figure G.4, and road states in Figure G.5. The test-route, located in Narvik, Norway, had a length of about 5 km and took 12 minutes to drive through, and the weather conditions were sunny with an average air temperature of -4 degrees Celsius. In the comparisons we do not expect to see two equal graphs for the measured variable, because we know that conditions were not exactly the same

for the two runs. The influence of other road users was present, as well as the impact from the sun, and the varying speed of the vehicle. However, we do expect to see similarities between the graphs in some areas.

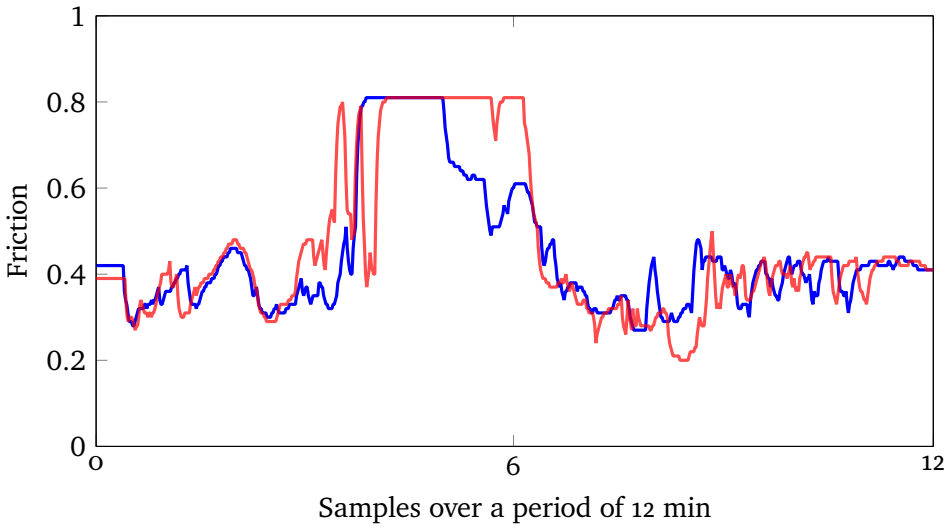

Figure G.3: RCM411 friction plots from two runs along the same test route. Blue: run 1. Red: run 2.

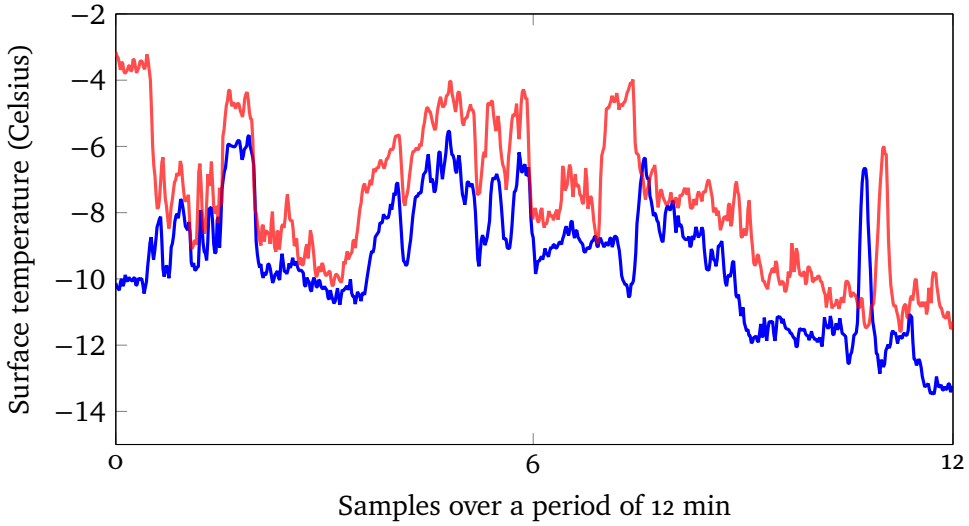

Figure G.4: RCM411 surface temperature plots from two runs along the same test route. Blue: run 1. Red: run 2.

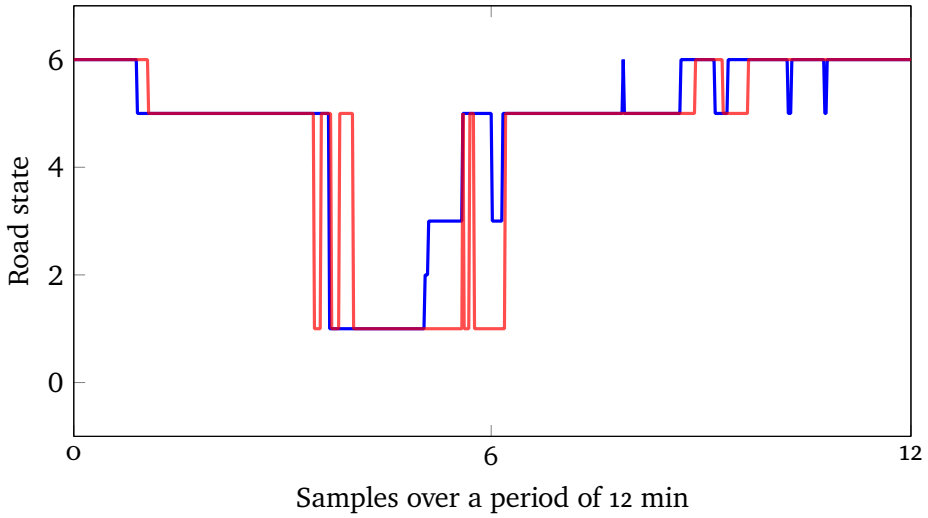

Figure G.5: RCM411 road state plots from two runs along the same test route. Blue: run 1. Red: run 2.

From the figures it can be observed that there are similarities between the variables when comparing the two runs. Especially in the friction and road state plots where the runs give equal values for the variables in certain areas, more so for the state than the friction, which is reasonable given that the friction can change within a road state. In the plot of the surface temperature, Figure G.4, the observation is that they have the same behavior but the values of the second run are consistently higher than for the first run. This can be explained by the sunny conditions where the air temperature was on average 1 degree Celsius higher during the second run compared to the first run. An overall conclusion to the consistency test is that the sensor appears to be stable when measuring, for the variables friction, surface temperature, and road state.

G.4.2 MARWIS

This section describes the sensor variables available from the MARWIS sensor, gives a discussion on the reliability of the sensor based on our experience, and comments on the collection and storage of the data. In addition a comparison between MARWIS and RCM411 friction is made.

Sensor variables

The MARWIS sensor offers many of the same variables as RCM411, and also some additional information that is relevant in winter road assessment. The

variables equal to RCM411 are; friction, road state, air temperature, surface temperature, and water layer thickness. For the road state from MARWIS a number in the range 1-8 is given where 1 = Dry, 2 = Damp, 3 = Wet, 4 = Ice, 5 = Snow + ice, 6 = Chemically wet, 7 = Water + ice, and 8 = Snow. The additional variables that MARWIS have are ice percentage, dew point temperature, and relative humidity (air and ground). Three examples of possible data can be seen in Figure G.6.

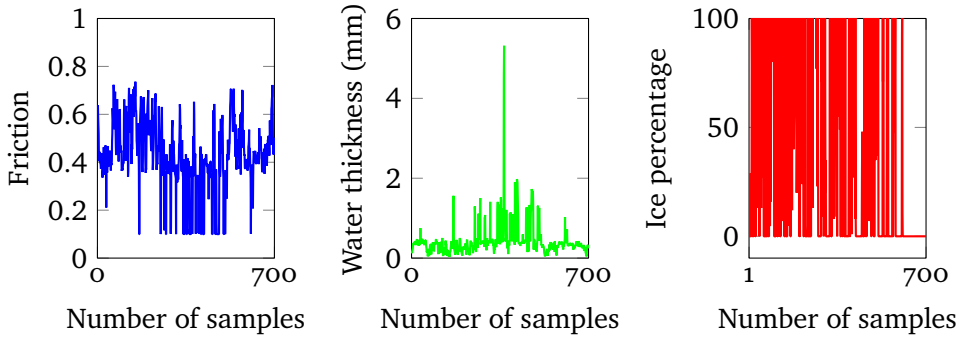

Figure G.6: Three of the possible data types that can be extracted from the MARWIS. Left: Friction. Middle: Water thickness. Right: Ice percentage.

Reliability

In the initial study we recognized problems with MARWIS almost immediately. Initially we had problems with MARWIS losing power, which was caused by an unstable/broken vehicle power adapter. Also, some issues were identified with the Bluetooth connection between MARWIS and our smart phone, which caused a disconnection between the two, and the application had to restart before further use. This issue was caused by the application itself, and related to the loss of power. Furthermore, the loss of power disrupted the Bluetooth connection to the sensors, which again led to the phone application crashing without any warnings or reconnects. Another problem included the powering of MARWIS where a converter that came with the sensor, converted 12V to 24V from the car adapter which MARWIS required under colder conditions (below a certain temperature the sensor need to heat up in order to work properly). The converter did not have any type of safety to limit the voltage, and when the car was accelerating the voltage from the adapter increased by a small amount, which lead to a higher voltage than MARWIS was made for frying one of the internal circuits.

Data collection and storage

The data collection and storage required a stable connection with no application crashes, and the initial reliability tests led to an evaluation of whether to continue with the commercial application. We had earlier discussed how to save the data for further analysis, and the remote server data upload was discarded since raw data was not available. The other option was to use the configuration tool and save locally, but the format of the data in .xml was only byte values, which we agreed was not suitable for our purpose. Since we had no idea if the remote server would let us download data in a useful format we created our own prototype application for communicating with MARWIS and storing the data. Doing research on the communication protocol, communication settings (Bluetooth), led to specific queries with a bytestream checksum directly to the MARWIS sensor. We got a working application which received data from the sensor based on our query and we identified some of the key problems which we experienced in the initial setup. One reason for the crashes in the commercial application was caused by variables not being initialized after a query, which again was caused by either delays in a response or malfunction in the power/bluetooth connection. Seeing that we now had control of the data we were able to save it in a useful format in the internal storage on the phone for further analysis.

Comparison

The initial test results from the MARWIS sensor were extracted on a test-run together with the RCM411 sensor. So, since MARWIS and RCM411 have many equal measurement variables, and they are both optical sensors, it was decided that comparing the two would be interesting in the initial phase. The variable that was compared was surface friction, because this is a key variable in winter road assessment. In Figure G.7 the graphs of the two frictions have been plotted, and it shows the data collected during a one hour drive.

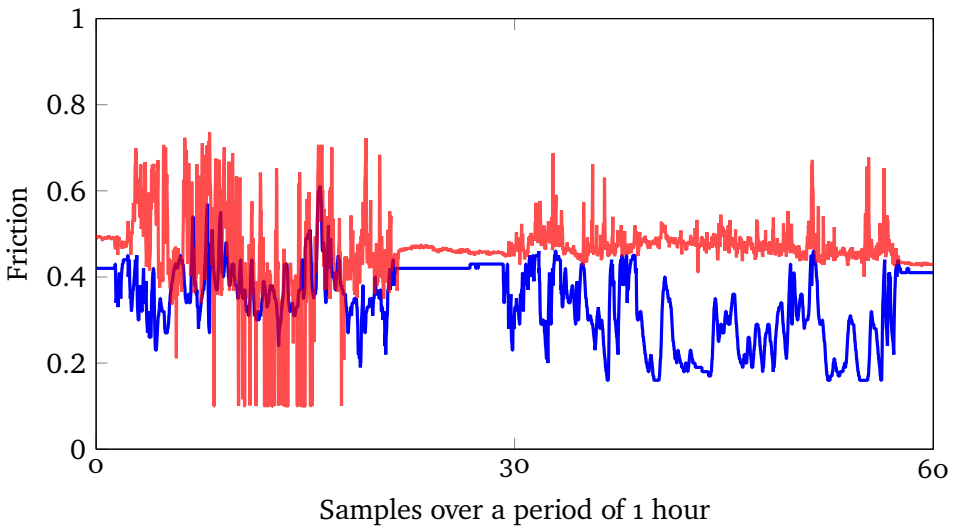

Figure G.7: The plots of friction data from RCM411 in blue and MARWIS in red, during a 1 hour drive.

From the figure it can be seen that the two sensors show different friction coefficients for almost the entire test drive. From the setup of the sensors we know that they do not measure the exact same spot, and that the area measured is larger for the MARWIS sensor than the RCM411 sensor. However, the expectation from our part, before analyzing the data, was that areas of equal or similar friction would be observed. Since this is not the case, it would be interesting to do more testing between these two sensors, and compare the results to previous work and comparisons connected to them.

G.4.3 Walabot

This section describes the sensor variables available from the Walabot sensor, and indicates which variables we found relevant. In addition, the section has a discussion on the reliability of the sensor based on our experience, comments on the collection and storage of the data, and shows a first comparison of Walabot image energy against RCM411 friction.

Sensor variables

The Walabot sensor is based on imaging data and can offer several types of output variables. The types are: 3D image, 2D image slice, raw signals, image energy (sum of raw signals), and imaging targets (a list of and the number of

identified targets). Figure G.8 shows three examples of possible outputs from the Walabot. In regards to using Walabot data in winter road assessment the

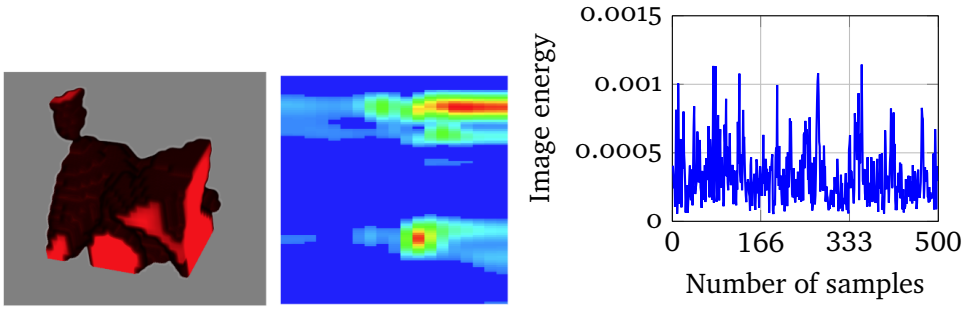

Figure G.8: Three of the possible data types that can be extracted from the Walabot. Left: 3D image. Middle: 2D image slice. Right: Image energy.

most suitable data output, having both storage and visual analysis in mind, was predicted to be image energy, since it gives one value every timestep, making it easy to create graphs that can be compared with the other sensor variables.

Reliability

All in all, the reliability of the Walabot sensor was adequate. After it was attached to the vehicle, and up and running, no problems occurred when performing the measurements, and data was collected without interruptions. Although collecting data from the initial test-runs went smoothly, the preparations of the Walabot leading up to the test-runs presented some challenges. Firstly, the connection between the Walabot and the Raspberry Pi, via USB, had a tendency to be lost due to sensitivity in the connection on the Walabot side, where the USB plug needed to be kept stable to secure a connection. This was solved by firmly securing the plug in the Walabot so that it had no room to move. Secondly, the Walabot does not have its own clock, and is therefore dependent on the clock of the device it is connected to. This caused some early headaches seeing that the Raspberry Pi, which the Walabot was connected to, only has a reliable clock as long as it has internet connection. So when the Raspberry Pi is without internet access, the clock starts counting from the time it had when the device was last turned off. The strategy used to solve the clock challenge was either setting up a hotspot on a mobile phone or manually setting the time on the Raspberry Pi before starting the Walabot.

Data collection and storage

The collection and storage method used for the Walabot worked well. Collecting the data in multiple files proved to be necessary given that on some test-runs small interruptions occurred leading to the loss of all data in the file that the Raspberry Pi was saving to in that moment. Since the Walabot gave 4-5 measurements every second a large amount of data was collected when the test-runs lasted an hour or more, so the method of assembling all the data into one file may not always be desirable. In our case, with the initial tests, putting the data into one file seemed like the best choice, in regards to simplifying analysis and comparisons later on.

A first comparison

In order to get a first impression of how the measurements from the Walabot behave when measuring winter roads, an experiment was conducted with the Walabot together with the RCM411. Both sensors were taken for a test drive and a segment over a period of 20 min was extracted from the sensors and compared. The plots of the two measurements can be seen in Figure G.9, where the blue graph is friction from the RCM411, and the red graph is image pixel energy from the Walabot.

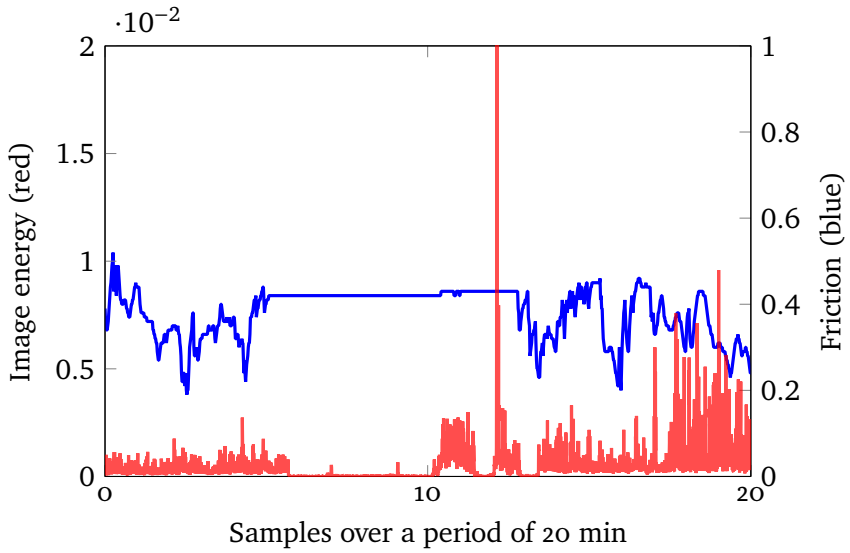

Figure G.9: The plots of friction data from RCM411 in blue, and Walabot image energy in red, during a 20 minute drive.

When comparing the two graphs in Figure G.9 it can be observed that in the

areas where the friction is close to constant, the image energy has the same behavior giving constant values close to zero, and for the areas where the friction fluctuates, the image energy also fluctuates. As a first impression this is a positive result showing that the Walabot radar may have potential in winter road assessment since it seems to have a correlation to, at least, road surface friction. The results from this initial test give strong reasons, and increase the interest, for further investigation of the experimental Walabot sensor for road assessment purposes.

G.4.4 Video, sound, OBD-II and smartphone

The measurements and captures collected from the devices/sensors in this section were not the main priority during the startup, and we had no specific goal or ideas of what to expect from the data. Since the measurement setup was mostly based on curiosity and future ideas, no type of analysis was performed regarding the data captured from the devices/sensors. However, the preliminary experiences are discussed.

Video

One of the ideas was to use video capture from in front of the car as a reference for what to expect from the friction measurements behind the car. Another interesting aspect here for future notice was to combine video with artificial intelligence (AI) and predict the road condition (friction) during the video analysis. An example is shown in Figure G.10. Capturing this amount of video for an entire trip (several hours) requires both storage capacities on the capturing device as well as storage for further use. Because we were using Box for storage purposes for the other measurement data, we included the video files as well in a folder. Experience showed that this was not a good idea with respect to the capabilities of Box and large file sizes.

Sound

We were also doing some experimental work regarding sound capture using a microphone. The idea was to attach a microphone to the car chassis, preferably something as tough as steel to get more accurate vibrations from the ground traveling through the car frame. There were only some initial sound captures and no post processing or analysis of the data has been undertaken yet. The file sizes were so small that they are negligible when uploading.

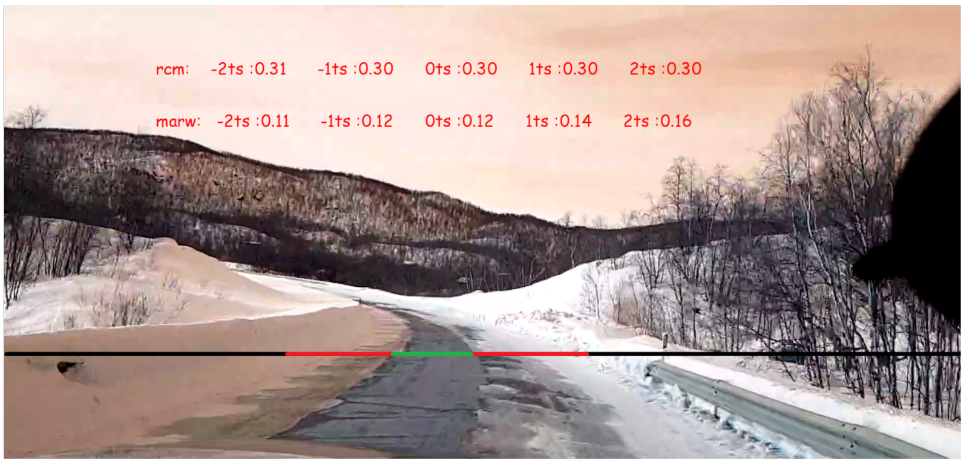

Figure G.10: Example image of how video can be preprocessed using AI to estimate road conditions. Figure by Kristoffer Tangrand.

OBD-II

Of the experimental sensors and devices, the OBD-II is already being used for car performance analysis and research purposes. The idea here was to extract information about the car, which is already available, and utilize post processing tools to analyze the data with regards to other measurements such as friction. There are a lot of variables available in the application, where the user can select which ones to record the output from. The available variables differ depending on the car model and make, for our use we selected those we found relevant, both for comparison with other sensors and for analysis purposes.

Smartphone

A smartphone is packed with sensors which can record data such as acceleration, orientation and sound. The commercial application we used for RCM411 had some experimental friction calculations based on measured forces on the phone, that is, using the accelerometer to estimate friction and breaking distance. This specific function was optional, and could be uploaded in the same file as the other variables, for comparison with the measured values. Based on these experimental calculations, we wanted to do our own experiments using smartphone sensors only, and no external information. There were some initial experiments, but this requires more work before doing any analysis on the data.

G.4.5 Hybrid sensor technology

In Table G.2 a brief summary is displayed of the previous results, based on the criteria from Table G.1 together with the price range of each sensor.

Criteria	Sensors						
	RCM411	**MARWIS**	**Walabot**	**Video**	**Sound**	**OBD-II**	**Smartphone**
S1	5	8 (9)	4	1	1	Optional	3
S2	High	High	Exp	High	Exp	Medium	Medium
R1	High	Medium	Low	High	High	High	High
R2	High	Medium	High	High	High	High	High
R3	High	Low (in-house: High)	Medium	High	High	High	High
D1	.csv	.xml (in-house: .csv)	.csv	.3gp	.3gp	.csv	.txt
D2	On stop	Yes	Yes	No	No	On stop	Yes
D3	Online	Both	Both	Both	Both	Both	Local
T1	Consistent	Dissimilar to RCM411	Interesting results against RCM411	N/A	N/A	N/A	N/A
PR	High	High	Low	Low	Low	Low	Low

Table G.2: Results of the criteria evaluation described in Table G.1, along with the price range (PR) of each sensor.

If we consider the previously discussed sensors in relation to creating a hybrid sensor in the future, there are already some interesting observations. The two optical sensors, RCM411 and MARWIS, have many of the same measured variables so in theory only one of them should be necessary in a hybrid sensor. However, from the friction plots in Figure G.7 of RCM411 and MARWIS an observation was made that the measured friction differed for most of the test drive. This opens up a possibility that the two sensors may be sensitive to different types of conditions, and if so, a combination of both sensors will be beneficial in a hybrid solution.

The experimental Walabot radar sensor shows, during the first comparison with RCM411 in Figure G.9, that there may be a correlation between RCM411 friction data and Walabot image energy data. This is of interest since our prediction is that the Walabot is less affected by snowy and foggy conditions compared to the RCM411 sensor, which will make it an asset during tough weather conditions. In addition the size and price range of Walabot is a major advantage in relation to a hybrid sensor.

For the device/sensors discussed in section G.4.4, the overall benefits are their small size and that the technology is available for a reasonably low cost. In addition, winter assessment research has been performed on all of them with positive results. The greatest potential probably lies within the use of video in winter road assessment, because it brings a new dimension to the

analysis that can involve other research areas. Above we presented an example of combining video with AI to predict friction measurements, but the possibilities are numerous. Thus, in our opinion, video will make a valuable inclusion in hybrid assessment. The OBD-II collects data from the vehicle, in contrast to RCM411, MARWIS, Walabot, and video that collect road data. This in itself makes it an important supplement to the hybrid measurements. Vehicle data can increase the reliability of the risk assessment, since vehicles may act differently under difficult road conditions. Regarding the two last measurements (sound and smartphone data), more experiments will have to be performed to find the strengths they may possess that the other sensors lack.

Implementation of the technology on the vehicle (placement of the sensors) is a topic that will have to be investigated more in future works. The placements chosen in this paper, as described in Figure G.1, were based on restrictions connected to the sensors, the type of vehicle used, and our opinion based on predictions and ideas. In a hybrid sensor technology it will be important to consider on which parts of the road measurements should be conducted, and if sensors should be spread out around the vehicle as opposed to gathered in one place. Gathering the sensors in one place can lead to information being lost (e.g. the two wheel tracks can have varying conditions), and spreading them out may require a larger number of sensors (increasing the price). A solution can be to implement sensors that can measure the whole width of the road and then extract condition data for given areas, for instance with a camera as shown in Figure G.10, however, this will enlarge the post-processing work. The pros and cons of various sensor placements should be identified and mapped so that a justified decision can be made based on the chosen hybrid technology.

G.5 Conclusions

Assessment of road conditions in Nordic countries is a necessity due to increasing amounts of transportation and heavy haulers, which brings about the need for accurate safety and risk assessment with strong focus on maintenance and estimates of the occurrence of critical conditions. In this paper we have performed a preliminary study of several sensor technologies with possible connections to hybrid sensor technology. We have tested two commercial and one experimental sensor, as well as four supplementary measuring devices or techniques. In addition, a set of classification criteria has been developed, see Table G.1, and used, see Table G.2, for evaluating the different sensors. The main findings can be summarized as follows:

- The difference in friction for RCM411 and MARWIS, on the test drive,

opens up the possibility that the two sensors have different sensitivity to various types of conditions.

- There is a possibility that the RCM411 friction and Walabot image energy correlate, but the data is currently not sufficient to verify this.

- Video can bring a new dimension to road assessment, by combining it with AI and sensor input.

- The OBD-II data is the only tested sensor data that gives information about the vehicle instead of the road, which makes it interesting in a hybrid technology.

These early studies establish connections between technologies that could potentially decrease risk and, hence, increase safety for all road users. The study has also focused on experimental technologies to improve and complement already existing winter road assessment devices. Experimental technologies can present cheaper solutions to replace commercial sensors if the measured variables correlate. The initial results show promising connections between the tested sensors and possible device combinations that would benefit from a hybrid solution. Implementing a form of hybrid sensor technology could both increase the reliability of risk assessment and have a more complete characterization of the road surface. Having a publicly available joint information source which could identify areas with higher risk that should, if possible, be avoided for safety reasons, will increase awareness of difficult conditions. The paper shows several experimental measurements and as previously mentioned, some of them need more work in order to find both strengths and weaknesses. A more thorough field test should also be performed, which incorporates all the above mentioned equipment to establish a complete view of the measurements compared to each other.

G.6 Acknowledgement

This research was part of the Interreg-Nord project “WiRMa”, project ID 20201092.

Bibliography

[1] Box. *Simplify how you work*. Online. https://www.box.com/home. (Accessed 2019-11-25) (cit. on p. 157).

[2] Jakob Döring et al. "A novel approach for road surface wetness detection with planar capacitive sensors." In: *Journal of Sensors and Sensor Systems* 8 (Jan. 2019), pp. 57–66. DOI: 10.5194/jsss-8-57-2019 (cit. on p. 154).

[3] Danish Farooq, Sarbast Moslem, and Szabolcs Duleba. "Evaluation of Driver Behavior Criteria for Evolution of Sustainable Traffic Safety." In: *Sustainability* 11.11 (June 2019), pp. 31–42. ISSN: 2071-1050. DOI: 10.3390/su11113142 (cit. on p. 153).

[4] Liping Fu and Taimur Usman. "Safety Effects of Winter Weather and Road Maintenance Operations." In: *Sustainable Winter Road Operations*. John Wiley & Sons, Ltd, 2018. Chap. 7, pp. 101–130. ISBN: 9781119185161. DOI: 10.1002/9781119185161.ch7 (cit. on p. 152).

[5] J Granlund and P Thomson. *Traffic safety risks with EU tractor-semitrailer rigs on slippery roads*. HVTT14: International Symposium on Heavy Vehicle Transport Technology, 14th, 2016, Rotorua, New Zealand. 2016 (cit. on p. 152).

[6] Kang Gui et al. "Road surface condition detection utilizing resonance frequency and optical technologies." In: *Sensors and Actuators A: Physical* 297 (2019), p. 111540. ISSN: 0924-4247. DOI: https://doi.org/10.1016/j.sna.2019.111540. URL: http://www.sciencedirect.com/science/article/pii/S0924424719300998 (cit. on p. 154).

[7] Taisto Haavasoja, Juhani Nylander, and Pauli Nylander. "Experiences of Mobile Road Condition Monitoring." In: *Proceedings of SIRWEC 2012, Helsinki, Finland*. May 2012 (cit. on p. 154).

[8] Y. Hou et al. "VehSense: Slippery Road Detection Using Smartphones." In: *2017 IEEE 85th Vehicular Technology Conference (VTC Spring)*. June 2017, pp. 1–5 (cit. on p. 154).

[9] Yumei Hu et al. "Modeling Road Surface Temperature from Air Temperature and Geographical Parameters—Implication for the Application of Floating Car Data in a Road Weather Forecast Model." In: *Journal of Applied Meteorology and Climatology* 58.5 (2019), pp. 1023–1038. DOI: 10.1175/JAMC-D-18-0145.1 (cit. on p. 152).

[10] M. Kalliris et al. "Machine Learning Algorithms for Wet Road Surface Detection Using Acoustic Measurements." In: *2019 IEEE International Conference on Mechatronics (ICM)*. Mar. 2019, pp. 265–270 (cit. on p. 152).

[11] Sten Löfving. *Road Eye*. Online. http://www.opticalsensors.se/roadeye.html. 2014 (Accessed 2019-12-12) (cit. on p. 154).

[12] Lufft. *MARWIS specifications*. Online. https://www.lufft-marwis.com/en_US/specifications. 2019 (Accessed 2019-09-05) (cit. on p. 154).

[13] MetSense. *MetRoadMobile - Mobile road friction monitoring*. Online. http://www.metsense.com/product?p=MetRoadMobile. 2017 (Accessed 2019-12-12) (cit. on p. 154).

[14] G. Pan et al. "Evaluation of Alternative Pre-trained Convolutional Neural Networks for Winter Road Surface Condition Monitoring." In: *2019 5th International Conference on Transportation Information and Safety (ICTIS)*. July 2019, pp. 614–620 (cit. on p. 154).

[15] Giovanni Pepe et al. "Detecting Road Surface Wetness Using Microphones and Convolutional Neural Networks." In: *Audio Engineering Society Convention 146*. Mar. 2019. URL: http://www.aes.org/e-lib/browse.cfm?elib=20326 (cit. on p. 154).

[16] Armando Piccardi and Lorenzo Colace. "Optical Detection of Dangerous Road Conditions." In: *Sensors* 19 (Mar. 2019), p. 1360. DOI: 10.3390/s19061360 (cit. on p. 154).

[17] Ziyuan Pu et al. "Road Surface Friction Prediction Using Long Short-Term Memory Neural Network Based on Historical Data." In: *Transportation Research Board 98th Annual Meeting, Washington DC, United States*. Jan. 2019 (cit. on p. 152).

[18] Yoshitaka Shibata et al. "IoT Based Wide Area Road Surface State Sensing and Communication System for Future Safety Driving." In: *Advanced Information Networking and Applications*. Ed. by Leonard Barolli et al. Cham: Springer International Publishing, 2020, pp. 1123–1132 (cit. on p. 152).

[19] Yoshitaka Shibata et al. "Realtime Road State Decision System Based on Multiple Sensors and AI Technologies." In: *Complex, Intelligent, and Software Intensive Systems*. Ed. by Leonard Barolli, Farookh Khadeer Hussain, and Makoto Ikeda. Cham: Springer International Publishing, 2020, pp. 114–122 (cit. on p. 152).

[20] OBD Solutions. *STN1100 Family Reference and Programming Manual*. https://www.scantool.net/downloads/98/stn1100-frpm.pdf. (Accessed 2019-10-21) (cit. on p. 156).

[21] OBD Solutions. *WHAT IS OBD?* Online. https://www.obdsol.com/knowledgebase/on-board-diagnostics/what-is-obd/. (Accessed 2019-10-21) (cit. on p. 156).

[22] Vegvesenet. *The directorate of public roads - Winter training for operators*. Online. https://www.vegvesen.no/_attachment/2365449/binary/1270205?fast_title=SVV+rapport+673+Oppl\T1\ae ring+i+

vinterdrift+for+operat\T1\o rer.pdf. (Accessed 2019-12-13) (cit. on p. 154).

[23] ViaTech. *Oscar*. Online. http://www.viatech.no/products.aspx?lang=no&id=3. (Accessed 2019-01-14) (cit. on p. 154).

[24] ViaTech. *RoAR mk6 Oppgradering*. Online. http://www.viatech.no/products.aspx?lang=no&id=2. (Accessed 2019-01-14) (cit. on p. 154).

[25] ViaTech. *ViaFriction brukes for å måle friksjonsnivåene på veg og flyplass*. Online. http://www.viatech.no/products.aspx?lang=no&id=1. (Accessed 2019-01-14) (cit. on p. 154).

[26] Johan Wåhlin et al. "Laboratory test of five different optical road condition sensors." In: *Proceedings of SIRWEC 2016, Ft. Collins, Colorado, USA*. Apr. 2016 (cit. on p. 154).

[27] Walabot. *Walabot - Technical Brief*. Online. https://walabot.com/docs/walabot-tech-brief-416?type=pdf. (Accessed 2019-09-05) (cit. on p. 155).

[28] Choongheon Yang et al. "Estimation Road Surface Temperature Variation Using Commercial Vehicle Ambient Sensor." In: *IOP Conference Series: Materials Science and Engineering* 603 (Sept. 2019), p. 022027. DOI: 10.1088/1757-899X/603/2/022027 (cit. on p. 154).